ACTA UNIVERSITATIS SZEGEDIENSIS

Acta Physica et Chemica

NOVA SERIES

TOMUS XXXV FASCICULI 1-4

AUSHAF 35(1-4)1989

HU ISSN 0324-6523 Acta Univ. Szeged

HU ISSN 0001-6721 Acta Phys. et Chem.

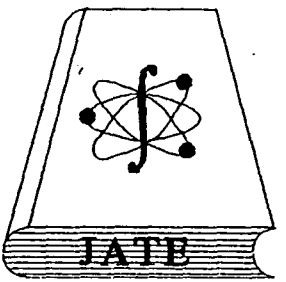

Szeged, Hungaria

1989

Adiuvantibus
M. BARTÓK, ZS. BOR, K. BURGER, L. CSÁNYI, J. CSÁSZÁR, I. DÉKÁNY,
P. FEJES, I. HEVESI, P. HUHN, I. NAGYPÁL, E. KAPUY,
I. KETSKEMÉTY, M. NOVÁK et F. SOLYMOSI

Redigit
MIKLÓS I. BÁN

Edit
Facultas Scientiarum Universitatis Szegediensis de
Attila József nominate

Editionem curant
J. ANDOR, I. BÁRDI, S. KÁDÁR, Á. MOLNÁR et Á. SÜLI

Nota
Acta Phys. et Chem. Szeged

Szerkeszti:
BÁN MIKLÓS

A szerkesztőbizottság tagjai:
BARTÓK M., BOR ZS.,BURGER K., CSÁNYI L., CSÁSZÁR J., DÉKÁNY I.,
FEJES P.,HEVESI I.,HUHN P.,NAGYPÁL I., KAPUY E.,
KETSKEMÉTY I., NOVÁK M. és SOLYMOSI F.

Kiadja:
a József Attila Tudományegyetem Természettudományi Kara
(Szeged, Aradi vértanúk tere 1.)

Szerkesztőbizottsági titkárok:
ANDOR J., BÁRDI I., KÁDÁR S., MOLNÁR Á. és SÜLI Á.

Kiadványunk rövidítése:
Acta Phys. et Chem. Szeged

ADSORPTION OF NITROGEN OXIDES IN ZEOLITES

I. HANNUS, J.HALÁSZ, I. KIRICSI,

GY. SCHŐBEL, GY. TASI and P. FEJES

Institute of Applied Chemistry, Attila József University,

Rerrich Béla tér 1., H–6720 Szeged, Hungary

(Received September 25, 1989)

THE ADSORPTION PROPERTIES OF DIFFERENT SYNTHETIC AND HUNGARIAN NATURAL ZEOLITES IN THE ADSORPTION OF NO AND NO_2 WERE INVESTIGATED BY X–RAY DIFFRACTION, DERIVATOGRAPHY, INFRARED SPECTROSCOPY, MASS SPECTROSCOPY AND CLASSICAL ANALYTICAL METHODS. NITRATE ION FORMATION WAS FOUND TO OCCUR IN THE ZEOLITE STRUCTURE DURING THE ADSORPTION OF NITROGEN OXIDES. THE SOLUBILITY OF NITRATE FROM NITRATE/NATURAL ZEOLITE SYSTEMS WAS INVESTIGATED. THE POSSIBILITY OF THE USE OF NATURAL ZEOLITES AS FERTILIZER ADDITIVES IS DISCUSSED.

Introduction

One of the current fundamental environmental problems is acidic rain, in which the main role is played by sulphur oxides and nitrogen oxides. The disadvantage of nitrogen oxides in the atmosphere is that they increase the acidity of rain, but the presence of nitrogen in rain has some advantages for plants (vegetables), too.

Adsorption is one of the possible methods for the removal of nitrogen oxides from waste and industrial flue gases. Zeolites, as excellent adsorbents, have been widely investigated in this process [1–3].

The present work had two aims: to determine the adsorption properties of natural and synthetic zeolites, and to investigate the possible agricultural application of Hungarian natural zeolites, to utilize both the nitrogen content that accumulates during adsorption and the original cations, as useful mineral components.

Experimental

Materials

The zeolites used in experiments were NaX (Union Carbide Co., Linde Div.), Na–mordenite (NaM) (Norton Co.), and natural mordenite (Hegyalja Works, Hungarian Ore and Mineral Mines, Bodrogkeresztúr) (BoM), with 30% mordenite content [4].

The nitrogen oxides were produced by classical preparation methods: NO from the reaction of HNO_3 with metallic copper; and NO_2 by the decomposition of $Pb(NO_3)_2$. N_2O was obtained commercially.

$NaNO_3$, NH_4NO_3 and chemicals for analytical work were REANAL products.

Methods

X–ray diffraction analysis with a DRON–3 diffractometer was carried out to check the crystallinity of the zeolites before and after different treatments.

The decomposition behaviour of nitrate in the zeolite structure was investigated with a MOM–Q derivatograph, usually operating at a heating rate of 10 degree/min.

Two infrared techniques were used: in a vacuum cell, the adsorption of nitrogen oxides was investigated by using self–supporting wafers appr. 10 mg cm^{-2} thick, pressed from zeolite; in other cases, the KBr pellet technique (with 1% zeolite in KBr) was used to determine the NO_3^- ion content under different experimental conditions. A SPECORD–75 IR spectrophotometer was used. The desorbed gas mixture was analysed with an MX–7301 mass spectrometer. In the quantitative determination of NO_2^- and NO_3^- ions in the washing water, classical analytical methods were used.

In the adsorption experiments, two methods were applied: the static method involved volumetric adsorption, while in the dynamic flow method a thermal conductivity detector was used for gas analysis.

Results and discussion

We initially investigated the adsorption of different nitrogen oxides (N_2O, NO, NO_2) on synthetic zeolite NaX by IR spectroscopy. These measurements were connected with our dealumination work with nitrosyl chloride [5].

Figure 1 shows infrared spectra of N_2O adsorbed under different conditions.

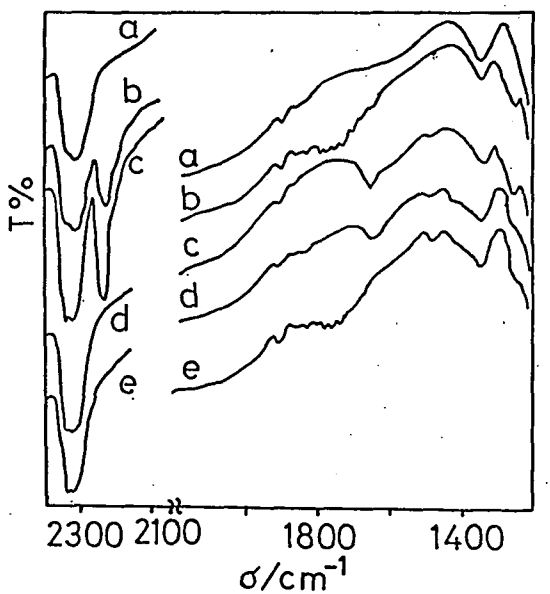

Figure 1: Infrared spectra of adsorbed N_2O

(a) pretreated NaX

(b) adsorption of 400 Pa N_2O at ambient temperature

(c) 840 min at 370 K

(d) evacuated for 30 min at 370 K

(e) evacuated for 30 min at 470 K

At room temperature, two adsorption bands were registered: at 2230 cm^{-1} and 1255 cm^{-1} (the vibration of adsorbed N_2O) [6]. After 840 minutes at 370 K, a new band appeared at 1630 cm^{-1}; this practically disappeared upon evacuation for 30 minutes at 470 K and the background spectrum of the zeolite was recorded, proving that N_2O adsorption is reversible under these conditions.

Infrared spectra of adsorbed NO are shown in Figure 2.

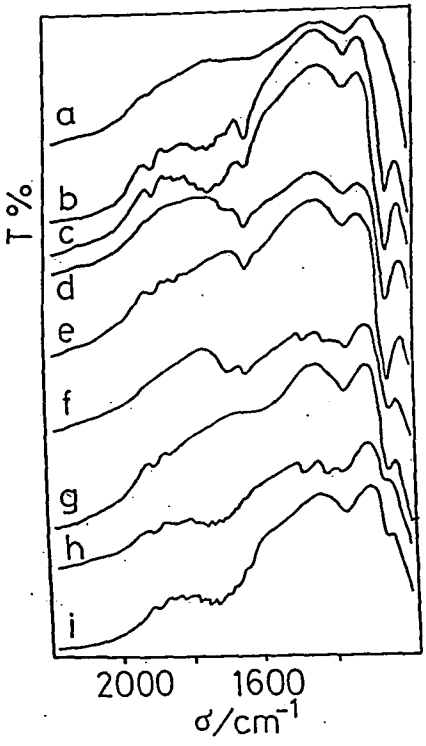

(a) pretreated NaX

(b) adsorption of 1000 Pa NO at ambient temperature

(c) 30 min at 370 K

(d) 930 min at 370 K

(e) evacuated for 30 min at 370 K

(f) 960 min at 470 K

(g) evacuated for 30 min at 470 K

(h) 150 min at 570 K

(i) evacuated for 30 min at 570 K

Figure 2: Infrared spectra of adsorbed NO

At room temperature, bands were found at 1630 cm^{-1} (due to adsorbed NO) and at 1240 cm^{-1} (due to NO_2^- ion in the zeolite structure) [7]. It can be clearly seen that with rising temperature the intensity of the band at 1240 cm^{-1} increases, and attaining a maximum decreases.

Heating resulted in two new bands, at 1470 cm^{-1} and 1410 cm^{-1}, but on evacuation for 30 minutes at 570 K the original spectrum was obtained.

Figure 3 shows spectra following the adsorption of NO_2 on NaX zeolite. At room temperature, bands appeared at 1915 and 1370 cm^{-1}, due to adsorbed NO_2 [8] and to NO_3^- ion present in the zeolite structure [9], respectively. A third band appeared in the range of framework vibration, at 810 cm^{-1}. This means that the formation of NO_3^- ion causes changes in the zeolite framework. At higher temperatures two other bands developed at 1690 and 1245 cm^{-1}, while the intensity of the 1370 cm^{-1} band decreased; however, this latter band, due to NO_3^- ion, was present even at 670 K, *i.e.* above the decomposition temperature of $NaNO_3$, proving that NO_3^- ion can be stabilized by salt occlusion in the framework.

In the next step of this work, the adsorption of nitrogen oxides in a Hungarian natural zeolite (BoM) was investigated.

The adsorption isotherms of NO and NO_2 at 423 and 573 K are shown in Figure 4. It can be seen that the adsorbed amounts are always higher in the case of NO_2 than for NO.

Table I gives the results of dynamic adsorption measured in the apparatus was described previously [10], at room temperature (298 K). The adsorbed amounts are in good agreement with literature data [2].

Figure 5 depicts infrared spectra of this zeolite, investigated with the KBr pellet technique, after desorption. It can be concluded that desorption is not complete, even at 570 K, and NO_3^- ion is formed in the zeolite structure from both NO_2 and NO. It is clear

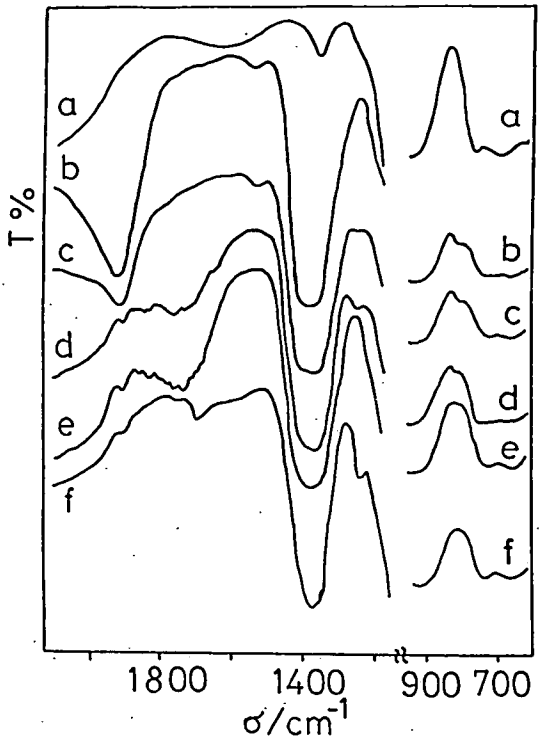

Figure 3: Infrared spectra of adsorbed NO_2

(a) pretreated NaX

(b) adsorption of 400 Pa NO_2 at ambient temperature

(c) evacuated for 30 min at ambient temperature

(d) 30 min at 570 K

(e) evacuated for 30 min at 570 K

(f) 30 min at 670 K

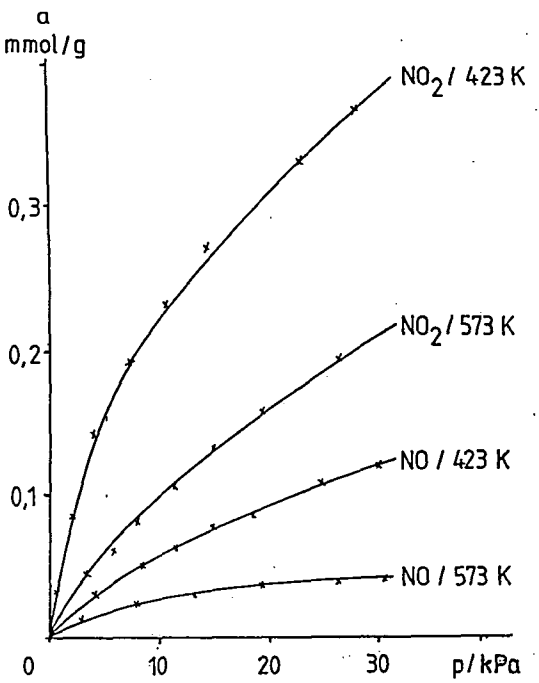

Figure 4: Adsorption isotherms of NO and NO_2 on Hungarian mordenite

that NO_2 yields a more characteristic NO_3^- ion band than NO.

Qualitative experiments were carried out to measure the composition of the desorbed gas mixture by mass spectrometry. In agreement with the infrared data, the composition of the desorbed gas indicated that reactions take place with the zeolite framework to form NO_3^- ion. The desorbed gases contain reduced molecules, for example N_2O and NO from NO_2 (see Fig. 6), and N_2 and N_2O from NO (Fig. 7).

In a further experimental series, we investigated the stabilization of NO_3^- ion in the

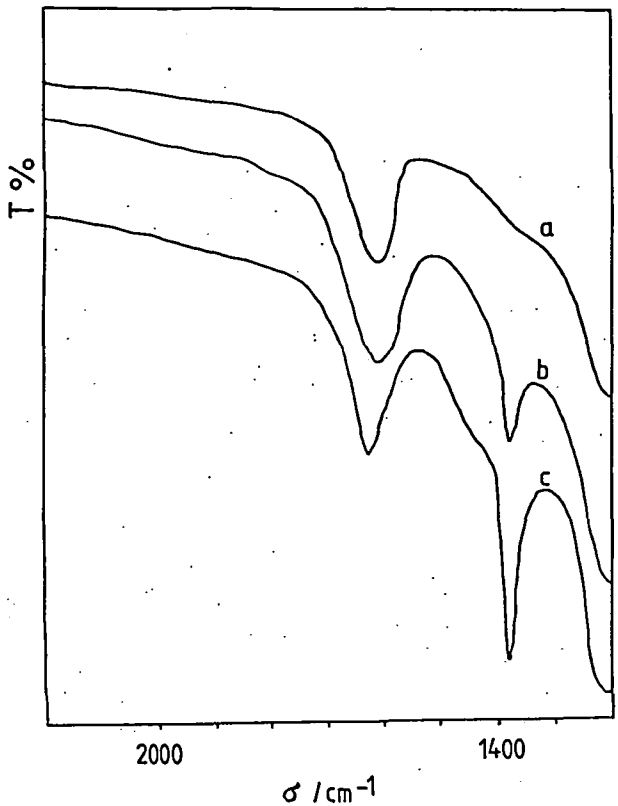

Figure 5: Infrared spectra of Hungarian natural mordenite

(a) original BoM

(b) after NO adsorption

(c) after NO_2 adsorption

mordenite structure. It is well known that inorganic ions can be formed in zeolites by the chemisorption of different gases at elevated temperatures, and guest ions or molecules can be occluded into the pore system of zeolites as well [11]. The occlusion of NO_3^- ion has been investigated in the case of A, X, and Y type synthetic zeolites, but not in the structure of synthetic mordenite and the natural zeolites.

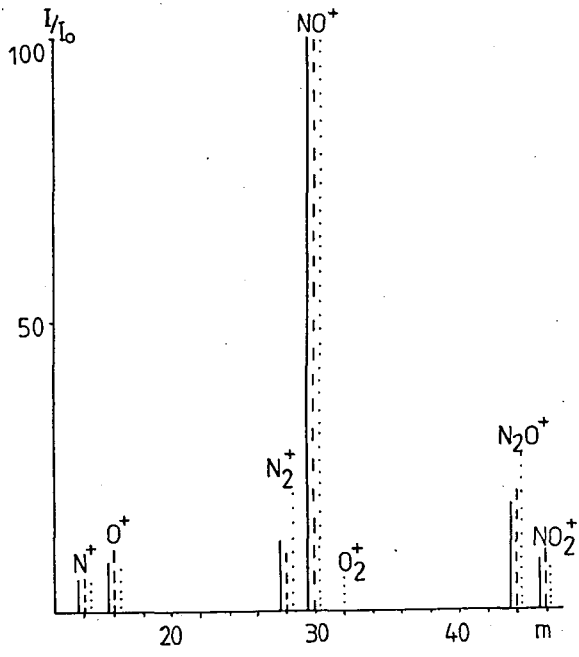

Figure 6: Mass spectra of desorbed NO_2
(—— at 373 K, – – – at 473 K, ... at 573 K)

Na–mordenite was treated with $NaNO_3$ solution and water was evaporated off to yield 5% $NaNO_3$ in Na–mordenite. Samples were treated for 5 hours at different temperatures in a furnace. The effects of heat treatment were investigated by derivatography. The adsorbed water desorbed from pure $NaNO_3$ up to 400 K and the sample melted at 580 K. Decomposition through $NaNO_2$ to Na_2O started at 870 K.

Figure 8 shows TG and DTG curves of heat–treated samples. The first step in the DTG curve relates to water loss, the second one to the decomposition of $NaNO_3$. The DTG curves reflect the decomposition in detail.

Figure 9 shows X–ray diffractograms of different samples. Reflexions of crystalline

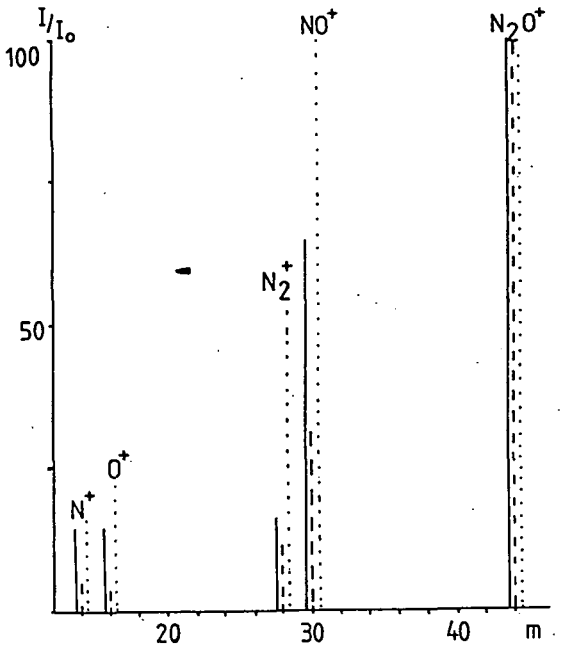

Figure 7: Mass spectra of desorbed NO
(—— at 373 K, – – – at 473 K, ... at 573 K)

$NaNO_3$ can clearly be seen in the diffractogram of the non–heated sample.

The results on the $NaNO_3$/Na–M system revealed that $NaNO_3$ was partially occluded in the pore system of mordenite. The $NaNO_3$ content of the sample obtained by heat treatement at 770 K was the same as originally added, but reflections of crystalline $NaNO_3$ were not detected in the X–ray diffractogram. The samples obtained by heat treatment at elevated temperatures had smaller $NaNO_3$ content, probably because of NO_3^- decomposition. The X–ray diffraction results indicated that the sample heat treated at 870 K had partially lost its crystallinity. It can be concluded that the optimum temperature for

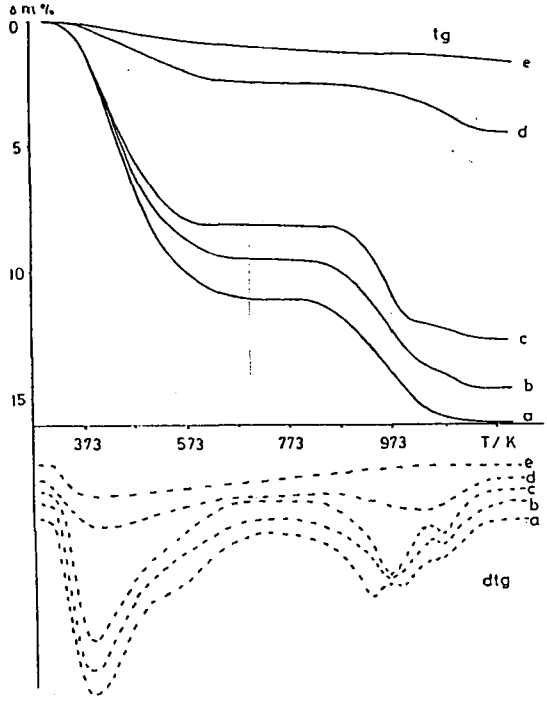

Figure 8: Derivatograms of 5 m% $NaNO_3$/Na–mordenite samples after different heat treatments
(a) at 370 K, (b) at 470 K, (c) at 570 K, (d) at 770 K
and (e) at 870 K

the stabilization of $NaNO_3$ in the mordenite structure is below 770 K.

The solubility of NO_2^- and NO_3^- ions from the zeolite framework was investigated in the case of natural mordenite. After the adsorption of NO and NO_2, 0.5 g BoM was washed with 50 cm^3 distilled water, and NO_2^- and NO_3^- contents of the solution were analysed by

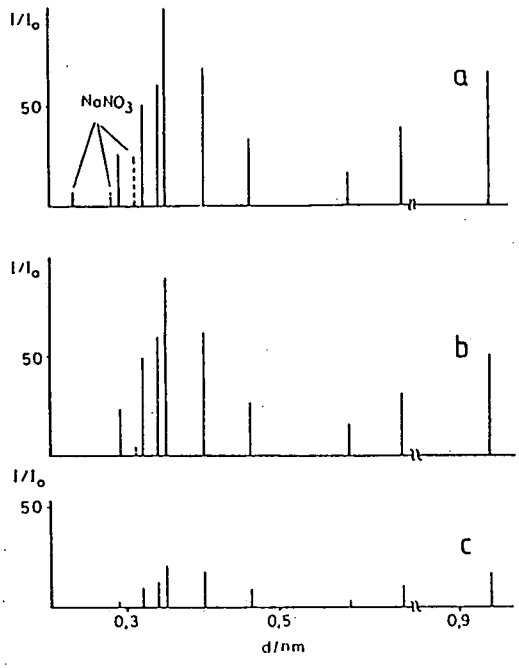

Figure 9: X–ray diffractograms of $NaNO_3$/Na–mordenite samples
(a) after evaporation of the $NaNO_3$ solution
(b) after heat treatment at 470 K
(c) after heat treatment at 870 K

classical methods. Typical results are given in Table II. From these data it can be concluded that the amounts of NO_2^- and NO_3^- ions formed following NO adsorption are of the same order of magnitude, whereas NO_2 adsorption led to a higher amount of NO_3^- ion without NO_2^- ion formation.

In the case of natural mordenite two preparation methods were used. In the first method, BoM powder and NH_4NO_3 powder were mixed to avoid the NH_4^+ ion–exchange, which was impossible in the second method, when the solvent of the NH_4NO_3 solution was

evaporated from the zeolite. The NH_4NO_3 content of the sample was the same in the two cases.

The solubility of NH_4NO_3 from the NH_4NO_3/BoM system was investigated in model experiments [12]. The soil was modelled with sand from the River Maros. The NH_4NO_3/BoM system was mixed with this sand. A glass column was filled with this mixture and distilled water was loaded on the bottom of the column. The conductivity of the outlet solution was measured. Figure 10 shows the results of a typical experiment. It is

Table I

Dynamic adsorption measurements

Reactants	Amount of adsorbent[#] (g)	Cross-section of column (cm^2)	Column volume (cm^3)	V_d:dead volume (cm^3)	w:flow rate (cm^3/min)	c^o:NO_x concn. (vol%)	$\bar{t}$:retention time (min)	Adsorbed* amount (mg/g)
BoM+NO	22 (A)	1.76	22	11	22.5	11	8	1.04
BoM+NO	22 (A)	1.76	22	11	12.5	20	10	1.26
BoM+NO	22 (A)	1.76	22	11	31.6	5	4	0.32
BoM+NO_2	12 (B)	0.50	12.4	6.4	25.3	21	58	47.67
BoM+NO_2	12 (B)	0.50	12.4	6.4	82.0	2.4	65	20.03
NH_4BoM+NO_2	12 (B)	0.50	12.4	6.4	20.5	17	84	45.71
NH_4BoM+NO_2	9.2(B)	0.50	9.5	4.9	40.5	1.2	40	3.97
NH_4BoM+NO_2	9.2(B)	0.50	9.5	4.9	92.6	7.2	30	43.09
BoM+NO_2	12 (A)	0.50	12	6.0	41.0	2.4	130	20.03
BoM+NO_2	10.5(C)	0.50	11.5	6.25	42.6	6.1	180	83.07

[#]Size fraction of adsorbent: A: 0.63–1.1 mm, B: 0.515–0.63 mm, C: 0.125–0.315 mm

*The equation $a = c^o(\bar{t}w - V_d)$ was used to calculate sorbed amounts

Table II

Removable anion content of saturated adsorbent

Reactant	Temperature of adsorption (K)	Washed–out anions (μmol/g zeolite)	
		nitrate	nitrite
NO	423	64	30
	573	38	18
NO_2	423	325	–
	573	272	–

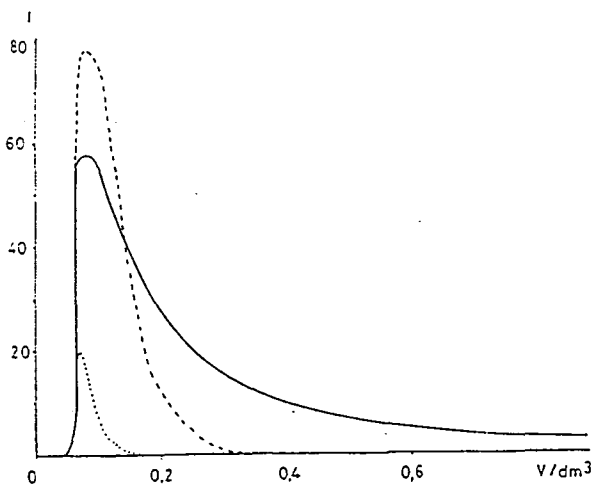

Figure 10: Conductivity of outlet solution vs. volume of solution

(... sand, – – – NH_4NO_3/sand, —— NH_4NO_3/BoM/sand)

clear from the curves that the dissolution of NH_4NO_3 requires more water and a longer time for the NH_4NO_3/BoM/sand system than for the NH_4NO_3/sand system.

Conclusions

–The adsorption of NO and NO_2 resulted in NO_3^- ion formation in the zeolite structure.

–NO_3^- ion was stabilized by salt occlusion in the mordenite framework.

–Natural zeolites can be regarded as possible fertilizer additives due to retardation of the dissolution of nitrates, especially in sandy soil.

References

[1] *Breck, D.W.:* Zeolite Molecular Sieves, J. Wiley Interscience Publ., New York, 1974.

[2] *Klopp, G., J.Sütő, I.Szebényi:* Magyar Kém. Lap., 34, 512 (1979).

[3] Occurence, Properties and Utilization of Natural Zeolites (Eds.: Kalló, D., Mumpton, F.), Akadémiai Kiadó, Budapest, 1988.

[4] *Hannus, I., I.Kiricsi, I.Dékány, P.Fejes:* Acta Phys. et Chem. Szeged, 30, 107 (1984).

[5] *Fejes, P., Gy.Schöbel, I.Kiricsi, I.Hannus:* Acta Phys. et Chem. Szeged, 31, 119 (1985).

[6] *Rabo, J.A.,:* Zeolite Chemistry and Catalysis, American Chemical Society, Washington, D.C., 1976, p.206.

[7] ibid: p.202

[8] *Wada, Y., K.Otsuka, A.Morikawa:* J. Catal., 81, 291 (1983).

[9] *Rabo, J.A.,:* Zeolite Chemistry and Catalysis, American Chemical Society,

Washington, D.C., 1976, p.338.

[10] *Hannus, I., A.Ádász-Szűcs, I.Firicsi, Gy.Tasi, P.Berger, J.Halász, P.Fejes:* Acta Phys. et Chem. Szeged, 35, 19 (1989).

[11] *Rabo, J.A.,:* Zeolite Chemistry and Catalysis, American Chemical Society, Washington, D.C., 1976, Chapter 5.

[12] *Hannus, I., Gy.Tasi, I.Firicsi, P.Fejes:* Hazai természetes zeolitok kutatása és felhasználása II. (Szerk: Hlavay, J., Pataki, K.), MTA VEAB, Veszprém, 1987, p.187.

АДЦОРБЦИЯ ОКСИДОВ АЗОТА В ЦЕОЛИТАХ

И.ГАННУШ, Я. ГАЛАС, У. КИРИЧИ, ДЬ. ШЕБЕЛ, ДЬ. ТАШИ и П. ФЕЕШ

Исследованы адсорбционные свойства различных синтетических и венгерских естественных цеолитов к NO и NO_2. Измерения были проведены с помощью рентгеновской диффракции, дериватографии, инфракрасной спектроскопии, масс-спектрометрии и классических аналитических методов. В процессе адсорбции оксидов азота в цеолитных структурах было найдено образование NO_3^- нонов. Изучена растворимость NO_3^- нонов из системы NO_3^-/естественный цеолит в связи с возможностью их применения в качестве компонента удобрений.

TREATMENT OF NATURAL GAS WITH ZEOLITES

I. HANNUS, A. ÁDÁSZ–SZŰCS[1], I. KIRICSI, GY. TASI, F. BERGER, J. HALÁSZ and P. FEJES

Institute of Applied Chemistry, Attila József University,

Rerrich Béla tér 1., H–6720 Szeged, Hungary

[1]Great Plain Oil and Natural Gas Company, Szeged, Hungary

(Received November 6, 1989)

NATURAL GAS CLEANING INVOLVING THE REMOVAL OF H_2O AND H_2S IMPURITIES AND MINIMIZATION OF THE CO_2 CONTENT, IS VERY IMPORTANT FROM BOTH ENVIRONMENTAL AND ECONOMIC ASPECTS. LITERATURE DATA INDICATE THAT ZEOLITES WOULD BE EFFECTIVE IN THE SOLUTION OF THIS PROBLEM. OUR LABORATORY AND EXPERIMENTAL RESULTS SUPPORT THIS PERCEPTION. DIFFERENT NATURAL AND SYNTHETIC ZEOLITES WERE COMPARED IN THE ADSORPTION PROCESS BY MEANS OF X–RAY, INFRARED, DERIVATOGRAPHIC AND GAS CHROMATOGRAPHIC TECHNIQUES.

Introduction

Zeolites, as excellent selective adsorbents compared with silica gel and activated carbon (see Figure 1), are useful for many phases of natural gas treatment [1].

Drying was the most obvious initial application for zeolites in the natural gas industry. With the classical method (glycol injection) it was possible to attain a dew point of 233 K (–40 °C), but with zeolites dew point of lower than 203 K (–70 °C) can be achieved easily and economically. The first installations were made in the late fifties and the early sixties in the United States [2–4].

Gas sweetening is the other important field of natural gas treatment in general, including Hungarian natural gas sources [5]. Among the different acidic components, mercaptans are the most strongly adsorbed sulphur compounds, followed by H_2S, and CO_2 is the most weakly adsorbed component in this series.

If the purpose is to remove only H_2O and CO_2 impurities, the task can be solved relatively easily (see Figure 2) [6].

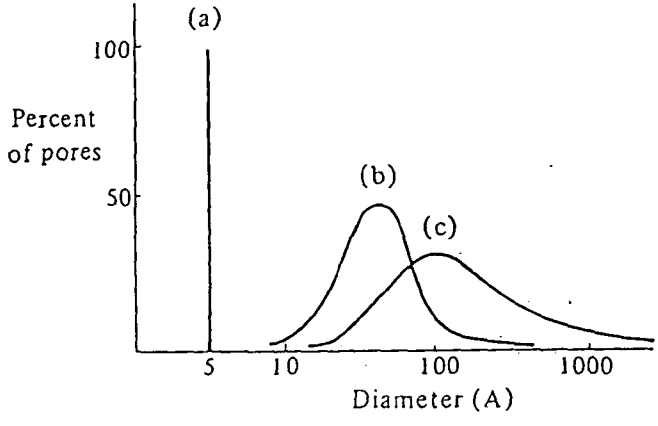

Figure 1: Distribution of pore sizes in microporous adsorbent (a) Dehydrated zeolite, *e.g.* type A, (b) typical silica gel, (c) activated carbon (from *ref.* [1]).

Various natural gases contain H_2S in different amounts; in some cases its content can reach 25% [7]. It is possible to dry such strongly acidic natural gases with zeolites and to remove the sulphur content with large–pore X–type zeolites [8].

It is a complex problem to remove the H_2O and H_2S impurities from a CO_2–rich natural gas and also to reduce the CO_2 content. An effective solution can be found in the literature: a mixed adsorption and absorption method [3]. In some cases, also the deep–cooling absorption process can be useful [9].

In this work we report laboratory results obtained with a natural gas of Hungarian origin, where the aims were to remove H_2O and H_2S impurities and to minimize the CO_2 using Hungarian natural zeolites and different Hungarian–made synthetic zeolites.

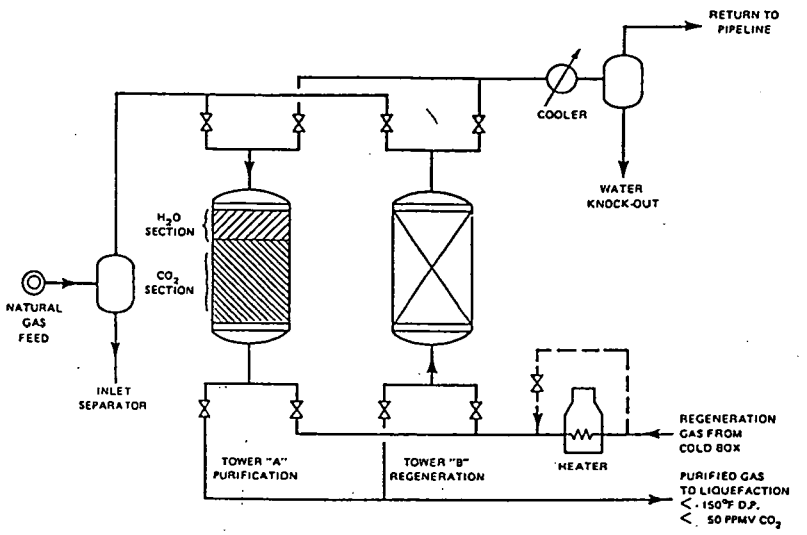

Figure 2: Zeolite adsorption system for combined natural gas dehydration and CO_2 removal (from *ref.* [6])

Experimental

Materials

The natural zeolites used in the experiments were from the Hegyalja Works of Hungarian Ore and Mineral Mines. Samples M_{30}, M_{70} and M_{80} contained 30, 70 and 80% mordenite, respectively. Zeolite ERSORB–4 was a product of Erdőkémia (Forest Chemistry) Co. and contained clinoptilolite.

Among the synthetic zeolites, we used Na–mordenite (Norton Co.), Linde 4A, 5A and 13X (Union Carbide Corporation), NaA zeolite (Merck) and Hungarian–made NaA. (Figure 3 illustrates the pore sizes of the different zeolites, as compared with the kinetic diameters of simple molecules.)

The natural gas used in the adsorption experiments was from the Algyő

gas–field, near Szeged, in South Hungary.

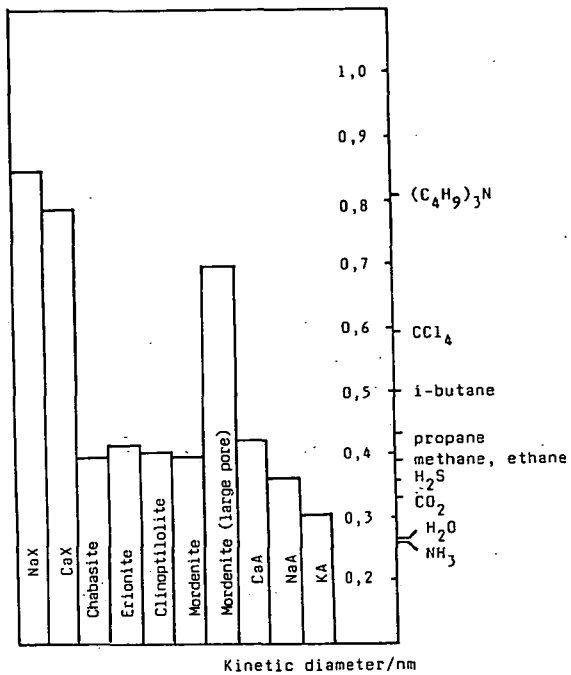

Figure 9: Pore sizes of different zeolites compared with kinetic diameters of simple molecules

Methods

The zeolite contents of the natural zeolites were determined by X–ray diffraction analysis at ambient temperature with a DRON–3 diffractometer.

The water contents of the samples were determined with a MOM–Q derivatograph, in ceramic crucibles, at a heating rate of 10 degree/min.

For the KBr pellet infrared technique, a SPECORD–75 IR spectrophotometer

was utilized. In each case, the spectra of wafers of 1 wt% zeolite in KBr were recorded vs. a standard KBr pellet.

In the adsorption experiments different methods were applied. The adsorption of CO_2 and CH_4 was investigated with a static method in volumetric adsorption equipment. The equipment and details of method were reported earlier [10].

In most of the adsorption investigations, a dynamic flow method was used, where either a thermal conductivity detector was applied for gas analysis or the volume of gas at the exit was measured directly [11]. In the industrial adsorption process, gaschromatographic analysis was used (CHROM–4 GC with a thermal conductivity detector).

Results and discussion

Laboratory investigations

Water adsorption

The water adsorption capacities of the samples were determined by derivatography. The pretreatment conditions were the same in every case, in order to obtain comparable results: equilibration in water vapour over saturated NH_4Cl solution for 2 days [12]. The weight losses of the different zeolites up to 1073 K are listed in Table I.

Figure 4 shows typical "water loss" curves for an "A"–type zeolite. From the data in Table I, it is clear that synthetic zeolites have much larger adsorption capacities than their natural counterparts. In the case of natural zeolites, the amount of water adsorbed correlates well with the amount of the zeolitic phase in the minerals.

H_2S adsorption

H_2S adsorption was studied with the dynamic method. Figure 5 shows the

Table I

Weight losses of different zeolites up to 1073 K, measured by thermogravimetry

Zeolite	mg H_2O/g dry zeolite
Linde NaX	272
Linde 5A	238
Linde 4A	228
Merck NaA	197
Hung. NaA	163
Na–mordenite	150
M_{80}	117
M_{70}	111
M_{30}	63
ERSORB–4	89

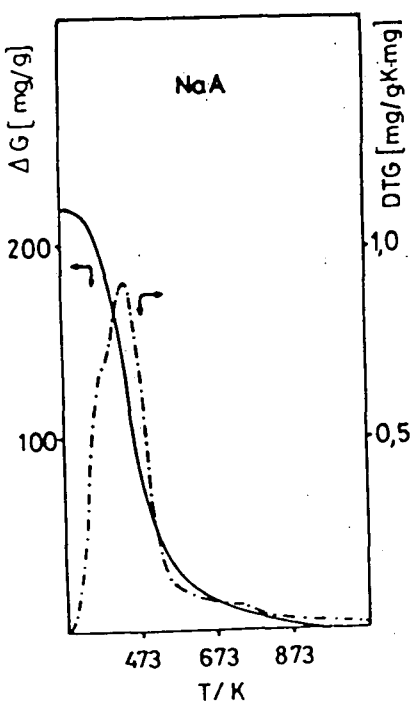

Figure 4: Water loss curves of zeolite NaA

TG curve ————

DTG curve — · — · —

experimental apparatus. Hydrogen was used as the carrier gas and H_2S was taken from a Kipp apparatus. The adsorbent was activated at 673 K in a system of flowing H_2 and the adsorption was carried out at room temperature. A thermal conductivity detector was used for gas analysis. Through measurement of the weight of the adsorbent column before and after the adsorption the adsorption capacity could be checked gravimetrically, too.

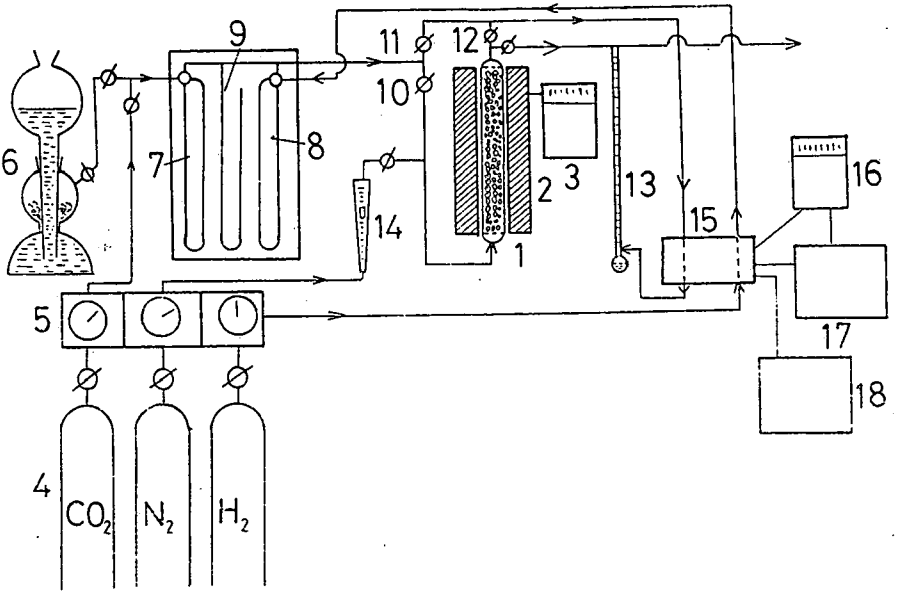

Figure 5: Dynamic adsorption apparatus with thermal conductivity detector (1) adsorber; (2) heater; (3) regulator; (4) gas tanks; (5) pressure gauge; (6) Kipp apparatus; (7,8,9) manometers; (10,11,12) valves; (13) soap film meter; (14) flow meter; (15) thermal conductivity detector; (16) regulator; (17) battery; (18) recorder.

For example, in the case of natural mordenite M_{70}, we measured (by weight) the

adsorption capacity of 60 mg H_2S/g dry zeolite for a gas stream containing 10% H_2S and obtained the same value by the dynamic method.

The adsorption of H_2S from natural gas containing 100 ppm H_2S was investigated. Figure 6 shows the adsorption curve and the increase in the adsorbent temperature measured in the middle of the adsorption column. The relatively high temperature increase illustrates that H_2S adsorbs more strongly than CO_2.

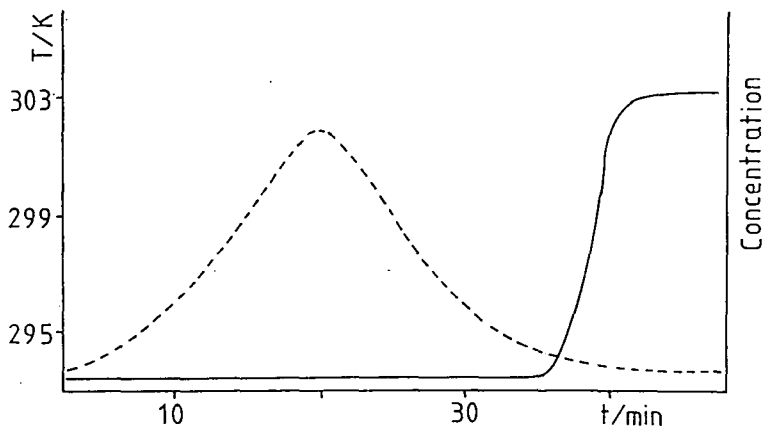

Figure 6: Breakthrough curve of natural gas with H_2S and CO_2 content over zeolite 4A (———), temperature in middle of column (– – –)

CO_2 adsorption

1. With a static method

Figure 7 shows the adsorption isotherms of CO_2 and CH_4 on NaA (Merck) and Hungarian NaA. CH_4 is practically not adsorbed, due to the apolarity of the hydrocarbon molecule.

Adsorption isotherms measured at different temperatures can be described by the well–known Langmuir equation. The experimental and theoretical results are similar.

The adsorption capacity of the Hungarian–made NaA proved to be 40% lower than that of the Merck NaA.

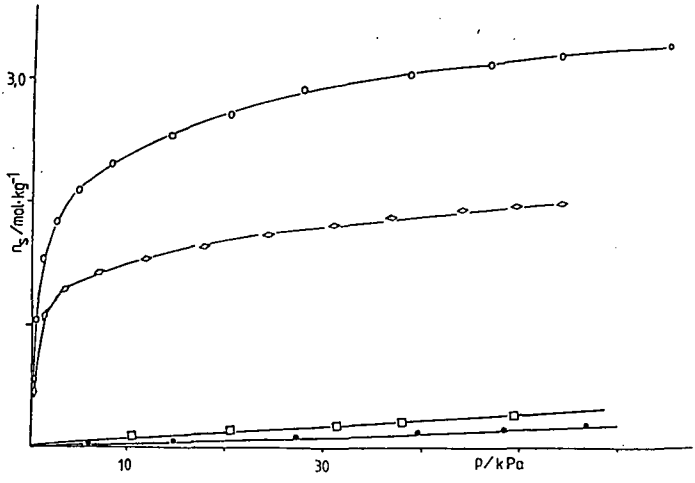

Figure 7: Adsorption isotherms of CO_2 and CH_4 at 298 K
CO_2 over Merck NaA (o); CO_2 over Hungarian NaA (⋄);
CH_4 over Merck NaA (□); CH_4 over Hungarian NaA (•)

2. With a dynamic method using a thermal conductivity detector

a. CO_2 adsorption from a H_2 stream

In these experiments, the CO_2 content was adjusted to 10%, which was similar to that in natural gas. During the adsorption, the temperature was measured in the adsorption column. The maximum increase in temperature due to the adsorption of CO_2 was about 6 degrees, showing a relatively weak adsorption of CO_2. Under similar conditions, H_2S adsorption caused a rise in temperature of about 8–10 degrees (see Figure 6).

The amount of CO_2 adsorbed (A) was calculated from the material balance equation [11]:

$$A = c_0(tw - V_h)$$

where c_0 = concentration of CO_2, t = time of breakthrough, w = flow rate, V_h = dead volume.

The specific adsorption capacity (a) was calculated from A. The experimental results are given in Table II. The calculated specific adsorption capacity and the gravimetrically measured data are in good agreement. The highest adsorption capacity was measured for synthetic zeolite 5A.

Table II

CO_2 adsorption from a H_2 stream

Zeolite	Loading (g)	V flow rate (cm^3/min)	$c^0_{CO_2}$ (%)	t/breakthrough time (min)	a/spec.ads. amount from t (mg/g)	gravi.
M_{30}	4.75	33.2	9.64	30	35.8	42.1
M_{70}	4.35	33.1	9.67	32	45.9	57.5
M_{80}	4.78	33.6	10.9	30	41.0	46.1
ER–SORB–4	4.9	33.4	10.9	31	50.6	47.1
LINDE 4A	4.7	32.1	10.9	66	84.1	85.0
LINDE 5A	4.9	32.9	8.8	80	104.1	107.1
HUNG. NaA	4.9	31.1	9.9	61	67.3	62.0

b. CO_2 adsorption from natural gas

In these experiments we used natural zeolite M_{70} (exhibiting the greatest adsorption capacity) and synthetic zeolites 4A and 5A. Table III shows the results. For

zeolites M_{70} and 4A, the specific adsorbed amounts were similar to those obtained from H_2 stream in the previous experiment, but for zeolite 5A the adsorption was found to be higher. In agreement with literature data, the reason is that the hydrocarbons of natural gas can adsorb in the larger pores of 5A (see Figure 3).

The breakthrough curve in Figure 8 supports this explanation, because a multistep curve was obtained over 5A instead of the smooth curves observed over natural zeolites and synthetic 4A.

9. CO_2 adsorption by measuring the gas volume leaving the column

The theoretical and experimental aspects of this technique were described by Fejes [11]. The schematic outline of the apparatus is shown in Figure 9.

The advantages of the soap film volume meter are as follows:

- the apparatus is simpler than that with a thermal conductivity detector (TCD)
- it is not necessary to determine the dead volume of the column in a separate experiment,

Table III

CO_2 adsorption from natural gas

Zeolite	Loading (g)	V flow rate (cm^3/min)	t/breakthrough time (min)	a/specific ads. amount (mg/g)	regeneration
M_{70}	5.1	31.6	–	49	673 K in H_2
M_{70}	5.1	32.0	38	49	673 K in H_2
5A	4.0	32.0	90	150	673 K in H_2
5A	4.0	31.6	92	150	673 K nat. gas
4A	4.1	31.6	44	85	673 K nat. gas
4A	2.05	30.0	45	82	473 K nat. gas

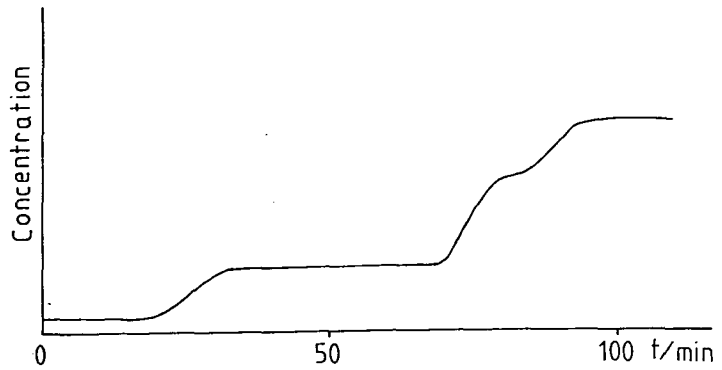

Figure 8: Breakthrough curve of CO_2 from natural gas over zeolite 5A

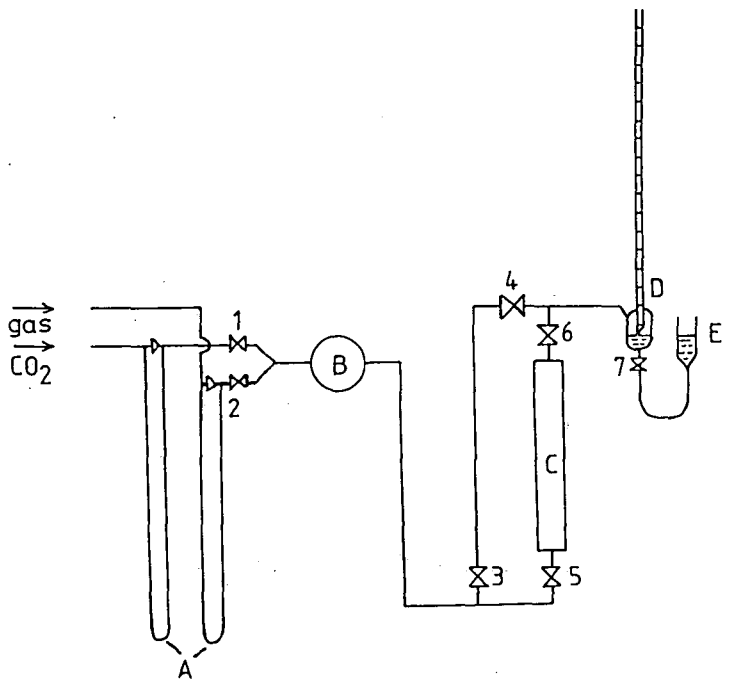

Figure 9: Dynamic adsorption apparatus with soap film meter

A: differential manometers; B: gas mixing vessel; C: adsorption column; D: soap film meter; E: liquid level regulator; 1–7: valves

– the experimental error is less than that in the case of TCD.

Measurement of the flow at the outlet in time, W(t), gave the characteristic curve shown in Figure 10.

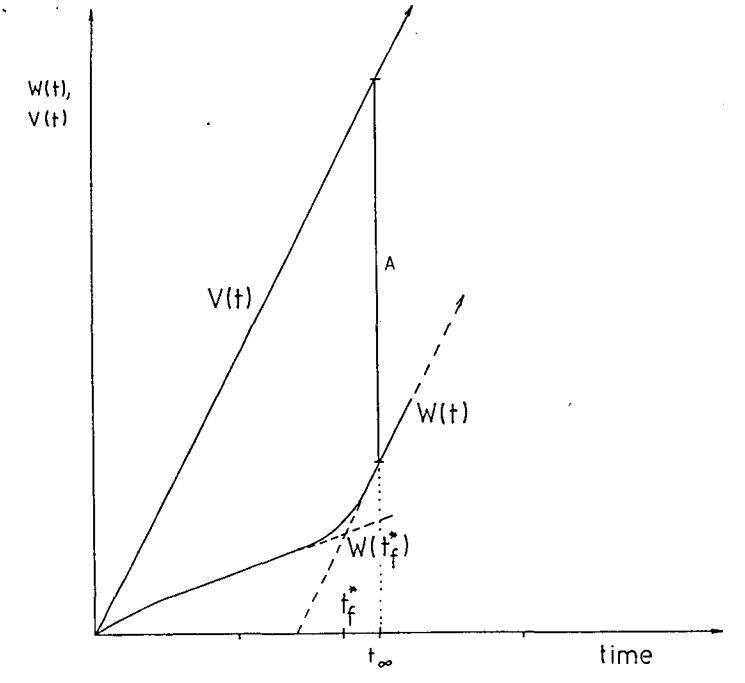

Figure 10: Determination of adsorption amount from dynamic measurements

V(t) is the flow at the inlet which is assumed to depend linearly on time. The difference between V(t) and W(t) at an appropriately chosen time, t, gives the equilibrium sorbed amount (A) [11]:

$$A = Lma_0 = V(t) - W(t)$$

where L = length of column,

m = mass of adsorbent per unit length,

a_0 = adsorbed amount per unit mass relating to inlet concentration, x_0.

This technique proved to be suitable due to its surprisingly good reproducibility (Figure 11).

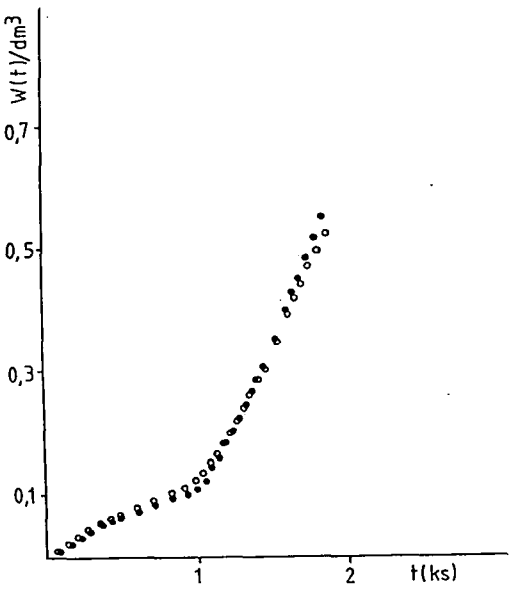

Figure 11: Reproducibility of measurements

Table IV shows the characteristic data on the columns used.

In the first series of experiments, the adsorption of pure CO_2 was measured at different flow rates with column 1. The conclusion to be drawn from the results is plausible: the smaller the flow rate, the greater the effective adsorption. The equilibrium adsorbed amounts, of course, are independent of the flow rate at t.

Figure 12 shows the results obtained with natural gas–CO_2 mixtures at different flow rates with column 2.

With adsorption column 3, the best result was observed at the smallest flow rate (2.41 mmol/g). This value is lower than that measured with the static method (3.33 mmol/g).

Table IV

Characterization of columns

No.	Length (cm)	Inner diameter (cm)	Volume (cm^3)	Loading (g)	Mass per unit length (g/cm)
1	16	0.9	10.1	7.5	0.5
2	20	2.2	75.9	47.0	2.35
3	18	1.5	31.8	24.5	1.36
4	29	1.5	51.2	36.0	1.24

Figure 13 shows the adsorption curves for adsorption column 4 filled with Hungarian–made NaA (a) and Merck NaA (b). The adsorption capacity of Merck NaA exceeds that of Hungarian–made NaA by a factor of 2. The results are given in Table V.

Table V

Results obtained from CO_2 adsorption by measuring gas volume leaving column

No.	Diameter of column (cm)	Mass of adsorbent (g)	Mass per unit length (g)	Inlet flow rate (cm^3/min)	CO_2 conc. x_0	Ads. CO_2 (cm^3)	Breakthrough time (min)
1	0.9	7.7	0.48	13.5	1.0	389	28.5
2	2.2	47.0	2.35	86.0	1.0	1040	21.3
3	2.2	47.4	2.37	50.0	0.9	380	13.3
4	2.2	47.2	2.36	35.7	0.86	1160	75.0
5	1.5	24.4	1.36	60.0	0.75	200	8.7
6	1.5	24.4	1.36	27.9	0.47	1320	75.0
7	1.5	35.5	1.22	60.0	0.75	1200	52.0
8	1.5	35.5	1.22	60.0	0.8	1480	52.0

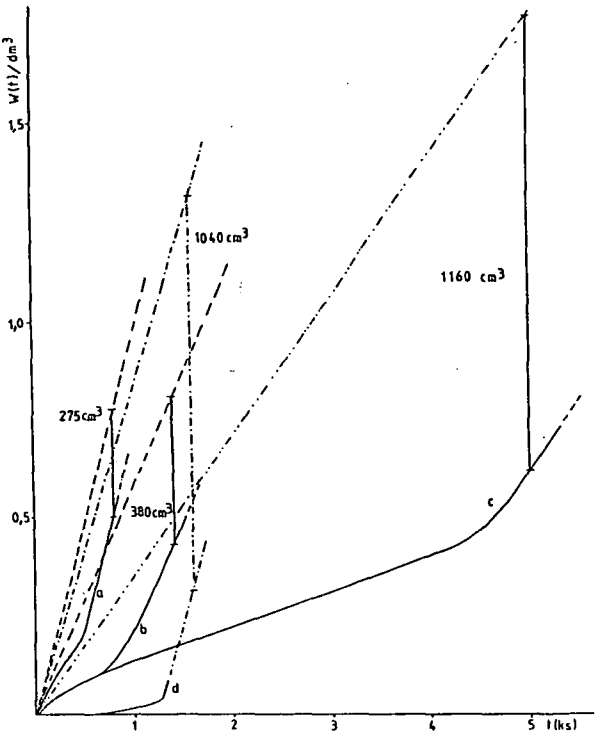

Figure 12: Breakthrough curves of CO_2 from gas mixture in column 2

a: $dV/dt = 88\ cm^3/min$; $x\%_{CO_2} = 0.77\ cm^3/cm^3$

b: $dV/dt = 50\ cm^3/min$; $x\%_{CO_2} = 0.90\ cm^3/cm^3$

c: $dV/dt = 36\ cm^3/min$; $x\%_{CO_2} = 0.86\ cm^3/cm^3$

d: $dV/dt = 86\ cm^3/min$; $x\%_{CO_2} = 1.00\ cm^3/cm^3$

The reversibility of CO_2 adsorption

Samples of Merck and Hungarian zeolites were saturated with CO_2 previously and the CO_2 was desorbed overnight at room temperature and atmospheric pressure. Infrared investigations were carried out with the KBr pressed pellet technique to check the formation of CO_3^{2-} in the zeolite channels. For the Hungarian–made NaA, a

characteristic CO_3^{2-} peak could be observed in the spectrum at 1380 cm^{-1} (see Figure 14).

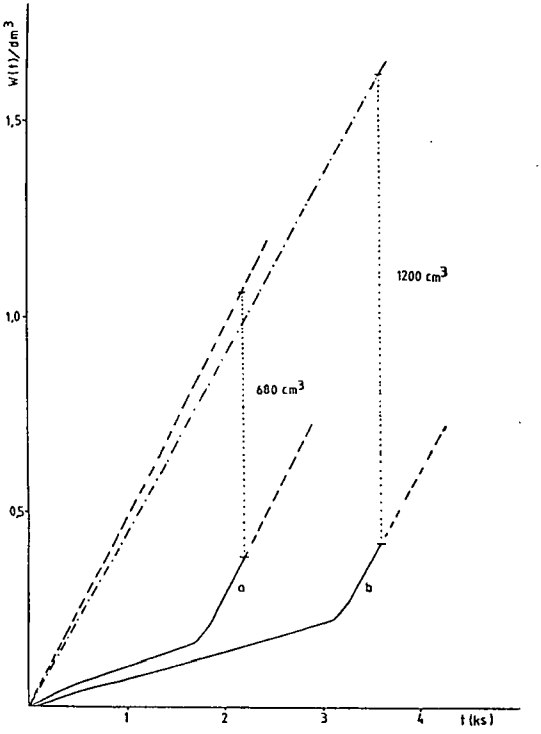

Figure 13: Breakthrough curves of CO_2 over Hung. NaA (a) and Merck NaA (b) zeolites in column 4 (dV/dt = 60 cm^3/min; $x_{CO_2}^{\&}$ = 0.75 cm^3/cm^3).

This means that CO_2 adsorption is not reversible for the Hungarian–made NaA in contrast with the Merck NaA. When the two samples were suspended in distilled water (0.5 g, in 50 cm^3 water, with stirring for 2 hours), the pH of the aqueous phase was almost the same in the two cases.

It is presumed that CO_3^{2-} formation is due to the presence of Al_2O_3–hydrogel from incomplete NaA zeolite crystallization.

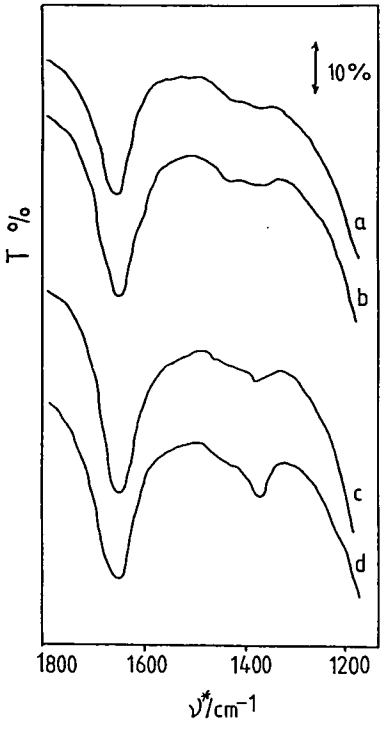

Figure 14: Infrared spectra
a: Original Merck NaA;
b: after CO_2 adsorption;
c: original Hung. NaA;
d: after CO_2 adsorption.

4. CO_2 adsorption under semiadiabatic conditions

In a real industrial separation, the adsorption is an adiabatic process because of the large dimensions of the column. The heat of adsorption causes a temperature increase in the adsorbent. This is of some advantage from the aspect of the transport, but this beneficial effect is counterbalanced by a large decrease in adsorption capacity. The investigation of adsorption under adiabatic conditions is very important from an industrial point of view.

Figure 15 shows a high–pressure column used in semiadiabatic measurements. The temperature of the adsorbent was measured at the beginning and the end of the

column with thermocouples. The breakthrough of the adsorptive was detected with a soap film flow meter. Three types of zeolites (H–NaA, M–NaA and L–NaX) and pure CO_2 were used in these experiments. Typical temperature curves are shown in Figure 16 for CO_2 adsorption at atmospheric pressure. Activation of the zeolites was carried out at 673 K. The adsorbed amounts are markedly lower than the equilibrium values due to the liberation of adsorption heat.

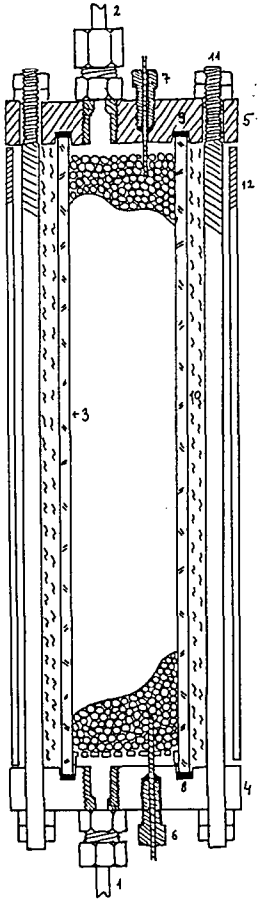

Figure 15: High–pressure adsorption column for semiadiabatic measurements
(1) inlet; (2) outlet;
(3) glass tube;
(4,5) covering plates;
(6,7) thermocouples;
(8,9) teflon rings;
(10) heat insulation;
(11) holding bars;
(12) protecting tube

When regeneration was carried out in vacuo during 2 hours without heating, the adsorption capacity led to losses of 27, 23 and 11%, respectively, for zeolites H–NaA, M–NaA and L–NaX, as compared with samples regenerated at 673 K (see Table VI). On increase of the CO_2 pressure from 1 bar to 2.5 and 5 bars, the adsorbed amounts increased, too.

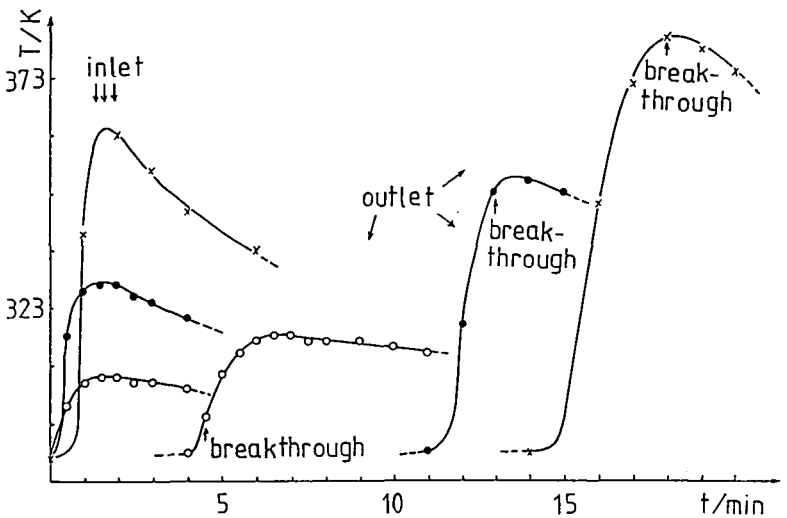

Figure 16: Semiadiabatic CO_2 adsorption; zeolites were actived at 673 K; p = 1 bar, W_{CO_2} = 0.5 dm³/min.

zeolite:	adsorbed CO_2:
Hung. NaA	0.59 mmol/g
Merck NaA	1.82 mmol/g
Linde NaX	2.78 mmol/g

Finally, the time of the desorption was decreased to 0.1 hour and the pressure to 0.1 bar. These conditions are similar to those in the industrial process when a pressure swing cycle is applied. The last row of Table VI shows the amount of CO_2 adsorbed.

The conclusion is that NaA is suitable for cleaning natural gases rich in CO_2, nevertheless, faujasites (NaX, NaY) are superior, because of their greater capacity and easy regeneration.

Table VI

Semiabiabatic CO_2 adsorption on three different zeolites under different pretreatment and adsorption conditions

Zeolite	Pretreatment	Pressure/bar	CO_2 mmol/g zeolite
H–NaA	at 673 K		0.59
M–NaA	in vacuo	1.0	1.82
L–NaX	2 hours		2.78
H–NaA	at room temp.		0.42
M–NaA	in vacuo	1.0	1.39
L–NaX	2 hours		2.47
H–NaA	at room temp.		0.59
M–NaA	in vacuo	2.5	1.44
L–NaX	2 hours		2.98
H–NaA	at room temp.		0.65
M–NaA	in vacuo	5.0	1.48
L–NaX	2 hours		3.42
H–NaA	at room temp.		–
M–NaA	0.1 bar	5.0	0.61
L–NaX	0.1 hours		1.74

Industrial investigations

The experimental set–up is shown in Figure 17.

The adsorber was filled with zeolite 4A. Gas samples at the inlet and outlet were analysed with a CHROM–4 gaschromatograph. In a typical experiment, the adsorbent filling was 1.7 kg, the pressure at the inlet was 50 bar and the flow rate of

the outlet, purified gas was 700 dm^3/hr at atmospheric pressure. The analytical data are shown in Table VII. Figure 18 depicts the breakthrough curve for CO_2.

If the requirement is to attain 0.5% CO_2 in the outlet gas, the breakthrough time is about 1.25 hr; this means in other words that about 0.5 m^3 gas can be purified per kg adsorbent per cycle. Under these conditions the adsorption capacity for CO_2 is 0.16 kg/kg zeolite. In the laboratory experiment, 0.13 kg CO_2/kg zeolite was measured at 1 bar.

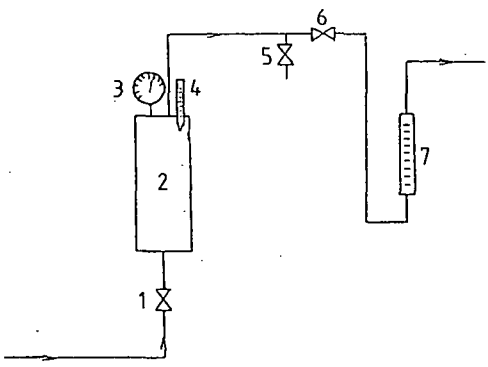

Figure 17: Industrial adsorption apparatus
(1,6) regulating valves; (2) adsorber; (3) pressure gauge; (4) thermometer; (5) blow–off valve; (7) flow meter

Conclusions

On the basis of literature data and the present results, it was shown that CO_2 can be removed from CO_2–rich natural gases effectively and economically by using adsorption techniques with zeolites as adsorbents.

Moreover, zeolites are the only adsorbents which are effective enough to solve this problem.

When zeolites NaA and NaX are compared for this task, NaX clearly surpasses NaA because of its greater adsorption capacity and easy regenerability.

Table VII

Typical analysis set from an industrial adsorption

Component	Time/hr										
	0.0	0.25	0.6	1.6	2.3	2.85	3.3	3.85	4.3	4.85	5.3
C_1	81.96	93.94	93.62	89.43	84.58	83.59	83.03	82.81	82.64	83.04	82.42
C_2	4.12	2.92	3.54	4.34	4.16	4.14	4.40	4.31	4.26	4.01	3.95
C_3	1.56	1.98	1.72	1.67	1.56	1.57	1.60	1.55	1.58	1.55	1.71
C_4	0.44	0.86	0.74	0.67	0.61	0.66	0.58	0.53	0.53	0.66	0.67
C_5	0.36	0.64	0.34	0.22	0.32	0.37	0.28	0.24	0.23	0.15	0.29
H_2O+H_2S	1.32	–	–	–	0.18	0.17	0.10	0.49	0.35	0.40	0.38
CO_2	10.31	–	–	3.64	8.58	9.50	10.01	10.14	10.41	10.19	10.58

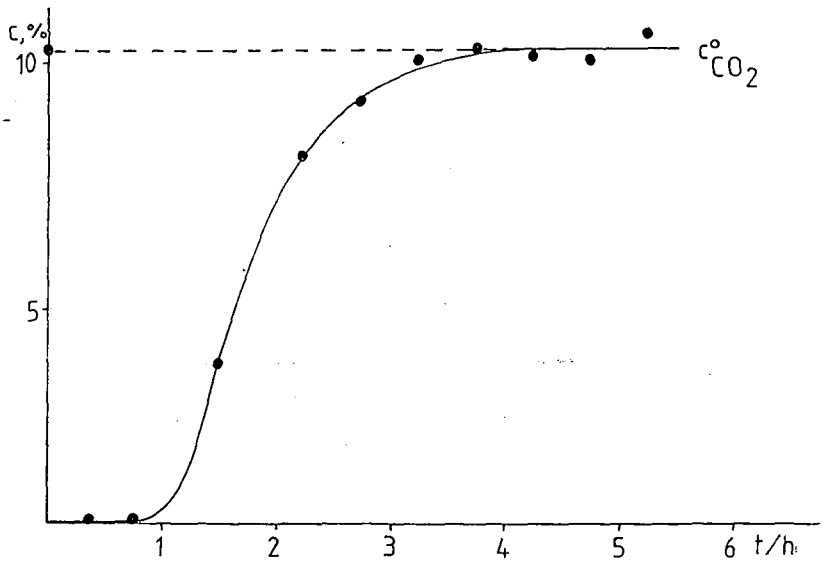

Figure 18: Breakthrough curve of CO_2 in an industrial experiment

References

[1] *Breck, D. W.*: Zeolite Molecular Sieves, J. Wiley, Interscience Publication, 1974.

[2] *Clark, E. L.*: Oil and Gas J., 57, 120 (1959).

[3] *Thomas, T. L., E. L. Clark*: Oil and Gas J., 65, 112 (1967).

[4] *Collins J. J.*: Chem. Eng. Prog., 66, 66 (1968).

[5] *Csákó D., L. Pető, P. Valastyán*: Kőolaj és Földgáz, 18, 353 (1985).

[6] *Anderson, A.*: ACS Symp. Ser., 40., 637 (1977).

[7] *Kraychy, P. N., A. Masuda*: Oil and Gas J., 64, 66 (1966).

[8] *Karge, H. G., J. Raskó*: J. Colloid Interface Sci., 64, 522 (1978).

[9] *Kulijev, A. M., P. D. Sihalizade, P. Valastyán*: Kőolaj és Földgáz, 14, 321 (1981).

[10] *Kiricsi, I., Gy. Tasi, H. Förster, P. Fejes*: Acta Phys. et Chem. Szeged, 33, 69 (1987).

[11] *Fejes, P.*: Dissertation, 1964.

[12] *Hannus, I., I. Kiricsi, P. Fejes*: Magy. Kém. Lapja, 39, 430 (1984).

ОБРАБОТКА ЕСТЕСТВЕННОГО ГАЗА ЦЕОЛИТАМИ

И.ГАННУШ, А.АДАС–СЮЧ, И.КИРИЧИ, ДЬ.ТАШИ, Ф.БЕРГЕР, Я.ГАЛАС, П.ФЕЕШ

На основании литературных и своих данных показано, что CO_2 эффективно и экономично может быть выделен из богатых CO_2 содержанием естественных газов с применением адсорбционной техники на цеолитах. Больше того, можно сказать, что цеолиты являются единственным видом адсорбентов, которые достаточно эффективны для разрешения этой проблемы. При сравнении применимости цеолитов NaA и NaX для этой цели, NaX значительно превосходит NaA тип, вследствие более значительной адсорбционной емкости и легкой регенерируемости.

COMPUTER–AIDED SCANNING ELECTRODE TECHNIQUE FOR THE INVESTIGATION OF CORROSION FAILURES IN ORGANIC–COATED TINNED PLATES

GY. KUTSÁN and Á. RAUSCHER

Institute of Physical Chemistry, Attila József University,

P.O.Box 105, H–6701 Szeged, Hungary

(Received October 23, 1989)

IN ORDER TO DETERMINE THE EXISTENCE AND LOCATION OF DEFECTS OF A COATING ON A METAL, A SCANNING ELECTRODE TECHNIQUE HAS BEEN DEVELOPED BY COMBINING THE RADIAL MOTION OF THE MICROELECTRODE WITH THE ROTATION OF THE SAMPLE. MEASUREMENT SYSTEM CONTROL, DATA COLLECTION AND EVALUATION WERE CARRIED OUT WITH A PROGRAM USING A MICROCOMPUTER.

THE DEFORMATION OF THE POTENTIAL FIELD CAUSED BY EXTENSIVE DAMAGE AND ACCUMULATED CORROSION PRODUCTS NECESSITATED AN EXACT MATHEMATICAL EVALUATION OF THE POTENTIAL MAPS. THROUGH THE METHOD OF GENERALISED SECOND DIFFERENCES, THE HEIGHT AND BASELINE WIDTH OF THE PEAKS CAN BE EXPRESSED NUMERICALLY. THE POINTS WHERE THE SECOND DIFFERENCES EXCEED A PRELIMINARILY CHOSEN LIMIT CAN BE DISPLAYED IN A DIAGRAM WHICH REPRESENTS THE SAMPLE. IN THIS WAY THE DEFECT SITES PROMOTING CORROSION CAN BE VISUALISED.

Introduction

Tinned cans protected with organic coatings may undergo certain corrosion failures when in contact with food products. Besides the corrosivity of the product and the quality of the tin and the organic coating (porosity, thickness and brittleness), the handling of the plates and the cannery technique can account for the increased corrosion of the inner side of the cans, *e.g.* the reinforcement embossing and identification numbers can cause fractures of the coating on the container ends. These techniques may cause not only mechanical damage, but also permanent stress.

When in contact with an electrolyte, the mechanically damaged areas are preferred sites for corrosion, due to the formation of local action cells. With a view to selecting

damaged series before use, it is reasonable to determine the possibility and distribution of the formation of local action cells by means of a non–destructive method.

The application of polarization methods may promote processes which do not occur during ordinary use. Optical methods, *e.g.* simple visual observations, are very useful, but need a long pretreatment or exposure time, may be affected by subjective factors and can hardly be automated. The scanning reference electrode technique provides an *in situ* method for studying the differences in electrochemical properties of a metal surface [1–9].

The existence and location of defects on a coating can be detected by a scanning micro–reference electrode with a fine capillary tip, situated close to the surface so as to intersect the potential field lines in the electrolyte due to the current of electrons in the metal and the ion migration in the solution [4,9].

The distance of the microelectrode from the surface affects the values on the potential contour map to a great extent. Changes in distance may result in noisy or hardly evaluable signals in the region of defects and may lead to the complete overlooking of certain defects near the reinforcement embossing. The microelectrode should be able to follow the embossed unevenness of the can ends.

The aim of this work was to develop a computer–aided scanning reference electrode technique and examine its performance on tinned can ends protected with organic coatings.

Apparatus and experimental technique

A schematic diagram of the applied measuring apparatus is shown in Fig. 1.

The embossed ends of containers served as test specimens (Fig. 1,1). The corroding medium was 0.05% NaCl. Signal generation was achieved with two Ag/AgCl reference electrodes. The potential distribution in the electrolyte close to the surface was measured by a scanning microelectrode (Fig.1,3) referred to the other Ag/AgCl electrode (Fig. 1,4). The sensing tip of the scanning electrode was set at a distance of some 20–30 μm from the surface, while the other one, in the bulk of the electrolyte, sensed the average potential of

the sample. The application of reference electrodes of the same type in this configuration increases the precision of the measurements.

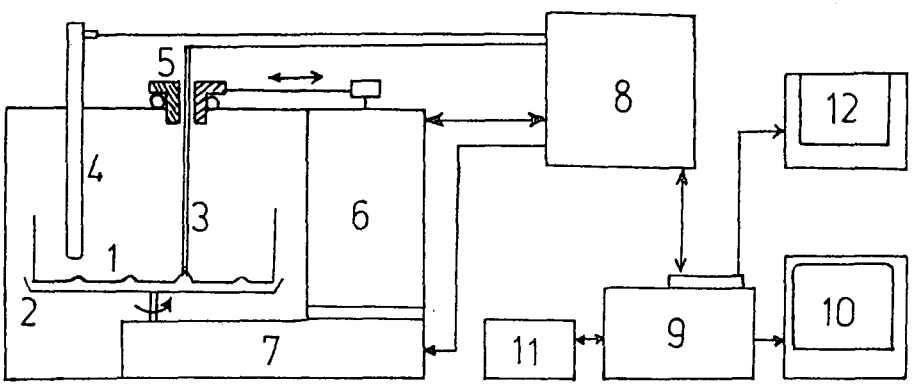

Figure 1: Block diagram of measuring system
1– sample, 2– sample holder, 3– micro–reference electrode, 4– stationary reference electrode, 5– carriage, 6– push–pull motor, 7– rotating motor, 8– AD–DA converter, 9– microcomputer, 10– monitor, 11– data storage, 12– printer

The scanning microelectrode was made in two different ways. A silver wire 0.25 mm in diameter was fixed in a glass capillary with "TORR SEAL" resin in the first case, and it was placed in a Teflon tube in the other case. The suitable profile of the resin or Teflon sliding foot of the electrode, which ensured the necessary 20–30 μm distance between the sample and the silver wire, was achieved by means of polishing. After formation of the electrode, an AgCl layer was electrodeposited onto it.

The microelectrode, fixed in a glass capillary, can move freely up and down in

accordance with the unevenness of the plate when placed in the Teflon sheath of the carriage (Fig. 1,5), which is equipped with bearings and pulled horizontally by an electric motor (Fig. 1,6). The sample holder with the can on it can be rotated around a vertical axis by another electric motor (Fig. 1,7). The electric motors (6) and (7) can operate either synchronised or individually.

As the container ends are symmetric with respect to rotation, a simple combination of the rotation of the container with the radial motion of the carriage carrying the electrode can result in a full coverage of the surface of the plate. Radial movements must be performed in such a way that the electrode is passed over the centre of the plate. Regular distribution of the scanning pathways can be ensured by synchronisation of the rotation and radial motion, and therefore electric motors with variable *rpm* values were applied. The method provides the possibility of variation of the scanning pathway distances (*i.e.* variation of the angle between the pathways). Of course, an increase of the scanning density results in an increase in the time required for testing, which cannot be compensated by increasing the sweep rate to any extent. Therefore, the optimal sweep rate and testing time should be determined experimentally.

Measurement system control, data collection and evaluation were carried out with a program for a personal microcomputer (Fig. 1,9). The computer is connected to an AD–DA converter (Fig. 1,8) through an interface which receives measurement data (positions and potentials) in two channels and is able to control relays for switching rotation and radial motion with reverse. The program controlling the AD–DA converter is written in ASSEMBLER code and is accessible from the main program in BASIC. The data–collecting segment (also in BASIC) stores about 6000 data pairs in a compact form. The intersections of the potential map and time data picked up are displayed on a monitor (Fig. 1,10).

The results of mathematical evaluation of intersections can be copied by a printer (Fig. 1,12) or saved (Fig. 1,11) and evaluated following the measurement process.

Results and discussion

In order to determine the optimal sweep rate and to test the reproducibility, the first experiments were conducted on plates subjected to intentional damage.

In the case of radial scanning (without rotation), the location and even the shape of the peaks referring to a given defect site depend on the sweep rate. This can be attributed to the facts that at greater speed the probe cannot be balanced sufficiently quickly and the potential distribution is perturbed by stirring of the solution.

In the experiments it was found that the reproducibility was acceptable if the sweep rate of the electrode did not exceed 30 mm/min. At higher sweep rates (*e.g.* at 60 mm/min.) the locations of the peaks depend on the scanning direction (Fig. 2).

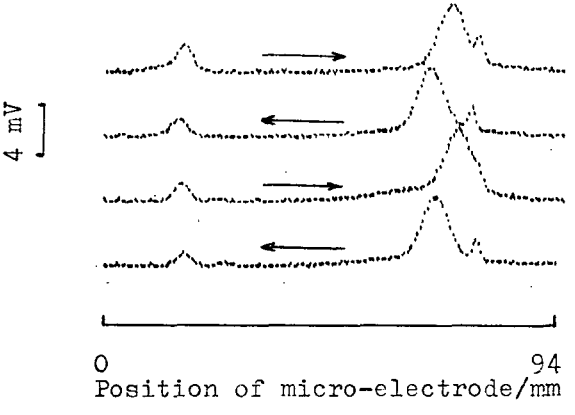

Figure 2: Influence of scanning direction on locations of potential peaks without sample rotation. Scanning rate: 60 mm/min

Optimal measurement time and scan rate could be achieved at 90 min/full rotation. As the advancing motor is stopped for only a few seconds at the endpoints, the route covered by the microelectrode is approximately symmetric and the distance between pathways do not exceed 5 mm anywhere.

Figure 3 shows a potential map of a container with a strongly corroded casing weld. Lines 3 and 4, which were recorded in the vicinity of the soldering, curve significantly. Deviation of the curves of this kind could be observed in every case when the damage was extensive and corrosion products had accumulated. Besides deformation of the potential field, data noise may also increase in such cases, and therefore an exact mathematical evaluation of the potential maps seemed to be reasonable in addition to simple observation of them.

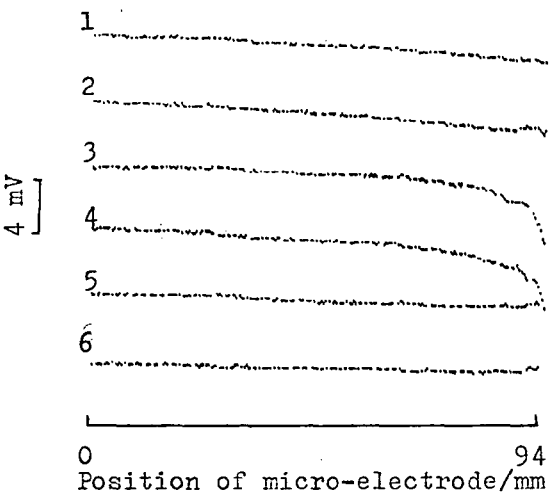

Figure 3: Influence of a strongly corroded soldering on contour lines. Scanning rate: 30 mm/min. Time of full rotation: 90 min.

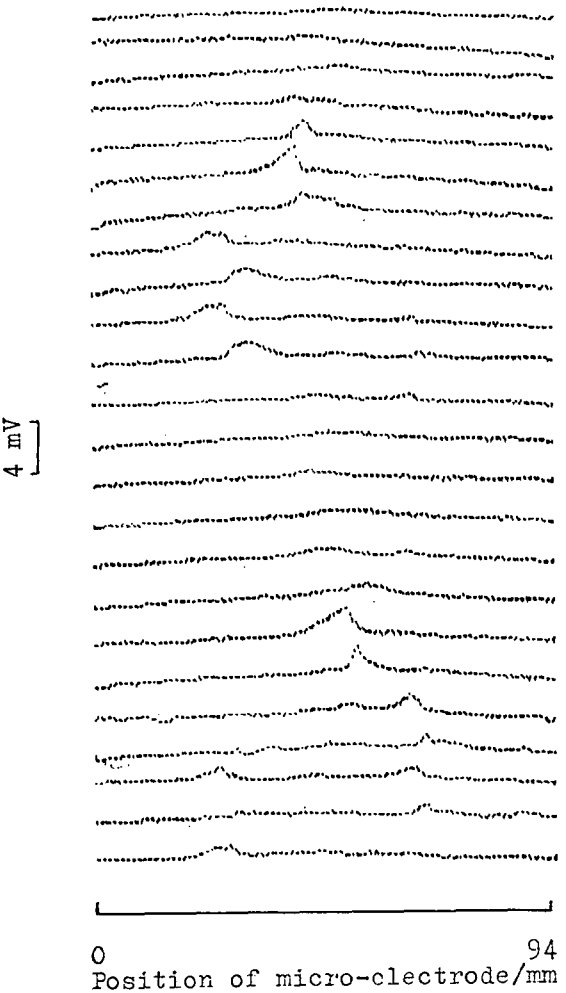

Figure 4: Potential contour map obtained on a can after 4 days exposure to electrolyte. Scanning rate: 30 mm/min. Time of full rotation: 90 min.

When the method of generalised second differences is applied, the height and baseline width of the peaks can be expressed numerically. The points where the second differences exceed a preliminarily chosen limit can be displayed on a monitor in a diagram which represents the can end. In this way the defect sites promoting corrosion can be visualised.

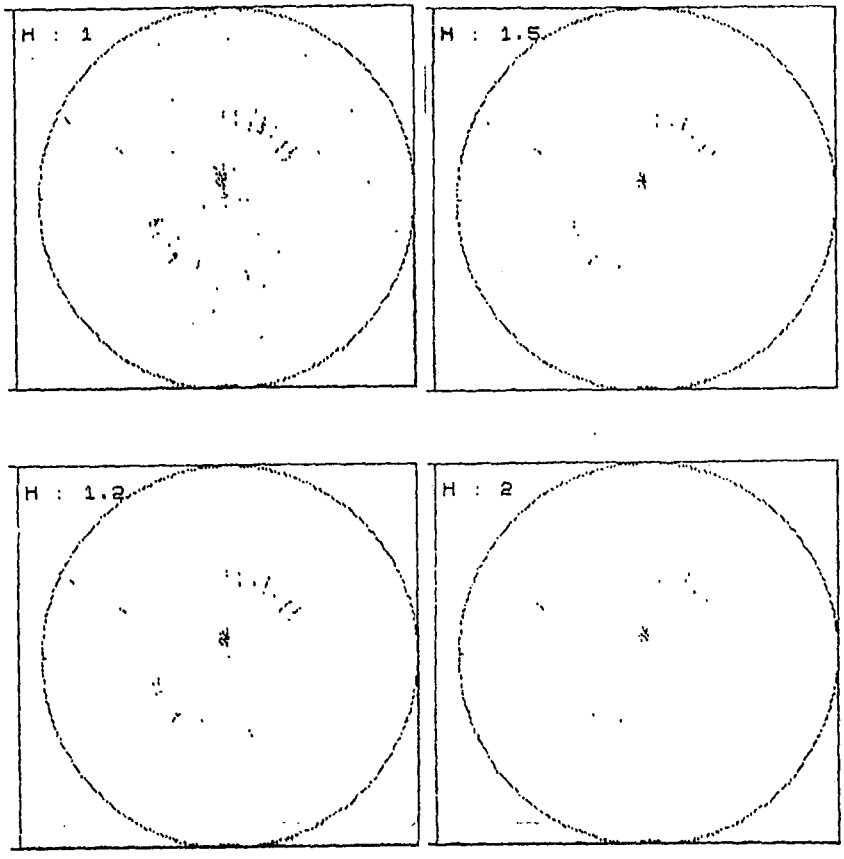

Figure 5: Distribution of defects evaluated from data of Fig. 4 according to different limiting values H.

Figures 4 and 5 depict the potential map intersections of a rotated sample exposed to 0.05% NaCl solution for four days, and the defect site distributions referring to different limiting values H of the second difference, respectively. The distributions reveal that corrosion occurs mainly at the innermost reinforcement embossing and at the identification numbers in the centre.

In a further series of experiments it was found that the height and width of the peaks increased with exposure time, showing the increase in local action cell activity, and the widening and deepening of the surface fractures and pits. As the probe passed over the defect sites, certain negative peaks also occurred in the diagrams of the intersections. This phenomenon must be connected with the formation of fractures and damage, and consequently cathodic and anodic sites of different sizes and characters. If the cut reaches the base metal, the steel functions as an anodic site and its environment as a cathodic site. In this case, the organic–coated surface, the passive tin layer and the steel corrosion products can all function, even simultaneously, as cathodic sites. If only the organic coating is damaged, the free tin surface can function as an active anode referred to the organic–coated surface. In the case of pitting corrosion of the tin, only a relatively small part of the surface functions as an anode. On the other hand, the cathodic character of the free tin surface referred to the defect sites reaching the steel is more marked than that of the organic–coated surface where the diffusion barrier of reducible components is much more expressed.

Though all these phenomena must influence the potential distribution in a very complicated way, there is no doubt that all of the sudden positive and negative shifts ("peaks" and "holes" in the map) indicate defect sites. Thus, the location and density of the points obtained by the method of generalised second differences (applying the empirically determined limiting factor H) are connected with the destruction of the surface layer.

References

[1] *Evans, U. R.:* The Corrosion and Oxidation of Metals, E. Arnold Ltd., London, p.862 (1960).

[2] *Rosenfeld, I.L., I.S. Danilov:* Proc. 3rd International Congress on Metallic Corrosion, Moscow, Vol.1. p.139 (1966).

[3] *Isaacs, H.S., G.Kissel:* J.Electrochem.Soc., 119, 1628 (1972).

[4] *Valker H.S., L.C. Rowe:* Electrochemical Techniques for Corrosion, Ed. R.Baboian p.79 (1977).

[5] *Gainer, L.J., G.R. Wallwork:* Corrosion, 35, 61 (1979).

[6] *Isaacs, H.S., M.W. Kending:* Corrosion, 36, 269 (1980).

[7] *Standish, J.D., H. Leidheiser:* Corrosion 36, 390 (1980).

[8] *Isaacs, H.S., R. Jackson:* Fundamental Aspects of Corrosion Protection by Surface Modification, Ed. E.McCafferty, p.339 (1984).

[9] *Schmauch, E.H., J.E. Finnegan:* Proc. of the Symp. on Computer Aided Acquisition and Analysis of Corrosion Data, Ed. M.W. Kending, U. Bertocci, J.E. Strutt, p.221 (1985).

[10] *Routti, J.T., S.G. Prussin:* Nuclear Instruments and Methods, 72, 125 (1969).

КОМПЮТЕР УПРАВЛЯЕМАЯ ЭЛЕКТРОДНАЯ ТЕХНИКА ДЛЯ ИССЛЕДОВАНИЯ КОРОЗИОННЫХ ПОВРЕЖДЕНИЙ СУРЬМИРОВАННЫХ ПОВЕРХНОСТЕЙ ПОКРЫТЫХ ОРГАНИЧЕСКИМ ВЕЩЕСТВОМ

Дь. КУЧАН, А. РАУШЕР

Для определения наличия и расположения изъянов в покрытиях металлов,

разработана сканирующая электродная техника при комбинации радиального движения микроэлектрода с вращением образца. Деформация потенциального поля, происходящая в результате расширения повреждений и накопления корозионных продуктов, требует точного математического расчета карты потенциалов. При применении обобществленного метода вторых разностей, высота и ширина базовой линии пиков могут быть численно выражены. Точки, в которых значения вторых разностей превосходят предварительно избранный предел, могут быть изображены на диаграмме, которая будет характеризовать образец. Таким образом положение дефектных мест, способствующих корозии, может быть визуализировано.

ABSORPTION SPECTRA OF NITRONES OF N–(2–HYDROXYBENZYLI–DENE)ANILINE AND N–(4–HYDROXYBENZYLIDENE)ANILINE IN VARIOUS SOLVENT MIXTURES

P. NAGY and R. HERZFELD

Chair of Chemistry, Gy. Juhász Teachers' Training College,

P.O.Box 396, H–6701 Szeged, Hungary

(Received September 4, 1989)

THE ABSORPTION SPECTRA OF THE EXAMINED NITRONES ARE NOT AFFECTED IN THE ESSENTIALS BY THE APPLIED SOLVENTS, WHEREAS THE SPECTRA OF THE CORRESPONDING SCHIFF BASES ARE GREATLY INFLUENCED BY THEM, MAINLY AT AROUND 400 nm.

THIS FINDING IS IN ACCORDANCE WITH THE SUPPOSITION OF BOTH THE ENOL ⇌ KETO AND ENOL ⇌ "ION–PAIR" EQUILIBRIUM. IT IS POSSIBLE THAT BOTH THE "ION–PAIR" AND THE KETO FORM PLAY A ROLE IN THE GIVEN SOLVENT EFFECT.

Introduction

In spite of extensive investigations, there is still no unanimously verified explanation for the characteristic solvent effect observed [1,2] at around 400 nm in the absorption spectra of certain types of Schiff bases.

DUDEK [3] and LEDBETTER [4] presume that a quinoline structure is formed on the action of the solvent, with an enol ⇌ keto tautomer equilibrium dependent on the solvent. In our opinion, the band at around 400 nm (the "fore–band") in the absorption spectra can be ascribed to the keto form. This explanation corresponds to the observation that this phenomenon can occur in those Schiff bases whose aromatic aldehyde component contains an OH group in the o– or p–position. Numerous experimental results are in accord with this explanation [5–10]. However, LEWIS and SANDORFY have postulated

the possibility of formation of an "ion–pair" structure [11]. The UV–VIS, IR and Raman spectra of N–(2–hydroxybenzylidene)aniline, however, did not reveal the presence of a substantial amount of either the quinone form or the "ion–pair" structure. On the basis of the Raman spectra of the amino acid Schiff bases of salicylaldehyde, LEDBETTER [12] explains this solvent effect in terms of the "ion–pair" structure. RANGANATHAN et al. [13] studied the PMR and electronic spectra of Schiff bases originating from substituted salicylaldehydes and 2–aminopyridine. They explained the solvent–dependent absorption band at around 400 nm as due to formation of the quinone structure. From an analysis of the electronic and Raman spectra of N–(2–hydroxybenzylidene)methylamine, LEE and KITAGAWA [14] attribute the absorption band at around 400 nm to the "ion–pair" structure. Accordingly, in spite of the fact that the investigations have been carried out with wide–ranging and varied methods, this problem has not been clarified unanimously so far.

The present paper reports on a study of the absorption spectra in various solvent mixtures of the nitrones of N–(2–hydroxybenzylidene)aniline and N–(4–hydroxybenzylidene)aniline, the two type–compounds as concerns the phenomenon in question. In these compounds, the non–bonding electron–pair of the azomethine N atom is involved in the N → O linkage, and it can therefore be expected that there will be a difference in the solvent effect relative to the corresponding Schiff bases, and that this may provide further data towards a better understanding of this solvent effect. It should be noted that KUBOTA et al. [15] made a detailed study of the spectroscopic behaviour of many nitrones, but they did not investigate Schiff bases originating from 2– and 4–hydroxybenzaldehyde, which are important from the aspect of the solvent effect in question.

Experimental

The following compounds

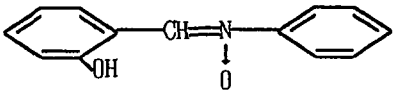

I

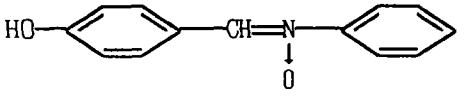

II

were prepared by mixing ethanolic solutions of the appropriate aldehyde and phenylhydroxylamine, and were subsequently purified by recrystallization. The analytical data are given in Table I.

Table I

Analytical data on compounds I and II

Com-pound	mp. (°C)		C(%)		H(%)		N(%)	
		*	Calc.	Obs.	Calc.	Obs.	Calc.	Obs.
I	118	51	73.24	73.30	5.16	5.21	6.57	6.22
II	210	192	73.24	73.32	5.16	5.16	6.57	6.58

* melting point of the corresponding Schiff base

The applied solvents were purified by means of the methods customary in spectroscopy, and were carefully freed from water. Freshly dried (dehydrated) calcium chloride was used for the investigation of the salt effect. The absorption spectra were recorded with a VSU2–P spectrophotometer at 298 K.

Results and discussion

The visible and UV spectra of compounds I and II were determined in absolute ethanol, in a 90% cyclohexene – 10% ethanol solvent mixture and in a 0.9 mol/dm^3 $CaCl_2$ solution in absolute ethanol. The absorption curves, together with those of the corresponding Schiff bases, are illustrated in Figs. 1 and 2. It can be seen that the absorption of the Schiff bases in the region 400–450 nm depends strongly on the solvent

used. On the other hand, the absorption curves of the nitrones are not appreciably influenced by the solvent. This experimental observation proves that conditions for the solvent effect are an OH group in the o– or p–position on the aldehyde ring, and also a non–bonding electron–pair on the azomethine N atom. If this electron–pair is involved in the bonding, the solvent effect is not observed.

This finding was next compared with the assumptions applied to date to explain the solvent effect. For the nitrones, the absence of the solvent effect would be in accord with the explanation that the hydrogen–bond between the solvent and the azomethine N atom causes the appearance of the new band and the change in the absorption spectrum, for this hydrogen–bond can not form in the nitrones. Nevertheless, this explanation is improbable for energetic reasons, and also because the solvent effect should then be observed for all Schiff bases. LEWIS and SANDORFY [11], among other authors, confirmed that a

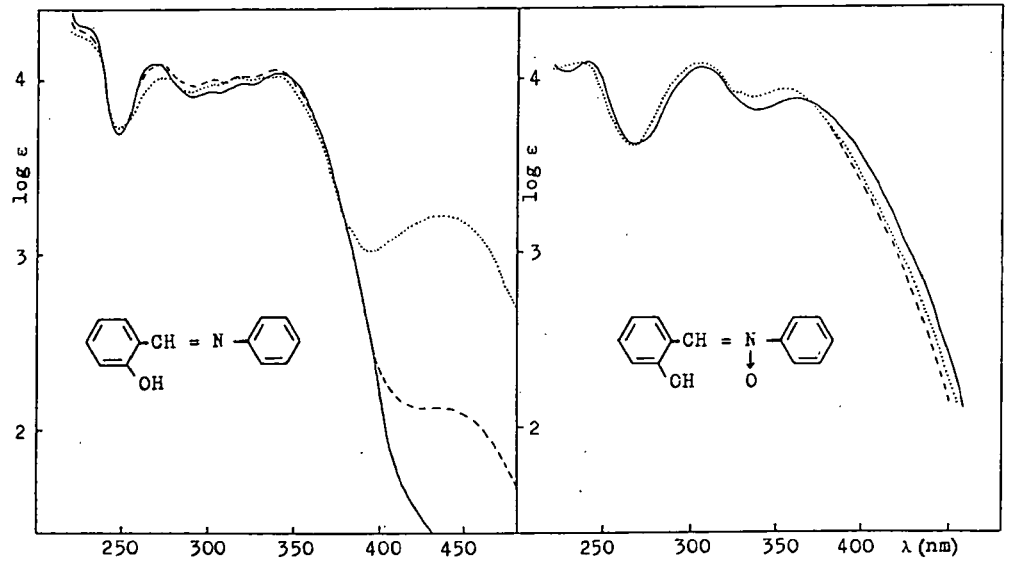

Figure 1: Absorption curves of compound I and the corresponding Schiff base in different solvents. Solvents: 90% cyclohexene – 10% ethanol (—), abs. ethanol(– –) and 0.9 mol/dm^3 $CaCl_2$ in abs ethanol(...)

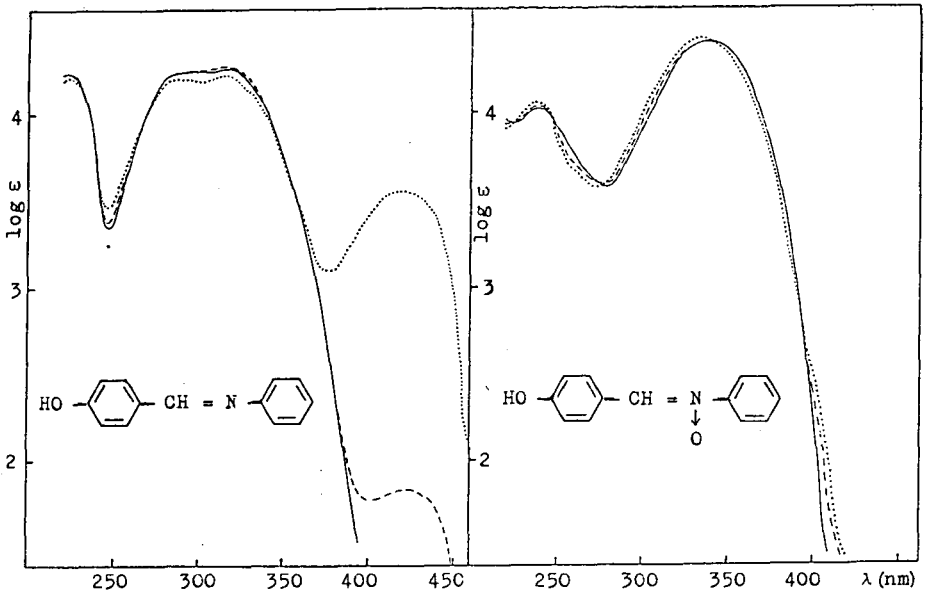

Figure 2: Absorption curves of compound II and the corresponding Schiff base in different solvents. Solvents: 90% cyclohexene – 10% ethanol (—), abs. ethanol(– –) and 0.9 mol/dm^3 $CaCl_2$ in abs ethanol(...)

hydrogen-bond is formed with benzalaniline, similarly as with N–(2–hydroxybenzylidene)-aniline, but the solvent effect in question can be observed only for the latter compound.

The data in Figs. 1 and 2 are in accord with the interpretation of the solvent effect in terms of either the enol ⇌ keto or the enol ⇌ "ion–pair" equilibrium. Both explanations correspond to the fact that the non–bonding electron–pair of the N atom plays a decisive role in the solvent effect. This is why the phenomenon is not observed for the nitrones. Via PMR and UV spectroscopic measurements, DUDEK presumed the enol ⇌ keto tautomeric equilibrium, on the basis of quantitative determination of the N–H bonding [3]. It is possible, however, that his experimental results can also be explained via the N–H bonds of the "ion–pair" structure. Apparently convincing evidence of the formation of the quinone structure is the fact that the solvent effect can be observed only if there is an OH group in

the o– or p–position on the aldehyde ring of the Schiff base. However, it can also be explained by the formation of the "ion–pair" structure, but less convincingly for the negative K effect of the azomethine group it can be expected that an OH group in the o– or p–position loses a proton more easily than one in the m–position, and therefore this solvent effect can not be observed for the m–derivatives.

The explanation of the phenomenon in terms of the formation of the "ion–pair" structure is in accord with our observation [6,10] that the solvent effect is greatly increased by various salts dissolved in absolute ethanol. Such an effect of $CaCl_2$ can be seen in Figs. 1 and 2. In our opinion, the charged particles of salts (in anhydrous solvent the salt molecules are largely non–dissociated) promote the formation of the "ion–pair" structure and therefore the ethanol $\rightleftharpoons$ "ion–pair" equilibrium shifts as a function of the salt concentration. We cannot explain the role of salts if the solvent effect is interpreted via the quinoidal transformation.

In their IR and Raman spectroscopic study of the solvent effect for N–(2–hydroxibenzylidene)aniline, LEWIS and SANDORFY [11] did not observe a perceptible change in the C = N force constant. Thus, formation of the quinone or "ion–pair" structure was not proved by their experimental data. Their suggested explanation, which they consider unlikely, is that one–two per cent of the molecules have the quinone or "ion–pair" structure in an ethanolic solution of the compound [10]. In contrast, there is a very considerable solvent effect for N–(2–hydroxibenzylidene)aniline, which DUDEK likewise investigated (Fig.3.); about 50 per cent of the molecules have the quinone (or "ion–pair") structure in ethanolic solution [3,10].

The reported results demonstrate that the findings relating to this solvent effect (perhaps with the exception of the role of the salts) can be explained with either the enol $\rightleftharpoons$ keto or the enol $\rightleftharpoons$ "ion–pair" equilibrium. However, in our opinion, these two explanations do not exclude, but rather presuppose one another: it is probable that the Schiff base molecules can assume the quinone form through the "ion–pair" structure

following hydrogen–bonding with the solvent:

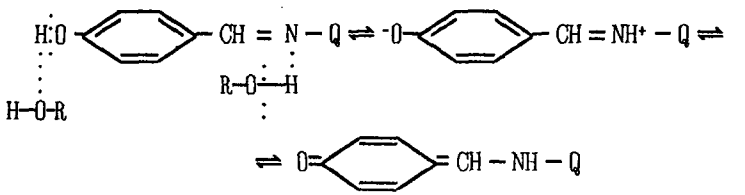

Of course, intramolecular hydrogen–bonding can also play a part in the reaction for the o–hydroxy derivatives.

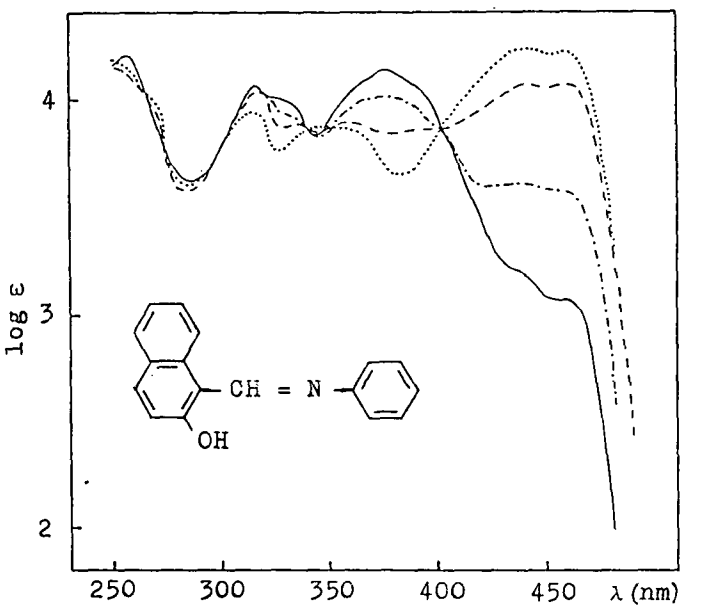

Figure 3.: Absorption curves of N–(2–hydroxy–1–naphthylidene)aniline in different solvents. Solvents: n–hexene (——), 90% n–hexene – 10% ethanol (–.–), abs. ethanol (– –) and 0.9 mol/dm^3 $CaCl_2$ in abs. ethanol (....)

The substituents on the aldehyde or amine component greatly influence the position of the above equilibria [5,13], and it must be taken into consideration that conjugation of the Schiff base molecule inhibits formation of the quinone structure. This may result in the solvent effect being perceptibly larger for the Schiff bases formed with aliphatic amines than for the aromatic derivatives [5]. In accordance with the stability difference between the naphthalene and benzene rings, the probability of formation of the quinone structure is larger for the Schiff bases formed with 2–hydroxy–1–naphthaldehyde than for the derivatives of salicylaldehyde. The solvent effect is essentially larger for the former. It is possible that virtually only the first equilibrium plays a role in the slight solvent effect observed for the 2– and 4–hydroxybenzylideneanilines. This would explain why the solvent effect basically occurs only in the "fore–band" region for these latter compounds (Figs. 1 and 2), whereas the whole absorption spectrum changes considerably for N–(2–hydroxy–1–naphtylidene)aniline, *e.g* see Fig. 3. The change in the spectrum is similarly considerable for the Schiff bases formed with aliphatic amines.

References

[1] *Tsuchida, R., T. Tsumaki:* Bull. Soc. Chem. Japan 13, 537(1938).

[2] *Hires, J.:* Kandidátusi disszertáció, Szeged, (1959).

[3] *Dudek, G.O., E.P. Dudek:* J.Amer.Chem.Soc. 86, 4283(1964); 88,2407(1966).

[4] *Ledbetter, J.W.:* J.Phys.Chem. 70,2245(1966).; 71, 2351(1967); 72, 4111(1968).

[5] *Nagy, P.:* Magy.Kém.Folyóirat 71, 11(1965); 72, 108(1966).

[6] *Nagy, P.:* Szegedi Tanárképző Főisk.Tud.Közl. 167(1965).

[7] *Nagy, P.:* Szegedi Tanárképző Főisk.Tud.Közl. 209(1970).

[8] *Császár, J., M. Novák-Bizony:* Acta Chim.Hung. 86, 9(1975).

[9] *Császár, J., J. Balogh:* Acta Chim.Hung. 86, 101(1975).

[10] *Nagy, P., E.Fövér:* Magy.Kém.Folyóirat 77, 100(1971).

[11] *Lewis, J.V., C.Sandorfy:* Can.J.Chem. 60, 1720(1982); 60, 1727(1982).

[12] *Ledbetter, J.V.:* J.Phys.Chem. 86, 2449(1982).

[13] *Ranganathan, H., T.Ramasimi, D.Ramaswamy, M.Santappa:* Chem.Lett. 1201(1979); Indian J.Chem. 25A, 127(1986).

[14] *Lee, H.,R.Kitagawa:* Bull.Chem.Soc.Japan 59, 2897(1986).

[15] *Kubota, T., M.Yamakawa, Y.Mori:* Bull.Chem.Japan 36, 1552,1564(1963).

АДСОРБЦИОННЫЕ СПЕКТРЫ НИТРОНОВ N–(2–ГИДРОКСИБЕНЗИЛИДЕН)АНИЛИНА И N–(4–ГИДРОКСИБЕНЗИЛИДЕН)АНИЛИНА В РАЗНЫХ СМЕСЯХ РАСТВОРИТЕЛЕЙ

П.НАДЬ, П.ГЕРЦФЕЛЬД

Адсорбционные спектры изученных нитронов в основном не зависят от применяемых растворителей, но в противоположность этому на спектры соответствующих Шиффовых оснований сильно влияют, в главном, в области 400 нм. Этот результат находится в соответствии с предположением наличия обоих энол ⇌ кето и энол ⇌ "ионная пара" равновесий. Возможно, что как "ионная пара" так и кето формы играют роль в эффекте растворителей.

THE DIELECTRIC BEHAVIOUR OF MONOCATIONIC MONTMORILLONITES

F. KÓCZÓ[1], Á. PATZKÓ[2] and M. BORBÉLY[3]

[1]ENERGOINVEST–RO Sigma, Subotica, Yugoslavia

[2]Institute of Colloid Chemistry, Attila József University, H–6720 Szeged, Hungary

[3]Training College, Subotica, Yugoslavia

(Received August 26, 1989)

Na,Ca–,Na– AND Ca–MONTMORILLONITES WERE USED AS DIELECTRICS IN A SEARCH FOR A RELATION BETWEEN THE ABILITY TO SWELL, X–RAY DIFFRACTION RESULTS AND DIELECTRIC PROPERTIES. THE CAPACITY AND CONDUCTIVITY OF MONTMORILLONITE TABLETS PLACED BETWEEN MINIATURE CONDENSING BLADES WERE MEASURED AS A FUNCTION OF TEMPERATURE, WHICH WAS VARIED VIA CONSTANT FREQUENCIES OF AN AC BRIDGE. THE PERMITTIVITY WAS DETERMINED FROM THE MEASURED CAPACITANCE. IT WAS FOUND THAT THE BEHAVIOUR OF THE SAMPLES WAS INFLUENCED PRIMARILY BY THE NATURE OF THE EXCHANGEABLE CATIONS AND BY THEIR MADE OF CONNECTION TO THE MONTMORILLONITE SHEET, AND SECONDLY BY THE PRESENCE AND NATURE OF THE ANIONS FORMING AN ELECTRIC DOUBLE LAYER ON THE OUTSIDE ARMATURE ON THE EDGES OF THE CLAY PARTICLES. IN FACT, THE DEPENDENCE BETWEEN THE CONDUCTIVITY AND THE TEMPERATURE CHANGES FAIRLY CLOSELY RESEMBLES THE SIMILAR DIAGRAMS FOR SEMICONDUCTORS. IT WAS CONCLUDED THAT THE GREATER RELATIVE PERMITTIVITY OF Na–MONTMORILLONITE IS DUE TO THE DIFFERENCE IN DISSOCIATIVE CAPACITY OF Na AND Ca CATIONS.

Introduction

Montmorillonites are anisodimensional plate–like particles which have an aluminosilicate network layer structure. Certain layers have a plane sheet structure: between two SiO_4 tetrahedral sheets there is an octahedral sheet consisting of $Al(O,OH)_6$ groups, linked by mutual oxygen atoms. It is presumed that the Al^{3+} partly replaces the Si^{4+}; the Al^{3+} can partly be replaced by Fe^{2+} or Mg^{2+}. Thus, in the triple layer complex there is always an excess of negative charge and, to compensate this, cations which can be exchanged by other cations (e.g. Na^+, Ca^{2+}, Mg^{2+}, H^+, etc.) occupy the space between the layers [1].

In the anhydrous state, the distance between the layers is 0.96 nm; in the case of complete hydration, however, the mineral can freely swell because of the small

layer–charge between the layers, which makes the internal and external surfaces free. Then depending on the nature of the cations, the interlayer distance increases from 2.0 to 5.0 nm. It is possible that a positive charge double layer is formed on the edges of the plates, due to the falling–off of tetrahedral silicate and octahedral aluminate layers. The capacity of montmorillonites for low anion–exchange can be explained by the presumed formation of positively charged double layers.

The nature and quantity of the attached ions determine the surface charge, the surface potential and the active adhesive forces of montmorillonite particles, which decisively influence the swelling ability , the possibility of peptization and the rheological properties [2,3].

During our examinations, we applied various monocationic montmorillonites as dielectrics and sought a connection between the physical–chemical and dielectric properties.

The aim of these examinations was essentially to improve the effects of the factors determining the corrosive aggressivity of the soil in the underground metallic structures by determining the typical dielectric properties of clay minerals, *i.e.* the colloid inorganic components of the soil.

Materials and methods

The crude bentonite used was from a mine at Mád. The colloid fraction obtained after peptization and fractionation contained only montmorillonites [4]. Peptization was performed with Na_2CO_3 and Na_3PO_4, which yielded the Na,Ca–montmorillonites. The montmorillonites (peptized by Na_2CO_3) which contained two kinds of cations were treated later with NaCl or $CaCl_2$ to produce Na– and Ca–montmorillonites [5].

From various samples we made tablets at 500 bar and dried these at 100 °C (373 K) until they showed conductivity saturation (G = const.). In order to ensure that the humidity was constant and typical for the given sample the measurements were made at an

equilibrated air humidity, which was determined with silica gel.

The tablets were placed between miniature condensing armatures and used as an element of an AC bridge. The capacitance and conductivity of the capacitor were measured as functions of temperature. Next the values of the relative permittivity (ϵ_r) were calculated. This method was described earlier [6].

Results and discussion

Typical data on the examined samples are shown in Table I. For the first three, there was no significant difference in the dry sample as concerned the distance between the plane sheets, measured by X–ray diffraction, or from the point of swelling. In an aqueous

Table I

Sample notation	Sample	Plane sheet distance d_{001} nm	Sediment vol. cm^3 Dose:1g substance in $10cm^3$ water
K1	Na,Ca–montmorillonite obtained by Na_3PO_4 peptization	1.265	stable suspension
K2	Na,Ca–montmorillonite obtained by Na_2CO_3 peptization	1.263	stable suspension
K3	Na–montmorillonite	1.228	stable suspension
K4	Ca–montmorillonite	1.426	3.7

medium a stable suspension is formed, and therefore no measurable sedimentation is present.

The dissociation of montmorillonites is determined by how strongly the

exchangeable cations are bound to the surface of the particles. The strength of the cation bond is determined by its valency and by the rule of the lyotropic series. Hence, in the dissociation of Ca–montmorillonite it is smaller than that of a Na–montmorillonite, and it is understandable that a Ca–montmorillonite does not swell in water so well, does not peptize and has a small volume of sedimentation (Table I).

The relative permittivity of various samples was measured as a function of temperature and the results are shown in Fig. 1. The samples treated with various Na^+ salts display almost the same behaviour; the only difference is the typical phase–change temperature.

All four samples have a very significant relative permittivity coefficient. As the temperature rises, the curves diverge more and more, which relates to the conclusion that the dipole moment is determined by some other induced polarization of equalizing ions.

In the presence of the same equalizing cations (samples K1 and K2) the permittivity is a function of number of exchangeable anions on the edges. Taking into consideration the van OLPHEN theory [3] about the positive double layer, the behaviour of the two dielectrics can be explained. Due to the interaction of the two dissimilar types of double layer, the molecules polarize differently. By examining the natures of cations in exchangeable positions (samples K3 and K4), it is obvious that the Na^+ ion, with high polarizability, predominates relative to the effects of the Ca^{2+} ion in Ca–montmorillonites. Samples K1 and K2 and samples K3 and K4 show similar dielectric behaviour, which is obvious from the $tg\delta$ vs. temperature diagrams in Fig. 2.

Figure 2 reveals that the behaviour of samples K1 and K2 differs significantly from that of samples K3 and K4. The ϵ_r vs. T diagrams of samples K1 and K2 (Fig. 1) show a phase change which can be seen in Fig. 2 as $tg\delta$ peaks. The phase–change temperature for sample K1 is –16 °C (257 K), while that for sample K2 is –22 °C (251 K). This means that the activation energy of sample K2 is smaller than that of sample K1. It also means that the "freezing" of different ions ceases. The course of the $tg\delta$ vs. T curve relates to a further

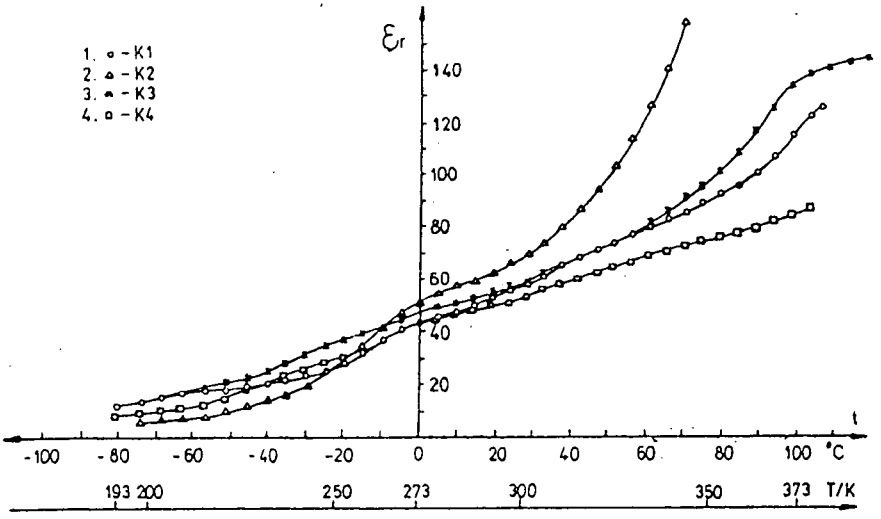

Figure 1: Relative permittivity of modified montmorillonites as a function of temperature

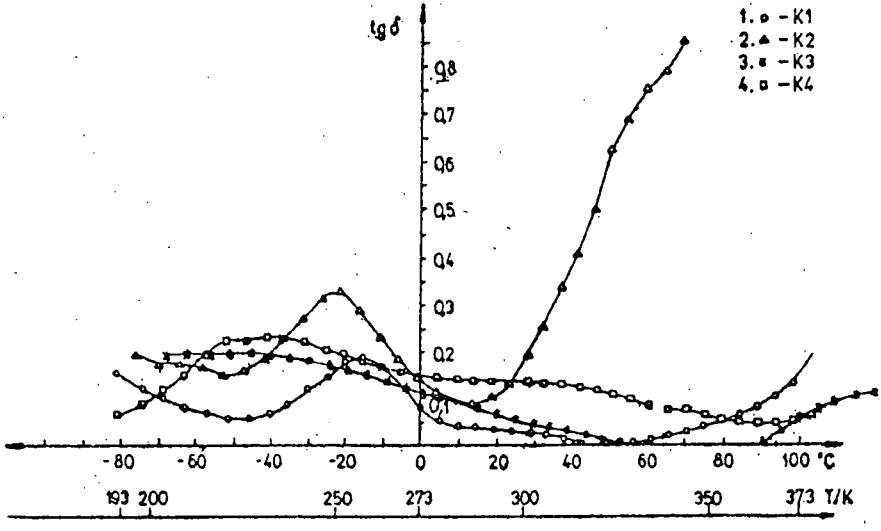

Figure 2: Dielectric loss of modified montmorillonites as a function of temperature

two "freezings" or "meltings". The characteristic rise in tgδ begins at 100 °C (373 K) for sample K2, whereas for sample K1 the tendency to a strong rise begins at 30 °C (303 K). The tgδ vs. T diagrams for monocationic Na–montmorillonites (K3) at –60 °C (213 K), and for Ca–montmorillonites (K2) at –45 °C (228 K), also show the phase change, but the further course of the curves is very different from the previous one.

Further, changes in specific conductivity (κ) as a function of temperature (logκ vs. 1/T) were tested (Fig. 3). The dielectric losses reveal that samples K1 and K2, and also samples K3 and K4, exhibit mutual similarity; this is clearly illustrated by the logκ vs. 1/T curves. Two typical plots are presented in Fig. 3. The plots for samples K1 and K2 comprise two linear sections their starting points being at the same temperature; the

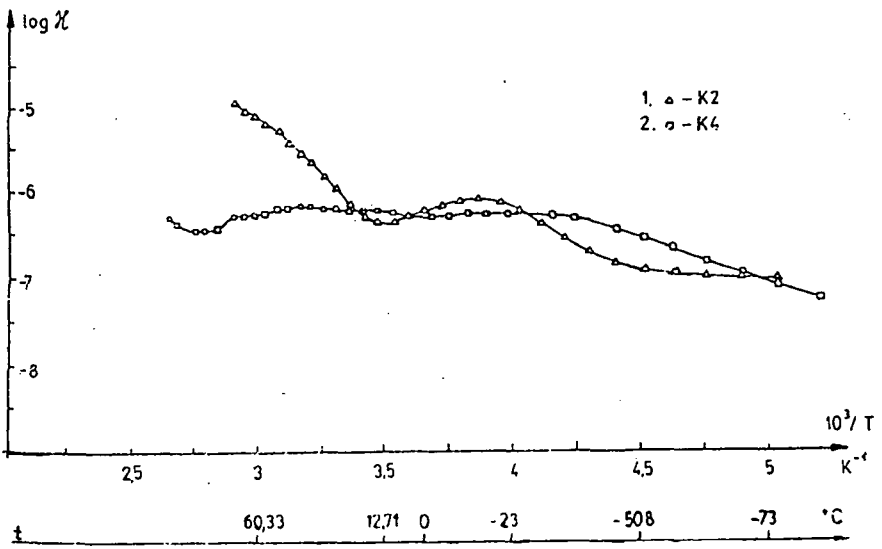

Figure 3: Dependence of logarithm of specific conductivity of modified montmorillonites on reciprocal absolute temperature

dielectric losses showed the maximum. The course of the curves is reminiscent of the similar curves (logγ vs. 1/T) for impure semiconductors [7]. It is assumed that these linear dependences originate from the increase in the number of dominant charge carriers with

temperature rise (resulting also in an increase in the specific conductivity). In contrast, the diagrams for monocationic montmorillonites (samples K3 and K4; Fig. 3 shows the diagram for sample K4) in the temperature interval from –40 °C to 40 °C the specific conductivity remains practically constant. The results obtained so far permit the conclusion that the relative permittivities of sample K1 and K2 (which are models of the montmorillonites in basic soils) are complex functions of the thickness of the negative double layers on the surfaces and the positive electric double layers on the edges. As the negatively charged networks are compensated by the same cations (Na,Ca–montmorillonite), the higher relative permittivity of sample K2 is attributed to the higher polarizability of the CO_3^{2-} ions in the exchange position on the edges of the network. If it is accepted that the dissociability of cations in the exchange position causes swelling and the possibility of peptization, and also influences zeta–potential (this determines the dipole moment of particles), then it is possible that the dissociability decreases the relative permittivities of Ca–montmorillonites relative to those of Na–montmorillonites.

To summarize, it is concluded that the dielectric characteristics of montmorillonites are function of the activities of the anions and cations in the system. The relative permittivities of the tested samples are relatively high (ϵ_r = 40–60 between –10 and +30 °C) and should therefore be taken into consideration in an evaluation of the corrosive aggressivity.

References

[1] *Nemecz, E.*: Agyagásványok, Akadémiai Kiadó, Budapest (1973).

[2] *Szántó, F.*: Földtani Közlöny 93. 142 (1963).

[3] *Olphen van, H.*: An Introduction to Clay Colloid Chemistry, Chap. 7., Int. Sci. Publ. John Wiley, New York (1963).

[4] *Szántó, F., M. Gilde-Farkas, B. Várkonyi, J. Balázs*: Acta Geol. Acad. Sci. Hung. 11, 409 (1967).

[5] *Patzkó, Á., P. Szántó:* 5th Meeting of European Clay Groups, Prague, 1983. Charles University (1985).

[6] *Koczó, F., M. Dulic, L. Horváth:* Acta Phys. et Chem. (Szeged) 30, 141 (1984).

[7] *Solymar, L., D. Walsh:* Szilárdtestek elektromos tulajdonságai, Műszaki Kiadó, Budapest (1972).

[8] *Borbély, M.:* Magistarski rad, Technoloski fakultet, Novi Sad (1975).

ДИЭЛЕКТРИЧЕСКИЕ СВОЙСТВА МОНОКАТИОНИТНЫХ МОНТМОРИЛЛОНИТОВ

Ф. КОЦО, А. ПАЦКО, И. БОРБЕЛЬ

Исследованы диелектрические свойства натриевого, кальциевого и смешанного натро–кальциевого монтморрилонитов и сопоставлены с их набухающей спасобностью и рентгено–структурными данными. Диэлектрические измерения проводились в зависимисти от температуры при постоянных частотах. Показано, что свойства образцов зависят в первую очередь от природы и способа связывания обменных катионов, а во вторую – от анионов, образующих двойной электрический слой на гранях минералных частиц. Температурная зависиность проводимости исследуемых монтмориллонитов соответствует в основном аналогичным зависимостям для полупроводников. Большая проводимость натриевных монтмориллонитов по сравнению с кальциевыми, обусловлена большей обменной емкостью натриевых ионов.

LOCATION OF STATIONARY POINTS OF POTENTIAL ENERGY SURFACES I. GUIDE TO A NEW PROGRAM SYSTEM DEVELOPED FOR THE DETERMINATION OF GRADIENT EXTREMAL CURVES

MIKLÓS. I. BÁN

Institute of Physical Chemistry, Attila József University

P.O.Box 105, H–6701 Szeged, Hungary

(Received October 10, 1989)

THE AIM OF THIS SERIES OF PAPERS IS TO PROVIDE THE INDISPENSABLE THEORETICAL BACKGROUND AND ALL PRACTICAL INSTRUCTIONS FOR USING A NEWLY DEVELOPED PROGRAM SYSTEM SUITABLE FOR THE EFFICIENT LOCATION OF SADDLE POINTS, MINIMA/MAXIMA AND POINTS OF GRADIENT EXTREMAL CURVES.

1. Introduction

Program system has been developed for the efficient location of saddle points, minima/maxima and points of gradient extremal curves[1]. It consists of two conceptually largely independent parts. Part I is designed for the determination of any kinds of stationary points of a function describing the potential energy surface of a chemical reaction. Part II relates to the determination of saddle points of gradient extremal curves.

The necessary theoretical considerations and technical instructions for the use of Part I are discussed in this paper, while Paper II will be devoted to the questions relating to Part II (see p.109 this volume).

Since a detailed theoretical discussion of the method has also been presented [1], the basic considerations concerning the algorithm will be mentioned here only when unavoidable. The FORTRAN code of the program is available; it will be submitted for distribution to the QCPE, but on request the author will send copies.

[1] The substantial comments provided in the program will also help the user.

2. The framework of the algorithm

To analyze the behaviour of the present algorithm, a quadratic objective function will be considered.:

$$f(x) = f(x_o) + g_o^t p + 1/2\, p^t G p \tag{1}$$

where x and x_o are the position vectors, $g_o = g(x_o)$ is the gradient, G is the matrix of second derivatives and $p = dx$ is the coordinate differential[2].

If the matrix of second derivatives (Hessian) is positive/negative definite, the stationary point of the function is a minimum/maximum. An indefinite Hessian determines a saddle surface and a saddle point for a critical point[3].

During the past two decades, the quasi–Newton algorithms[4] have proved to be very powerful in finding minima, and therefore they have also begun to be used for the location of saddle points [3]. If a genuine quasi–Newton method is applied to an indefinite objective function, several serious inherent problems occur.

With indefinite Hessians, singular vectors exist which satisfy the condition

$$v^t G v = 0. \tag{2}$$

Such singular directions of search cause the total breakdown of the algorithm. Neither the step size nor the update of the H–matrix is defined along a path of zero/very small curvatures. The existing techniques developed for handling such functions explicitly modify a parent quasi–Newton method for adaptation to indefinite optimization problems. The concept of the present algorithm approaches the problem of location of a saddle point in a different way. Instead of modifying a parent quasi–Newton algorithm, it seems more

[2]Small letters denote scalars and vectors, capital letters denote matrices, and superscript t refers to transposition.

[3] A saddle point can be of first or higher order, depending on the number of negative eigenvalues.

[4] For the common properties of the quasi–Newton family, see [2].

attractive to define a new (associated) surface, which is convex and contacts the original surface at its saddle point. This means that, in the sense of this idea, the two surfaces are in a first order touching contact characterized by identical function values and first derivatives, but their second derivatives differ in nature. While the critical point of the original surface is a saddle point, the "associated convex surface" has a minimum with the same coordinates. The introduction of the associated convex surface allows the use of any quasi–Newton method to find its minimum located at identical coordinates as the saddle point of the original surface. The present algorithm will carry this out.

The procedure is defined in an area around the saddle point where a constant direction vector (z_1) exists, along which the curvature of the surface is negative[5]:

$$z_1^t G z_1 < 0. \tag{3}$$

With the help of z_1 and $w_1 = Gz_1$ the reflector matrix

$$B = I - 2\frac{w_1 z_1^t}{z_1^t w_1} \tag{4}$$

can be constructed. The matrix B is used for the transformation

$$\tilde{g} = Bg, \tag{5}$$

the new gradient (5) being related to the convex surface[6].

If the algorithm is applied for the location of a minimum, the construction of (4)

[5] It has been presumed for chemical reasons that in the area to be explored the Hessian has only one negative eigenvalue.

[6] The transformation (5) of the gradient involves the implicit transformation

$$\tilde{G} = BG$$

of the Hessian and yields a positive definite quadratic form:

$$x^t \tilde{G} x > 0; \quad \forall x \in R^n.$$

and the transformation (5) are omitted. The further steps in both cases follow the general scheme of the quasi–Newton family. The minor changes introduced into the algorithm are of a practical nature and do not affect the common inherent structure of these procedures.

The peculiarities of the linear search, the properties of the update of the H–matrix and numerical examples will be presented in the forthcoming sections.

3. The linear search

The present description concerns the practical performance of the linear search step of a modified quasi–Newton algorithm suitable for the location of saddle points[7]. At any general point, the associated convex surface is defined exclusively on its derivative properties because the function value of the associated surface can not be evaluated from the primary data relating to the saddle surface[8].

The consequences of this fact are twofold:

i) the linear search must be based on the behaviour of the gradient, disregarding the continuous descent of the function value, which is an essential property of the quasi–Newton family, and

ii) the function value of the original (saddle–)surface becomes superfluous, saving part of the computational work.

In the search for a saddle point, the basic requirement is to know a constant vector (z_1) satisfying condition (3). The line segment connecting the minima at the "endpoints" of the reaction path is generally a suitable estimate.

At a point (x) of a general (non–quadratic) function the gradient and the (locally defined) B–matrix (4) have to be evaluated[9]:

---

[7]The essence of the necessary modifications relates to any member of the family, and therefore the method used will not be specified more closely.

[8]The function value is given only at the critical point.

[9]This is generally performed in a finite–difference approximation:

$$w_1(x) = g(x + \eta z_1) - g(x); \qquad \eta << 1.$$

$$B(x) = I - 2\frac{w_1(x)z_1^t}{z_1^t w_1(x)}. \tag{6}$$

The gradient will be transformed into the form

$$\tilde{g}(x) = B(x)g(x), \tag{7}$$

relating to the associated convex surface.

The direction of search (s) will be chosen according to the parent algorithm. The i^{th} search direction can generally be written as

$$s_i = -H_i\tilde{g}_{i,1}, \tag{8}$$

where H_i is a positive definite matrix, the double–index (i,1) is to be read "the gradient at point 1 along the i^{th} search direction" and the vector s_i must satisfy the condition

$$r_{i,1} = \tilde{g}_{i,1}^t s_i < 0. \tag{9}$$

The position (r) of a point is measured by the component of the gradient parallel to the path (directional derivative):

$$r \equiv r(x) = \tilde{g}^t s. \tag{10}$$

A point (x*) will be accepted as a local stationary point if the condition

$$r(x^*) = \tilde{g}^t(x^*)s = \epsilon \approx 0 \tag{11}$$

is fulfilled.

The step length (α) will be determined in a slightly different way if the point is on the side of descent/ascent around the local minimum, and therefore the linear search process will be discussed separately.

i) Side of descent:

The first step (at x_1) is

$$x_{i,2} = x_{i,1} + \alpha_{i,1} s_i \tag{12}$$

and the second step (at x_2) is

$$x_{i,3} = x_{i,2} + \alpha_{i,2} s_i. \tag{13}$$

The step length will be determined by using the information obtained on the curvature of the surface. The average curvature of the surface relating to the first step is

$$GS_{i,2} = (r_{i,2} - r_{i,1}) / \alpha_{i,1} \tag{14}$$

where $r_{i,2}$ and $r_{i,1}$ are the values of (9) at $x_{i,2}$ and $x_{i,1}$.

If

$$GS_{i,2} > 0, \tag{15}$$

the length ($\alpha_{i,2}$) of the step will be chosen as

$$\alpha_{i,2} = -r_{i,2} / (\omega_1 GS_{i,2}) \tag{16}$$

where

$$\omega_1 < 0. \tag{17}$$

The factor ω_1 accounts for the possible diminishing of the curvature and it is chosen for slight overestimation of the step length (generally, $\omega_1 = 0.8$).

If

$$GS_{i,2} < 0, \tag{18}$$

the step length will be estimated for a fixed factor ($\alpha_{i,2} = 4.0$).

The k^{th} step on the descent side at x_3 will be

$$x_{i,k+1} = x_{i,k} + \alpha_{i,k} s_i. \tag{19}$$

If both of the average curvatures ($GS_{i,k}$, $GS_{i,k-1}$) are positive, the change of the curvature will be approximated by

$$\omega_1^i = GS_{i,k}/GS_{i,k-1} \tag{20}$$

determining the step length:

$$\alpha_{i,k} = -r_{i,k}/(\omega_1^i GS_{i,k}). \tag{21}$$

If $GS_{i,k-1}$ is negative, $\alpha_{i,k}$ will be determined by (16) if $GS_{i,k}$ is positive, $\alpha_{i,k} = 4.0$.

This procedure is repeated until the actual point can be accepted as a local minimum on the descent side, or the point passes the minimum having reached the ascent side.

There are two criteria to be fulfilled at the local minimum. The first criterion requires an acceptable reduction of the gradient along the path. It is applied in two forms of optional use:

$$\text{a)}\ r_{i,k} < r_{i,1} \tag{22}$$

and

$$\text{b)}\ r_{i,k} < \omega_2 r_{i,1}. \tag{23}$$

The form condition (22) is a loose requirement used at the beginning of the iteration, while (23) is used if the point is closer to the minimum. The second criterion tends to ensure an acceptably close distance from the exact local minimum. This means that the step length of the k^{th} step will be reevaluated (and checked) through use of the data obtained in the k^{th} step:

$$GS'_{i,k} = (r_{i,k+1} - r_{i,k})/\alpha_{i,k}, \tag{24}$$

$$\alpha'_{i,k} = -r_{i,k}/GS'_{i,k}. \tag{25}$$

Before taking steps, the step length (21) is determined by using data on the curvature relating to the $(k-1)^{th}$ step (see(14)).

If

$$\alpha_k/\alpha'_k > \omega_3 \tag{26}$$

(generally, $\omega_3 = 0.8$), the point can be taken as acceptable.

If the first and second criteria are fulfilled simultaneously, the point will be accepted as a local stationary point. The last (approximating) point will always be stored.

ii) Side of ascent:

The $(k+1)^{th}$ point (reached in the k^{th} step and corresponding to x_4) is defined by (19). The local minimum has been passed:

$$r_{i,k} > 0, \quad (r_{i,l} < 0; \quad \forall l < k). \tag{27}$$

It will first be checked whether $x_{i,k}$ is too far from the minimum, *i.e.* the change of r must be smaller than a given limit:

$$|r_{i,k}|/|r_{i,k-1}| < \omega_4. \tag{28}$$

If this condition is not fulfilled, a step back (based on the measured curvature) will correct this situation. If the point is in a suitably close position, it will be stored (as will every successive approximation) and a bracketing process begins.

The $(l+2)^{th}$ point (corresponding to x_5 or x_5^l) is

$$x_{i,k+2} = x_{i,k} + \alpha_{i,k+1} s_i. \tag{29}$$

Using the (directional) first derivatives, the second derivatives will be approximated:

$$GG1 = (r_{i,k} - r_{i,k-1})/\alpha_{i,k-1}, \tag{30}$$

$$GG2 = (r_{i,k+1} - r_{i,k})/\alpha_{i,k}. \tag{31}$$

If both of them are positive, then an (approximate) third derivative is also computed:

$$GGG = (GG2 - GG1)/(\alpha_{i,k-1} + \alpha_{i,k}). \tag{32}$$

Because of the averaged nature of the second derivatives (GG1, GG2), the local value at point x_k will be approximated by the weighted sum:

$$GG(x_k) = GG_c = (\alpha^{-1}_{i,k-1} + \alpha^{-1}_{i,k})^{-1}(\alpha_{i,k-1} GG1 + \alpha^{-1}_{i,k} GG2). \qquad (33)$$

When the change in the function up to third order is taken into account, the two step lengths are:

$$(\alpha_{i,k+1}; \alpha'_{i,k+1}): \rightarrow (-GG_c \pm \sqrt{DISCR})GGG^{-1} \qquad (34)$$

where

$$DISCR = GG_c^2 - 2r_{i,k} GGG. \qquad (35)$$

The solution is chosen to be closer to

$$\alpha_{i,k+1} = -r_{i,k}/GG2 \qquad (36)$$

which provides the result of the second–order interpolation. If GG1 or DISCR is negative, (36) is used for estimation of the step length.

The new point ($x_{i,k+2}$ and also all subsequent points) can be on the descent side or the ascent side. After storage in the appropriate array, the bracketing process will be repeated, taking into account the points (k+2). If one of the two second derivatives GG2 is negative, the third–order interpolation will be substituted by the second–order step (36).

The conditions for exit are the same as discussed previously. The accuracy of the line search can be controlled via the parameter ω_2. The usual choice ($\omega_2 = 0.1$) prescribes a moderate accuracy, implying simultaneously a small number of gradient evaluations (generally in the range 1.8–2.3 per search direction).

4. Update of the H-matrix

To absorb the explored characteristics of the surface, the H–matrix will be updated

in each step. Because of the widely proved computational qualities, the present procedure allows the optional use of the DFP [4] and BFGS [5] update schemes.

The formulas

$$H_{i+1}^{DFP} = H_i^{DFP} + \frac{\delta_i \delta_i^t}{\tilde{\gamma}_i^t \delta_i} - \frac{(H_i \tilde{\gamma}_i)(\tilde{\gamma}_i^t H_i)}{\tilde{\gamma}_i^t H_i \tilde{\gamma}_i}, \tag{37}$$

$$H_{i+1}^{BFGS} = H_i^{BFGS} + \left[1 + \frac{\tilde{\gamma}_i^t H_i \tilde{\gamma}_i}{\tilde{\gamma}_i^t \delta_i}\right] \frac{\delta_i \delta_i^t}{\tilde{\gamma}_i^t \delta_i} - \frac{\delta_i (\tilde{\gamma}_i H_i) + (H_i \tilde{\gamma}_i) \delta_i^t}{\tilde{\gamma}_i^t \delta_i}. \tag{38}$$

These are formally strikingly similar to the original definitions in [4,5] ($\tilde{\gamma}_i$ and δ_i will be given below).

Since the coordinates and gradients relating to the last points (on both sides) are always preserved, there is some freedom in determining the curvature. Including the last point (accepted as a local minimum), there are altogether three points (and gradients) for this purpose (x_3, x_4, x_5, $(x_5^l)(k=3)$). Theoretical considerations and computational experience show that the best choice is the use of the weighted composition

$$\tilde{\gamma}_i = \tau_1(\tilde{g}_{i,k+2} - \tilde{g}_{i,k}) + \tau_2(\tilde{g}_{i,k+1} - \tilde{g}_{i,k+2}), \tag{39}$$

$$\delta_i = \gamma_1(x_{i,k+2} - x_{i,k}) + \tau_2(x_{i,k+1} - x_{i,k+2}) \tag{40}$$

where

$$\tau_1 = \alpha_{i,l+1}/\alpha_{i,l}, \tag{41}$$

$$\tau_2 = 1 - \tau_1. \tag{42}$$

The storage of the last points ensures a significant exclusion of higher than second–order effects.

The above update strategy yields a significant (30–40 percent) decrease in the number of steps (and gradient evaluations) necessary to attain the same accuracy as with the parent algorithm. The algorithm ensures a second–order convergence on quadratic surfaces.

5. The necessary conditions of the procedure

The explicit necessary condition is the knowledge of a vector (z_1) satisfying condition (3) in the whole region around the saddle point. Transformation (5) accounts for the reversion of the negative curvature of the surface (along z_1) into a positive one.

If the Hessian has more than one negative eigenvalue, the directions of negative curvature (conjugated to the Hessian) must be known to construct separate B–matrices.

Those areas where the Hessian has more than one negative eigenvalue are not of chemical importance, and therefore the present scheme of the algorithm covers the needs of chemical interest. The assumption that the Hessian has only one negative eigenvalue in the region of search is an implicit condition.

Acknowledgement

In writing up this paper thanks are due to Dr. Imre Bálint for the consent of using many results of his work, consultations and advice during the period working in my group between January 1985 and July 1987. The support of this work is acknowledged to the Hungarian Ministry of Higher Education (grant Nos. P–437/84. and 746/86).

References

[1] *Bálint I., M.I.Bán:* Theoret.Chim.Acta 63, 255 (1983),
Bálint, I.: Candidate dissertation, Szeged, 1986.

[2] *Fletcher, R:* Practical Methods of Optimization I.–II.,
Wiley, New York, 1980.
Powell, M.J.D.: Math.Progr.1,26 (1971).

[3] *Bálint,I.,M.I.Bán:* Int.J.Quant.Chem.25, 667 (1984).

[4] *Davidon,W.C.*: AEC Res.Dev.Rep.ANL–5990 (1959),
Fletcher,R.,M.J.D.Powell: Comp.J.6, 163 (1968).

[5] *Broyden,C.G.*: Maths. Comput.21, 368 (1967).
Fletcher,R.: Comp.J.13, 317 (1970).
Goldfarb,D.: Maths. Comput.24, 23 (1970).
Shanno,D.F.: Maths. Comput.24, 647 (1970).

РАСПОЛОЖЕНИЕ СТАЦИОНАРНЫХ ТОЧЕК ПОВЕРХНОСТЕЙ ПОТЕНЦИАЛЬНОЙ ЭНЕРГИИ I. ВВЕДЕНИЕ К НОВОЙ СИСТЕМЕ ПРОГРАММ ДЛЯ УСТАНОВЛЕНИЯ КРИВЫХ С ЭКСТРЕМАЛЬНЫМ ГРАДИЕНТОМ

М.И. БАН

Цель данной серии публикаций заключается в представлении необходимого теоретического обоснования и всех практических инструкций требуемых для пользования новь развитой системы программ пригодной для успешного установления седловных точек минимумов/максимумов и точек кривых с экстремальным градиентом.

A RAPID ITERATIVE DIAGONALIZATION METHOD FOR LARGE MATRICES

MIKLÓS. I. BÁN

Institute of Physical Chemistry, Attila József University

P.O.Box 105., H–6701 Szeged, Hungary

(Received November 7, 1989)

AN ACCELERATED ITERATIVE MATRIX DIAGONALIZATION TECHNIQUE REDUCING THE COMPUTATIONAL WORK IS DESCRIBED. THE METHOD IS USEFUL WHEN THE RATE OF CONVERGENCE IS NOTORIOUSLY SLOW AND THE ITERATIVE PROCEDURE CAN NOT BE AVOIDED.

1. Introduction

Iterative procedures used to determine the eigenvectors (and the spectrum) of matrices yield the eigenvector belonging to the eigenvalue largest in absolute sense . The overall rate of convergence depends on the structure of the spectrum very strongly and the usual procedures require in most cases too many iterations to be of practical value. In order to determine the rest of eigenvectors (and eigenvalues) several methods reducing the rank of the matrix, or projective elimination techniques are generally used.

The diagonalization of large matrices is an acute problem extending to many fields of computational sciences (molecular physics, quantum chemistry, *etc.*). A typical computational task in recent molecular physics and quantum chemistry is the determination of some (*e.g.* generally the largest) eigenvalues and eigenvectors of the Hamiltonian at the post–SCF level.

In this paper an effective acceleration procedure reducing substantially the number of iteration steps necessary to reach convergence will be described. The procedure is especially useful in cases where the separation of eigenvalues is small.

2. Method

Let us consider a positive (semi–)definite matrix A with real elements and denote the ordered set of its eigenvalues by λ_j:

$$\lambda_j := (\lambda_1 > \lambda_2 \geq \lambda_3 \geq \ldots \geq \lambda_n) \in R, \qquad j=1,..,n \tag{1}$$

and its eigenvectors by e_i, where R is the assembly of real numbers.

As is well known, the existence of the following limit values[1] can be verified[2][1–4]:

$$\lim_{k\to\infty} \frac{1}{\lambda_1^k} A^k {}^0u = \alpha_1 e_1, \qquad {}^0u = {}^0\alpha_1 e_1 + {}^0\alpha_2 e_2 + \ldots + {}^0\alpha_n e_n, \tag{2}$$

$$\min_{(u)} Q = \frac{\bar{u}\ A\ u}{\bar{u}\ u} = \lambda_n, \tag{3}$$

and

$$\max_{(u)} Q = \frac{\bar{u}\ A\ u}{\bar{u}\ u} = \lambda_1, \tag{4}$$

where k is the sequential number of the iteration step, ${}^0\alpha_i$ is the 0^{th} coefficient vector and the vector[3] u in the formulas (3) and (4) run over the whole configuration space, while Q is the so called Rayleigh quotient [5]. The classic iterative procedure, the "power method"[5] consists of consecutive multiplications by a trial vector. In the following section a modification of this method will be described.

Let us examine the following schemes (in the left and right columns the steps of the power method and the modified procedure respectively, are compared):

[1]The superscripts on the left and right of symbols refer to the sequential number of iteration and the exponents, *resp.*

[2]Theorem of von MISES.

[3]$\bar{u}$ is the transpose of u.

$$
\begin{array}{lll}
{}^{1}u = A\,{}^{0}u, & {}^{1}v = {}^{1}u, & \\
{}^{2}u = A\,{}^{1}u, & {}^{2}v = {}^{2}u, & \\
\vdots & \vdots & \\
\vdots & \vdots & \\
{}^{s}u = A\,{}^{s-1}u, & {}^{s}v = {}^{s}u, & {}^{s}w = \hat{B}_s\,{}^{s}v, \\
 & {}^{s+1}v = A\,{}^{s}w, & \\
\vdots & \vdots & \\
\vdots & \vdots & \\
{}^{s+r}u = A\,{}^{s+r-1}u, & {}^{s+r}v = A\,{}^{s+r-1}v, & {}^{s+r}w = \hat{B}_{s+r}\,{}^{s+r}v.
\end{array}
$$

The operator $\hat{B}_s$ performs a non–linear transformation of the trial vector. This step is embedded into the basic procedure and it will repeatedly be applied by using the actual vectors stored in the given cycle.

Now we try to construct the operator $\hat{B}_s$ in such a manner that the vector ${}^{s+1}v = A^s w$ approximates a vector ${}^{k}u$ of the basic procedure where $k>s+1$ (or even more favourably: $k\gg s+1$).

3. Details of the procedure

To define the operator $\hat{B}_s$ we express ${}^{0}u$, ${}^{k}u$, *etc.* by the eigenvectors $\{e_i\}$ in the space used for the computations[4]:

$$
{}^{0}u = \alpha_1 e_1 + \alpha_2 e_2 + \ldots + \alpha_n e_n, \tag{5}
$$

$$
{}^{0}u_i = \alpha_1 x_{i1} + \alpha_2 x_{i2} + \ldots + \alpha_n x_{in}, \tag{6}
$$

$$
{}^{k}u = \alpha_1 \lambda_1^k e_1 + \alpha_2 \lambda_2^k e_2 + \ldots + \alpha_n \lambda_n^k e_n, \tag{7}
$$

$$
{}^{k}u_i = \alpha_1 \lambda_1^k x_{i1} + \alpha_2 \lambda_2^k x_{i2} + \ldots + \alpha_n \lambda_n^k x_{in}. \tag{8}
$$

[4]The coordinates of the eigenvectors in this system are: $\{e_j\} = \{x_{ij}\}$.

By constructing the sequence (2) we obtain:

$$^{k}\tilde{u}_i = \alpha_1 x_{i1} + \alpha_2\left[\frac{\lambda_2}{\lambda_1}\right]^k x_{i2} + \ldots + \alpha_n\left[\frac{\lambda_n}{\lambda_1}\right]^k x_{in} \approx \alpha_1 x_{i1} + M\left[\frac{\lambda_2}{\lambda_1}\right]^k, \tag{9}$$

where M is constant.

Each component vanishes separately according to a function

$$f_{ij}(k) = \gamma_{ij} a_j^k, \tag{10}$$

where $a_j = (\lambda_j/\lambda_1)$ and the meaning of γ_{ij} follows from *eqn.*(9). Regarding (10) and (1) the rate of convergence is apparently determined by the second largest eigenvalue.

Now combining (9) and(10)

$$^{k}\tilde{u}_i = \alpha_1 x_{i1} + \sum_{j=2}^{n} \gamma_{ij} a_j^k \tag{11}$$

is obtained.

The next goal is to determine a single function

$$\Theta_i(t) = \xi_i e^{-\nu_i t}, \quad 0 \le t < \infty \tag{12}$$

which approximates satisfactorily the function[5]

$$F_i(k) = \sum_{j=2}^{n} f_{ij}(k). \tag{13}$$

[5]Function (13) having an integer argument is not a continuous function in contrast to (12) which has a real argument.

Substituting $f_{ij}(k)$ by

$$\varphi_{ij}(t) = \gamma_{ij} e^{-\beta_{ij} t}, \tag{14}$$

then for integer values of t the equality

$$\overset{k}{\tilde{u}}_i = \alpha_1 x_{i1} + \sum_{j=2}^{n} f_{ij}(k) = \alpha_1 x_{i1} + \sum_{j=2}^{n} \varphi_{ij}(t)\Big|_{t=k} \tag{15}$$

will hold. It can readily be shown that as an exact substitute for (13) no function of type (12) is expected to be found. To realize this, let us consider the difference function $\omega_i(t)$ and its derivatives $\omega_i^{(r)}(t)$:

$$\omega_i(t) = \Theta_i(t) - \sum_{j=2}^{n} \varphi_{ij}(t) = \xi_i e^{-\nu_i t} - \sum_{j=2}^{n} \gamma_{ij} e^{-\beta_{ij} t} =$$

$$= \sum_{j=2}^{n} \left[\frac{1}{n-1} \xi_i e^{-\nu_i t} - \gamma_{ij} e^{-\beta_{ij} t} \right], \tag{16}$$

$$\omega_i^{(r)}(t) = (-1)^r \xi_i \nu_i^r e^{-\nu_i t} - \sum_{j=2}^{n} (-1)^r \gamma_{ij} \beta_{ij}^r e^{-\beta_{ij} t} =$$

$$\sum_{j=2}^{n} (-1)^r \gamma_i^r \left\{ \frac{1}{n-1} \xi_i e^{-\nu_i t} - \gamma_{ij} \left[\frac{\beta_{ij}}{\nu_i} \right]^r e^{-\beta_{ij} t} \right\}. \tag{17}$$

From (16) and (17) follows that at a given point, in general, $\omega_i(t)$ and its derivatives can not simultaneously be zero unless one of the following conditions is

fulfilled[6]:

$$\frac{\beta_{ij}}{\nu_i} = 1, \quad j = 2,\ldots,n,$$

$$\beta_{i1} \neq 0, \quad \text{but } \beta_{ij} = 0 \text{ if } j \neq 1,$$

$$\gamma_{i1} \neq 0, \quad \text{but } \gamma_{ij} = 0 \text{ if } j \neq 1.$$

Now for judging the possibility of an approximation, let us examine the behaviour of (15) describing the changes of the components of the iterated vectors in the course of iteration. We represent first (15) in the form

$$\overset{k}{\tilde{u}}_i = \alpha_1 x_{i1} + \sum_{j=2}^{n} \gamma_{ij} e^{-\beta_{ij} t} = \alpha_1 x_{i1} + \left\{ \sum_{j=2}^{n} \gamma_{ij} e^{-z_{ij} t} \right\} e^{-\xi_i t}. \tag{18}$$

The expression in the parentheses can be transcribed as follows:

$$\sum_{j=2}^{n} \gamma_{ij} e^{-z_{ij} t} = \sum_{j=2}^{n} \gamma_{ij} e^{-\delta_i(t) t}, \tag{19}$$

where

$$\delta_i(t) = -\frac{\ln\left[\sum_{j=2}^{n} \gamma_{ij} e^{-z_{ij} t} \Big/ \sum_{j=2}^{n} \gamma_{ij} \right]}{t} =$$

[6]All these cases lie outside the region of practical importance.

$$= -\frac{\ln \sum_{j=2}^{n} d_{ij} e^{-z_{ij} t}}{t}, \tag{20}$$

$$d_{ij} = \frac{\gamma_{ij}}{\sum_{l=2}^{n} \gamma_{il}} \tag{21}$$

and

$$\sum_{j=2}^{n} d_{ij} = 1. \tag{22}$$

The sum in the argument of the logarithm is increasing or decreasing strictly monotonously depending upon the signs of z_{ij}. In the first case ($z_{ij} < 0$) the range of the argument function is between 1 and ∞ if $0 \leq t < \infty$ and the relations[7]

$$\ln \left[\sum_{j=2}^{n} d_{ij} e^{-z_{ij} t} \right] < \ln \left[\sum_{j=2}^{n} d_{ij} e^{-z_{i,\min} t} \right] \equiv$$

$$\equiv \ln(e^{-z_{i,\min} t}) = |z_{i,\max}|^{t} \tag{23}$$

hold.

If the second case ($z_{ij} > 0$) occurs, the argument function ranges between 1 and 0 if $0 \leq t < \infty$ and the relations

$$\ln \left[\sum_{j=2}^{n} d_{ij} e^{-z_{ij} t} \right] < \ln \left[\sum_{j=2}^{n} d_{ij} e^{-z_{i,\min} t} \right] \equiv$$

[7] $z_{i,\min}$ and $z_{i,\max}$ denote the minimum and maximum elements in the set z_{ij}.

$$\equiv \ln(e^{-z_{i,\min}t}) = |z_{i,\min}|^t \tag{24}$$

will be satisfied.

For $z_{ij} < 0$

$$\lim_{t\to\infty} \delta_i(t) = -\frac{\ln e^{|z_{i,\max}|^t}}{t} = -|z_{i,\max}| \tag{25}$$

and for $z_{ij} > 0$

$$\lim_{t\to\infty} \delta_i(t) = -\frac{\ln e^{|z_{i,\min}|^t}}{t} = -|z_{i,\min}| \tag{26}$$

will be valid.

It seems that in any case $\delta_i(t)$ becomes constant in the course of iteration. By using these last results we get an approximation for the exact formula[8]:

$$k\tilde{u}_i = \alpha_1 x_{i1} + \sum_{j=2}^{n} \gamma_{ij} e^{-\delta_i(t)t}\, e^{-\zeta_i t} \approx \alpha_1 x_{i1} + \sum_{j=2}^{n} \gamma_{ij} e^{-(z_{i,\max/\min} + \zeta_i)t}. \tag{27}$$

We expect this approximating formula (27) to be satisfactory for practical purposes only if it is used after having reached the required accuracy.

The computations proceed as follows:

i) Because of the possibility of the presence of negative eigenvalues (in contrast

[8]The subscript max/min means either maximum or minimum in conformity with the former remarks.

to our assumption about the positive semidefinite nature of A), if the accuracy is below a predetermined limit, each second vectors start to be stored. For computational efficiency it is practical and enough to use but three vectors.

ii) The formula (27) will be used in the form

$$^{k}\tilde{u}_i \approx S_i(t) = \Theta_i(t) + K_i. \tag{28}$$

To have a descending sequence, if necessary, the i^{th} components of the vectors used are to be transformed. By supposing that the following equation system can be set up for each component of the trial vector separately, it will be solved for all the unknown parameters[9]:

$$\xi_i e^{-\nu_i k_1} + K_i = {}^{k_1}b_i, \tag{29}$$

$$\xi_i e^{-\nu_i k_2} + K_i = {}^{k_2}b_i, \tag{30}$$

$$\xi_i e^{-\nu_i k_3} + K_i = {}^{k_3}b_i. \tag{31}$$

k_1; $k_2 = k_1 + 2$; $k_3 = k_2 + 2$ are the serial numbers of iteration, ${}^{k_j}b_i$ are the i^{th} components of the iterated vectors, and ξ_i, ν_i and K_i are the unknown parameters to be determined. To get ν_i one has to solve a second order equation, however, ξ_i and K_i are in linear dependence.

[9]It is justifiable to use an equation system, instead of using a least–square type procedure, only if we assume that (27) is exactly valid. Computational experience shows this procedure to be admissible without any significant deterioration concerning the accuracy of the results.

iii) The i^{th} component of the last vector will be replaced by the limit value[10] of (28):

$$\lim_{t\to\infty} S_i(t) = K_i. \tag{32}$$

iv) The original iterative scheme will be continued by repeating the same procedure, until the accuracy is above a predetermined limit.

If there are only positive eigenvaluee, to enchance the efficiency of the procedure three consecutive vectors are to be used in *eqns.* (29–31). In special cases, for increasing the separation of eigenvalues any usual method (*e.g.* raising the matrix to power, *etc.*) can be appealed to.

Examples

The results obtained in the course of testing the procedure are summarized in Table I. In the columns 1, 2 and 3 the dimensions of matrices (MD)[11], the ratios of the total number of iterations (NIR) in the accelerated procedure related to that in the basic procedure and the ratios of the total iteration times (TIR) formed similarly as NIR are displayed. For testing purposes real symmetrical matrices having pseudo random number elements were used.

All the testing examples –quite independently from the dimensions of the matrices used–show the savings in the total numbers and times of iterations mainly to be between 0.4 and 0.6, *i.e.* the acceleration reduces both quantities roughly to the halves of their original values, thus giving hope to expect similar gains at larger matrices. When using a backstorage device for the high dimension of the matrix to be diagonalized, the gain in

[10]If necessary, it has to be retransformed.

[11]The dimensions of matrices were confined to 55 regarding that –for practical reasons– the method was tested on a microcomputer.

computer time is expected to be even larger.

Table I

Data comparing results

MD	NIR	TIR
3	0.52	0.60
3	0.56	0.69
4	0.59	0.68
5	0.60	0.70
6	0.52	0.58
6	0.48	0.52
7	0.60	0.68
8	0.51	0.58
8	0.52	0.55
10	0.51	0.54
10	0.32	0.44
12	0.48	0.51
20	0.51	0.53
30	0.56	0.57
55	0.56	0.57

Acknowledgement

In writing up this paper thanks are due to Dr. Imre Bálint for the consent of using many results of his work, consultations and advice during the period working in my group between January 1985 and July 1987. The support of this work is acknowledged to the Hungarian Ministry of Higher Education (grant Nos. P–437/84. and 746/86).

References

[1] *Varga, R.S.*: Matrix Iterative Analysis. Prentice Hall, Englewood Cliffs, 1962.

[2] *Householder, A.S.*: Principles of Numerical Analysis. McGraw–Hill Book Co., New York, 1953.

[3] *Householder, A.S.*: The Theory of Matrices in Numerical Analysis. Blaisdell, New York, 1964.

[4] *Lánczos, C.*: Applied Analysis. Prentice Hall, Englewood Cliffs, 1961.

[5] *Axelsson, O.*: "Solution of Linear System of Equations: Iterative Methods" in Sparse Matrix Techniques (V.A. Barker, ed.), Springer, Berlin–Heidelberg–New York, 1977.

МЕТОД БЫСТРОЙ ИТЕРАТИВНОЙ ДИАГОНАЛИЗАЦИИ ДЛЯ БОЛЬШИХ МАТРИКСОВ

М.И. БАН

Описана ускоренная техника итеративной диагонализации матриксов, позволяющая сократить время необходимое для проведения расчетов метод особенно полезень, когда скорость конвергенции чрезвычайно мала и итерационный процесс не может быть завершен.

AN ACCELERATION METHOD FOR ITERATIVE QUANTUM CHEMICAL PROCEDURES

MIKLÓS I. BÁN

Institute of Physical Chemistry, Attila József University,

P.O.Box 105, H–6701 Szeged, Hungary

(Received October 26, 1989)

A PROCEDURE CHANGING THE SEQUENCE OF ITERATED VECTORS AT THE SCF LEVEL OF QUANTUM CHEMICAL OR MOLECULAR PHYSICAL COMPUTATIONS INTO A MORE RAPIDLY CONVERGING SEQUENCE IS PRESENTED. THE METHOD IS BASED UPON A NON–LINEAR TRANSFORMATION OF FOCK MATRICES FURNISHING THE ITERATED VECTORS.

Introduction

The acceleration of the convergency rate of iterative quantum chemical or molecular physical calculations involving procedures mainly of SCF or post–SCF types is one of the principal possibilities to obtain results of high accuracy. For instance, when evaluating gradients the wavefunctions are required to be much more accurate than is needed for attaining only energies of satisfactory precision. Especially post–SCF level calculations suffer notoriously from low rate of convergence, however, some groups of compounds (*e.g.* transition metal complexes, organometallic clusters, *etc.*) behave in the same way even at the SCF–level.

These experiences explain the increasing interest in developing methods which reduce the time of computation by accelerating the rate of iteration convergence. The continuously increasing number of papers dealing with such problems retain us from giving a full account of the different theories on this subject. Therefore we only refer to some recent fundamental literatures [1–11] with preceding important papers cited therein. In one of our former papers [12] also a possible way of accelerating iteration was reported,

however, in the present one an even more powerful procedure working at the SCF–level has been described.

Description of the procedure

The minimum of the energy functional is usually searched for in a multi–dimensional parameter space. In the quadratic region around the minimum the general scheme of iteration can be given as a quasi–Newton type procedure. As parameters of the functional the independent elements of the density matrix or the Fock matrix are equally suitable. In SCF calculations the requirement for the conservation of idempotency unfits the density matrix to use it as a parameter vector, nevertheless the Fock matrix seems to remain fully appropriate for this purpose.

In a formal description we have the iteration scheme as follows:

$$ {}^{n}v = {}^{n-1}v - H_0^{-1}\,{}^{n-1}g = {}^{n-1}v - H_0^{-1}\left\{H({}^{n-1}v - {}^{m}v)\right\} = $$

$$ = {}^{m}v + (I - H_0^{-1}H)({}^{n-1}v - {}^{m}v) = G^{n-1}\,{}^{1}v + C(n-1), \qquad (1) $$

where ${}^{1}v$, ${}^{n-1}v$ and ${}^{n}v$ are the parameter vectors (*i.e.* the independent elements of the Fock matrix) belonging to the given iteration step. ${}^{m}v$ is the parameter vector at the minimum, g is the gradient of the energy functional, H is the exact Hessian, H_0^{-1} is the inverse of an approximate Hessian of the energy functional, I is the unit matrix and the meaning of G^{n-1} and $C(n-1)$ are evident from the above equalities[1].

The iterative procedure will converge to the minimum only if

$$ S(G) < 1 \qquad (2) $$

[1]The superscripts on the left and the right refer to the serial numbers of the iteration and to the exponent, *resp.*

holds for the spectral radius[2] of G. When describing (1) by the help of the eigenvectors of G, we obtain that

$$ {}^{n}v_i = \sum_{j=1}^{\nu} \left\{ {}^{m}\alpha_j x_{ij} + \lambda_j^{n-1}({}^{1}\alpha_j x_{ij} - {}^{m}\alpha_j x_{ij}) \right\}, \tag{3} $$

where x_{ij} is the matrix of the eigenvectors, ${}^{m}\alpha_j$ is the coefficient vector at the minimum and ${}^{1}\alpha_j$ is that of the first point. Each vanishing component in (3) diminishes according to the function

$$ f_{ij}(n) = \gamma_{ij}\, \lambda_j^{n-1}, \tag{4} $$

where γ_{ij} stands for $({}^{1}v_i - {}^{m}v_i)$ and the other notations are as previously defined. Using (4) equation (3) turns to a simpler form:

$$ {}^{n}v_i = \sum_{j=1}^{\nu} \gamma_{ij}\, \lambda_j^{n-1} + K_i. \tag{5} $$

After replacing $f_{ij}(n)$ by the continuous function

$$ \varphi_{ij}(t) = \gamma_{ij} e^{-\beta_{ij} t}, \qquad 0 \le t < \infty \tag{6} $$

we get the following equality for integer values of t:

$$ {}^{n}v_i = \sum_{j=1}^{\nu} \gamma_{ij}\, \lambda_j^{n-1} + K_i = \sum_{j=1}^{\nu} \gamma_{ij} e^{-\beta_{ij} t} + K_i \Big|_{t=n-1}. \tag{7} $$

[2] $S(G) = \max_j |\lambda_j|$, where $|\lambda_j|$ are the eigenvalues of G.

Our aim is now to find a single function[3]:

$$\Theta_i(t) = \xi_i \, e^{-\eta_i t}, \qquad 0 \leq t < \infty \tag{8}$$

approximating satisfactorily the summation term in (5):

$$^{n}v_i \approx S_i(t) = \xi_i \, e^{-\eta_i t} + K_i. \tag{9}$$

Let us now accept the statement –as described in *ref.* [13]– that a function of type (8), suitable to mimic in the course of iteration the exact behaviour of the parameter vector, can generally be found, we are going to make extrapolations to infinity by using *eqn.* (9):

$$\lim_{t \to \infty} S_i(t) = K_i. \tag{10}$$

Afterwards, the limit vector (10) will be used as a substitute for the position vector at the minimum searched for. The steps of the procedure at the computational level are as follows:

i) If the accuracy[4] is below a predefined limit[5] then –by collecting only three vectors for computational efficiency– each second vectors[6] start to be stored.

ii) To form a descending sequence, if necessary, the i^{th} components of the parameter vectors used are to be transformed. Upon the supposition that the equation system

[3]We are here not concerned with the conditions of finding such a function. For these details of the basic procedure see [13].

[4]Measured, for instance, as the norm of the difference vector between consecutive Fock matrices.

[5]This is an important condition for the successful application of the method.

[6]In order to have a monotous sequence of elements.

$$\xi_i e^{-\eta_i k_1} + K_i = {}^{k_1}b_i, \tag{11}$$

$$\xi_i e^{-\eta_i k_2} + K_i = {}^{k_2}b_i, \tag{12}$$

$$\xi_i e^{-\eta_i k_3} + K_i = {}^{k_3}b_i \tag{13}$$

can be set up for each component of the parameter vector, this equation system is to be solved for the unknown quantities[7]. In *eqns.* (11–13) k_1, $k_2 = k_1 + 2$, $k_3 = k_2 + 2$ are the serial numbers of iteration, ${}^{k_j}b_i$ are the i^{th} components of the vector ${}^{k_j}v$ and ξ_i, η_i and K_i are the unknown parameters in (9) to be determined. In order to get η_i one has to solve a second order equation while ξ_i and K_i are only linearly dependent.

iii) The i^{th} components of the parameter vector are to be replaced by (10) and –in case of necessity– retransformed.

iv) The original iterative schemes will be continued by repeating the procedure until the accuracy reaches its predetermined limit.

Examples

Although the experience we gathered so far is based on a limited number of computations, yet it shows the following univocal nature of the method: the slower the unaccelerated process converges the larger the savings in iteration steps.

In Table 1 CNDO/2 level computations are illustrated by various molecules (HF, CN^+, CO^{2+} and CO; bond lengths are in parentheses) with and without using the

[7]To use an equation system instead of choosing a least–square procedure we rely on the conjecture that *eqn.* (9) is not an approximation. Computational experience verifies this neglect to be admissible.

acceleration procedure. For practical reasons all the computations were done on a microcomputer[8].

Table I.

SCF convergence of CNDO/2 calculations with and without using acceleration procedure

iteration cycle	convergence indicator*			
	HF (r=139pm)	CN^+ (r=115pm)	CO^{2+} (r=115pm)	CO (r=113pm)
4	3.0E–02	1.2E–02	3.0E–02	2.5E–02
6	4.2E–03	6.7E–03	8.6E–03	8.3E–03
8	1.0E–03	2.1E–03	2.3E–03	2.7E–03
10	2.6E–04	6.8E–04	8.7E–04	8.8E–04
12	6.9E–05	2.7E–07	2.8E–04	2.8E–04
14	1.0E–05	6.7E–05	8.8E–05	9.1E–05
16	6.6E–06	2.3E–05	2.8E–05	2.9E–05
18	4.2E–06	6.7E–06	8.4E–06	8.6E–06
20	1.1E–06	4.6E–06	3.0E–06	3.0E–06
22	—	2.8E–06	9.1E–07	9.9E–07
24	—	—	5.4E–07	6.7E–07
26	—	—	—	4.4E–07
6–8–10#	8.6E–06	2.6E–06	7.1E–07	6.2E–07

*The i^{th} convergence indicator is the norm of difference vector between the i^{th} and $(i+1)^{th}$ Fock matrices.

#The three iterated vectors involved in the acceleration procedure.

Acknowledgement

In writing up this paper thanks are due to Dr. Imre Bálint for the consent of using many results of his work, consultations and advice during the period working in my

[8]This is why the accuracy is relatively low even at the end of iteration, which fact, of course, does not concern the comparabilities of the results.

group between January 1985 and July 1987. The support of this work is acknowledged to the Hungarian Ministry of Higher Education (grant Nos. P–437/84. and 746/86).

References

[1] *Goscinski, O., E.Brändas*: Phys.Rev.182,42(1969).

[2] *Brändas, E.,O.Goscinski:* Phys.Rev. A1,552(1970).

[3] *Roos, B.*: Chem.Phys.Lett.15,153(1972).

[4] *Neilsen, V.B.*: Chem.Phys.Lett.18,225(1973).

[5] *Saunders, V.R., I.H.Hillier*: Int.J.Quantum Chem.7,699(1973).

[6] *Sadlej, A.J.:* Chem.Phys.Lett.58,561(1978).

[7] *Pulay, P.*: Chem.Phys.Lett.,73,393(1980).

[8] *Bacskay, G.B.:* Chem.Phys.61,385(1981).

[9] *Bacskay, G.B.:* Chem.Phys.65,383(1982).

[10] *Zhixing, Ch.:* Chem.Phys.Lett.87,455(1982).

[11] *Pulay, P.:* J.Comput.Chem.3,556(1982).

[12] *Bálint, I., M.I.Bán:* Chem.Phys.Lett.101,153(1983).

[13] *M.I.Bán:*This volume, p.89.

МЕТОД УСКОРЕНИЯ ИТЕРАЦИОННЫХ КВАНТОВО–ХИМИЧЕСКИХ РАСЧЕТОВ

М.И БАН

Представлен метод изменения порядка итерационных векторов SCF уровня квантово–химических и молекулярно–физических расчетов в более быстро конвергируемый ряд. Метод основан на нелинейной трансформации матриксов Фока служащих итерационным векторам.

LOCATION OF STATIONARY POINTS OF POTENTIAL ENERGY SURFACES II. A NEW PROCEDURE FOR FINDING SADDLE POINTS

MIKLÓS I. BÁN

Institute of Physical Chemistry, Attila József University

P.O.Box 105, H–6701 Szeged, Hungary

(Received November 12, 1989)

A NEW, QUASI—NEWTON—TYPE PROCEDURE HAS BEEN DEVELOPED FOR FINDING SADDLE POINTS. BY ASCRIBING THE INDEFINITE OPTIMIZATION PROBLEM TO A POSITIVE DEFINITE ONE THE HIGH NUMERICAL EFFICIENCY CHARACTERISTIC OF THIS CLASS OF ALGORITHMS (IN MINIMIZATIONS) HAS BEEN RETAINED WHILE THE INHERENT PROBLEMS OCCURING IN INDEFINITE OPTIMIZATIONS COULD BE AVOIDED.

Introduction

Theoretical (and in many respects also practical) investigations of chemical reactions require some knowledge of the geometrical features of the Born–Oppenheimer potential energy surfaces.

Among the many geometrical characteristics of the potential surface, the most important ones are the minima, the saddle points and the reaction path. The minima correspond to stable molecular configurations and are characterized by the matrix of second derivatives (Hessian) having only positive eigenvalues. The saddle point of the potential surface is a critical point where the Hessian also has one negative eigenvalue[1]. The reaction path is the unique curve of steepest descent, which starts at the saddle point and goes to the minima. The saddle point corresponds to the transition state of the chemical reaction.

[1]The existence of only one negative eigenvalue (first order saddle point) has only chemical reasons [22], *i.e.* it is not a mathematically motivated restriction.

and represents the maximum of the reaction path.

The main difference between the problems of finding a minimum and a saddle point is significant. Whereas the knowledge of the slope of the surface is enough to reach a minimum, to find a saddle point the curvature of the surface is also needed, the computational work thereby increasing substantially.

In a short survey on the multitude of methods used to determine saddle points, the pioneering work of McIVER and KOMORNICKI [1,2] should be mentioned first. Their algorithm is based on minimization of the square of gradient norm. Since their procedure is theoretically well established, it is widely used in spite of the relatively high numerical cost and the possible collapse to a minimum/maximum. During the past two decades, many other techniques have appeared for finding the transition state [3–8], together with excellent surface walking algorithms [9–13] which are suitable for controlling of the walking process to any kind of stationary points. Quite recently the quasi–Newton methods have begun to be used to locate saddle points [14–19]. Their power in finding minima justifies the significant efforts that have been made to solve the problems which arise when these algorithms are used for indefinite optimizations.

The aim of the present work was to establish a method which does not require the evaluation of the full matrix of second derivatives, but furnishes a high computational efficiency. This intention has been realized in a quasi–Newton–type algorithm using the first derivative of the function and a one–dimensional projection of the Hessian.

The paper is structured in several sections. In Section 1 the frame of quasi–Newton algorithms will be discussed briefly. Section 2A contains the basic idea, while 2B presents the general development of the method. Section 3 discusses the main properties of the algorithm, and Section 4 is devoted to the numerical illustrations. The Appendix gives a short account of the relation of the present method and the BELL-CRIGHTON-FLETCHER [17] algorithm.

1.) The quasi-Newton procedure

To outline the main properties of a quasi–Newton algorithm, a quadratic function will be considered:

$$f(x) = f(x_o) + g_o^t p + \frac{1}{2} p^t G p, \tag{1.1}$$

where f is a scalar, x_o and x are position vectors, g_o ($\equiv g(x_o)$) is the gradient, p ($\equiv dx$) is the change of coordinates, and G is the Hessian[2].

The gradient at point x is given by

$$g(x) \equiv g = g_o + Gp. \tag{1.2}$$

If a symmetric, positive definite H matrix is given (playing the role of an approximation to the inverse of the Hessian), the successive steps (from the k^{th} one) will be generated as follows [21,24–26].

a.) Generation of the step direction:

$$d_k = -H_k g_k, \quad (g^t d_k < 0) \tag{1.3}$$

b.) Estimation of the step-length:

$$x_{k+1} = x_k + \alpha_k d_k, \tag{1.4}$$

$$\alpha_k = \{ \alpha_k \,/\, g^t(x_k + \alpha_k d_k) d_k \equiv g_{k+1}^t d_k = 0 \} = -g_k^t d_k / d_k^t G d_k. \tag{1.5}$$

The parameter α_k is determined by the requirement that the acceptable point (x_{k+1}) must be a local minimum, implying that the gradient (g_{k+1}) has no component along the

[2]Small letters denote scalars and vectors, capital letters matrices, and superscript t refers to transposition.

step–vector.

c.) Evaluation of quantities which can be derived from primary data and *characterize the curvature of the surface:*

$$p_k = x_{k+1} - x_k = \alpha_k d_k, \tag{1.6}$$

$$\gamma_k = g_{k+1} - g_k = G p_k \tag{1.7}$$

(on a quadratic surface, g_{k+1} is given by (1.2)).

d.) The previously evaluated quantities are used to *update the H matrix* by absorbing the information collected on the curvature of the surface. This means that a correction term is added to H_k. Taking the DFP procedure [21,24–26] as an example:

$$H_{k+1}^{\gamma} = H_k \frac{p_k p_k^t}{\gamma_k^t p_k} - \frac{(H_k \gamma_k)(\gamma_k^t H_k)}{\gamma_k^t H_k \gamma_k}. \tag{1.8}$$

The correction ensures a perfect description of the portion of the surface explored by the actual step. This point distinguishes mainly the various quasi–Newton algorithms.

e.) After checking results *stop or return to step a.*

Some important characteristics of the whole quasi–Newton family are the following [21,24–26]:

- one dimensional searches are used successively;
- only the function values and gradients relating to the actual and immediate previous points are used;
- the location of the stationary point of a quadratic function requires (at most) as many steps as the number (n) of independent variables (quadratic convergence property).

For an indefinite matrix, non–zero (singular) vector(s) exist(s), satisfying the relation:

$$d_1^t G d_1 = 0. \tag{1.9}$$

If a quasi–Newton algorithm is applied to an indefinite objective function, such a singular vector may cause the total breakdown of the algorithm. Neither the step–length nor the update (1.8) of the H matrix can be defined [18].

When a native quasi–Newton algorithm is used, the presence of a negative eigenvalue prevents the approximation of the saddle point by an incorrect choice [11] of the search direction, even in the absence of a singular direction of search.

The existing techniques [14–18] developed for handling such functions explicitly modify a parent quasi–Newton method for adaption to identify optimization problems.

The framework of this very significant class of algorithms has been presented briefly in order to show the most important problems which occur when these methods are applied to indefinite objective functions.

In the following sections the theoretical background and technical aspects of the present algorithm will be discussed.

2.) Definition of the method

A. Qualitative considerations

The idea of the present algorithm was born from the intention to exploit the full computational efficiency of the quasi–Newton methods by avoiding somehow the problems of their application to indefinite functions.

Instead of modifying the algorithm itself, it seemed more attractive to define a new (associated) surface, which is convex and contacts the original surface at its saddle point.

This means that (in the sense of the idea) the two surfaces are in a first–order touching contact characterized by identical function values and first derivatives, but their

second derivatives differ in nature. While the critical point of the original surface is a saddle point, the "associated convex surface" has a minimum with the same coordinates.

The introduction of an associated convex surface would allow the application of quasi–Newton methods to find the minimum, which is located at the same point as the saddle point of the original surface .

B. The family of "associated convex surfaces"

Let the quadratic surface be determined by (1.1) and let its Hessian have one negative eigenvalue ("saddle surface"). Because of the quadratic nature of the function, the surface is unambiguously defined if the coordinates of the stationary point and its Hessian are known.

Let the eigenvectors and eigenvalues of G be

$$\{ u_i \} , \{ \lambda_i \} ; \qquad i \in [1,n] \tag{2.1}$$

and let a set of independent vectors be given:

$$\{ z_i \} , \qquad i \in [1,n] \tag{2.2}$$

which satisfy the following inequalities:

$$z_1^t \, G \, z_1 < 0, \tag{2.3}$$

$$z_j^t \, G \, z_j > 0 ; \qquad j \in [2,n] \tag{2.4}$$

and

$$z_i^t \, G \, z_j = z_i^t \, w_j = 0 ; \qquad \forall (i \neq j). \tag{2.5}$$

Relations (2.3) and (2.4) account for the indefiniteness of G, while (2.5) expresses the conjugated nature of the vectors (2.2) and the biorthogonality[3] of the dual vector pairs:

$$\{ z_i \} \text{ and } \{ w_i = Gz_i \} ; \qquad i \in [1,n]. \tag{2.6}$$

With the help of the specially chosen vector systems (2.1) and (2.2), projector matrices will first be constructed:

$$P_n^{(u)} = \overline{P}_n^{(u)} = \sum_{i=1}^{n} u_i u_i^t, \tag{2.7}$$

$$P_n^{(z)} = \sum_{i=1}^{n} \frac{w_i z_i^t}{w_i^t z_i}, \tag{2.8}$$

$$\overline{P}_n^{(z)} = \sum_{i=1}^{n} \frac{w_i z_i^t}{z_i^t w_i}, \tag{2.9}$$

where $P_n^{(u)}$ and $\overline{P}_n^{(z)}$ denote adjoint matrices. The projectors are of rank n, and yield the identity:

$$x = P_n^{(u)} x = P_n^{(z)} x = \overline{P}_n^{(z)} x \tag{2.10}$$

and the general projector property:

$$P_n^{(u)} = P_n^{(u)^2} ; \qquad P_n^{(z)} = P_n^{(z)^2} ; \qquad \overline{P}_n^{(z)} = \overline{P}_n^{(z)^2}. \tag{2.11}$$

(In general, our statements will be formulated with the help of the (orthogonal) eigenvectors (2.1) and the biorthogonal vector systems (2.6).)

Through the use of (2.7)–(2.9) the Hessian and its inverse will be represented in

[3]The upper/lower indices for contravariant/covariant vectors will not be used.

factorized forms:

$$G = P_n^{(z)} G\, P_n^{(z)} = \sum_{i=1}^{n} \frac{w_i w_i^t}{z_i^t w_i} = P_n^{(u)} G\, P_n^{(u)} = \sum_{i=1}^{n} \lambda_i u_i u_i^t, \tag{2.12}$$

$$G^{-1} = P_n^{(z)} G^{-1} P_n^{(z)} = \sum_{i=1}^{n} \frac{z_i z_i^t}{w_i^t z_i} = P_n^{(u)} G^{-n}\, P_n^{(u)} = \sum_{i=1}^{n} \lambda_i^{-1}\, u_i u_i^t. \tag{2.13}$$

The sign of the individual terms in (2.12) and (2.13) depend on the signs of the diagonal elements

$$\left\{\lambda_i\right\}; \qquad \left\{z_i^t\, w_i = z_i^t G z_i = w_i^t G^{-1} w_i\right\} \tag{2.14}$$

of the Hessians transformed by the (congruence) transformations

$$\left[U^t\right] G \left[U\right]; \qquad \left[Z^t\right] G \left[Z\right]; \qquad \left[W^t\right] G^{-1} \left[W\right] \tag{2.15}$$

into new (orthogonal and non–orthogonal) vector systems. ([U], [Z] and [W] are matrices whose columns are vectors { u_i }, { z_i }, { w_i } ; i$\in$ [1,n].) Since the number of diagonal elements having negative, zero and positive signs is conserved by the congruence transformation (SYLVESTER inertia theorem [23]). The number of terms with a given sign in (2.12) and (2.13) is equal to the number of eigenvalues with the same sign.

As our future aim is to manipulate the signs of the individual terms in (2.12) and (2.13), the (reflector) matrices

$$B^{(u)} = I - 2\, u_1 u_1^t, \tag{2.16}$$

$$B^{(z)} = I - 2\, \frac{w_1 z_1^t}{z_1^t w_1} \tag{2.17}$$

will be introduced (I is the identity matrix[4]).These matrices change the sign of that component of a vector which is parallel to u_1 or z_1.

With the help of (2.16) and (2.17) new matrices (of second derivatives) will be constructed by evaluating the following products:

$$B^{(u)}G = -\lambda_1 u_1 u_1^t + \sum_{j=2}^{n} \lambda_j u_j u_j^t, \tag{2.18}$$

$$B^{(z)}G = -\frac{w_1 w_1^t}{z_1^t w_1} + \sum_{j=2}^{n} \frac{w_j w_j^t}{z_j^t w_j}. \tag{2.19}$$

(It has been assumed that the Hessian has one negative eigenvalue ordered on the first place.) The negative signs (introduced only into the first terms) ensure the positive definiteness:

$$x^t(B^{(u)}G)x > 0; \qquad \forall\, t \in R^n, \tag{2.20}$$

$$x^t(B^{(z)}G)x > 0; \qquad \forall\, t \in R^n. \tag{2.21}$$

The first Hessian (2.18) differs from G in the reversion of the sign of the first eigenvalue. It therefore determines a convex surface the main curvature of which has been the same absolute values as G. The second new Hessian (2.19) represents a somewhat different case. To show this, the effect of multiplication by the projectors (from the left and right in (2.12) and (2.13)) has to be investigated. This is a two–step procedure, consisting of a congruence transformation (2.15) converting G into a non–orthogonal basis, and a back–transformation by the inverse matrices. The congruence transformation into a non–orthogonal basis changes the values of the diagonal elements. The multiplication by (2.17) reverses the sign of the first term, and therefore the back–transformation provides a

[4]They have also the following property:

$$I = B^{(u)^2} = B^{(z)^2}.$$

new Hessian (2.19) having main curvatures[5] (*even in absolute values*) other than G.

By this point, two Hessians (2.18) and (2.19) have been constructed, both of them determining convex surfaces. The first matrix (2.18) requires a knowledge of the eigenvector relating to the (one) negative eigenvalue and determines a surface of fully identical shape in the subspace of eigenvectors relating to the positive eigenvalues. The second matrix (2.19) requires exclusively a knowledge of a vector (z_1) satisfying the relation

$$z_1^t \, G \, z_1 = z_1^t \, w_1 < 0 \tag{2.22}$$

and determines a surface differing from G in its curvature properties, in the "positive subspace" too. Since the eigenvectors are usually not known, only this last case is of practical significance. This last surface will henceforward be referred to as the "associated convex surface".

Although the associated convex surface has different main curvatures (also in absolute values) from those of the original surface (determined by G), the position of the critical point (where the gradient is the zero–vector) remains unaffected. This implies that the critical points of the two surfaces are common first–order touching points, *i.e.* their function values and first derivatives are equal:

$$f(x_{cr}) = \tilde{f}(x_{cr}), \tag{2.23}$$

$$g(x_{cr}) = \tilde{g}(x_{cr}) = 0, \tag{2.24}$$

where x_{cr} is the coordinate of the critical point, and the designation $\sim$ will denote quantities defined on the convex surface.

[5]The difference between the convex surfaces determined by $B^{(u)}G$ (2.18) and $B^{(z)}G$ (2.19) depends on the non–orthogonality of the basis vectors $\{z_i\}$.

The associated convex surface depends on the choice of the vector (z_1) fulfilling the condition (2.22). Since an infinite number of such suitable vectors exists, an infinite numbers of surfaces contact at the critical point constitute the "family of associated convex surfaces".

The coincidence of the critical points (relating to the saddle–surface and the associated surface) allows a search for a minimum instead of a saddle point of identical location. This fact is of particular importance in establishing the new algorithm.

3.) The algorithm

The frame of the algorithm strictly follows the ideas described previously. Only the main properties will be discussed in a form which is rather 'conceptual' regarding that a detailed and neat program description will be presented (as a manual) elsewhere[6].

A. Generation of the convex surface

To show clearly the mechanism of the algorithm, a quadratic function will be considered with a Hessian having one negative eigenvalue[7].

There are two explicit requirements:

– an objective function to have a form which allows the evaluation of its first derivative is assumed,

– the existence of a vector (z_1) which fulfills condition (2.22) is assumed.

A suitable guess for z_1 is usually the line–segment connecting the minima at the "endpoints" of the reaction path (or an initial Hessian can provide a good choice). The vector w_1 will first be evaluated (by a finite difference):

$$w_1 = g_2 g_1 = G z_1 \tag{3.1}$$

[6]The FORTRAN code of the program is available, and it will also be submitted for distribution to the QCPE. On request copies will be sent by the author.

[7]The extension to higher–order saddle points (which have more than one negative eigenvalues) involves no new theoretical problem.

following afterwards the construction of (2.17).

If the reference frame is fixed to the stationary point, the gradient (at point x) of the saddle–function is given by

$$g(x) = G\,x \tag{3.2}$$

and the gradient of the associated convex function by

$$\tilde{g}(x) = B^{(z)}G\,x = B^{(z)}g(x). \tag{3.3}$$

The function value (at any general point) of the associated convex function can not be drawn from the data relating to the saddle–surface. The information on the associated convex function is therefore restricted (at any general point) to its derivative(s). This means that (in the course of searching) the associated convex surface is given only partially, without its function value. A full description of the surface becomes possible *a posteriori*, if the function value at the stationary point fixes the position of the graph of the function. Fortunately, the function value (of the saddle–function) is not necessary at all for the perfect working of the algorithm, and this substantially reduces the computational work.

B. The linear search

As the function value of the associated convex function is lacking, the line–search must be made without any reference to it. The point acceptable as a local stationary point has to be determined by the condition (see (1.5)):

$$\tilde{g}_{k+1}^{t}\,\tilde{d}_k = \epsilon \approx 0. \tag{3.4}$$

The important pecularities of the performance of the line–search do not influence its

structure and therefore they will not be discussed here.

C. Updating of the matrix–H

Again, an example (see (1.8)) by the DFP [21] procedure:

$$\tilde{H}_{k+1} = \tilde{H}_k + \frac{\tilde{p}_k \tilde{p}_k^t}{\tilde{\gamma}_k^t \tilde{p}_k} - \frac{(\tilde{H}_k \tilde{\gamma}_k)(\tilde{\gamma}_k^t \tilde{H}_k)}{\tilde{\gamma}_k^t \tilde{H}_k \tilde{\gamma}_k}, \tag{3.5}$$

$$\tilde{\gamma}_k = \tilde{g}_{k+1} - \tilde{g}_k, \tag{3.6}$$

$$\tilde{p}_k = x_{k+1} - x_k = \tilde{\alpha}_k \tilde{d}_k. \tag{3.7}$$

Although the formula (3.5) contains quantities relating to the associated convex surface the strict formal identity with the parent update scheme is obvious.

If the above conceptual modifications are introduced into a quasi–Newton algorithm, the new algorithm will be able to locate saddle points. Without going into details, the separate steps will be formally the same as in Section 1, but the designated quantities

$$\tilde{d}_k, \tilde{p}_k, \tilde{\alpha}_k, \tilde{g}_k, \tilde{\gamma}_k, \tilde{H}_k \tag{3.8}$$

in relation to the associated convex surface will appear everywhere.

The whole discussion so far referred to a quadratic objective function having a Hessian with one negative eigenvalue. For general functions, the structure of the algorithm remains the same as already defined, but minor changes and restrictions are indispensable to ensure the necessary conditions.

For non–quadratic functions, the Hessian has only a local meaning sense, so the reflector matrix will also be locally defined:

$$B^{(z)}(x) = I - 2\frac{w_j(x)z_j^t}{z_j^t w_j(x)} \tag{3.9}$$

and

$$\tilde{g}(x) = B^{(z)}(x)\, g(x). \tag{3.10}$$

All other quantities differ from those in the quadratic case by the appearance of (3.10). The vector z_j is constant but $w_j(x)$ will be reevaluated at any point. In consequence of the local character of the quantities the algorithm is defined in a region where the condition

$$z_j^t w_j(x) < 0 \tag{3.11}$$

is fulfilled.

A continuous approach to the stationary point is ensured only in that area where the Hessian has the assumed one negative eigenvalue.

To reach higher–order saddle points separate matrices (3.9) are needed for each independent direction of negative curvature.

The properties peculiar to the present quasi–Newton–type procedure have been discussed while other characteristics conform to the general behaviour of the whole quasi–Newton family.

To summarize the leading aspects:

i) The algorithm is defined in a region where a constant vector exists, pointing in the direction of negative curvature. It is assumed implicitely that the Hessian has one negative eigenvalue.

ii) On construction of the reflector matrix (3.9) the gradient of an "associated convex surface" can be obtained through (3.10). The convex surface is only partially defined by its derivative(s) and evaluation of the function value of the original (saddle–) function is not necessary.

iii) Through the use of the quantities (3.8) relating to the associated convex surface, any quasi–Newton algorithm (with the minor technical changes mentioned) will provide a minimum at the same coordinates as those of the saddle point of the original surface.

4.) Applications

The algorithm has been tested on various model surfaces and quantum chemical problems. Although the BFGS [21] and DFP [21] methods can equally be used, the examples will refer to the DFP algorithm.

A. The Adams model–potential [12]

$$E(x_1,x_2) = 2x_1^2(4 - x_1) + x_2^2(4 + x_2) - x_1x_2(6 - 17e^{-r^{0.5}}) \qquad (4.1)$$

has a minimum and two saddle points. The walk from the point (1.8,–0.2) to one of the saddle points is displayed in Table I.

The following quantum chemical examples have been chosen to test the efficiency of the algorithm in comparison with other procedures. BAKER's paper [27] presents convergence data of several rearrangement reactions. These computations have been done by the SIMON's algorithm [12] which was implemented and incorporated into the standard GAUSSIAN 82 program package. The tests of the present algorithm are relating to

Table I

	x_1	x_2	RMS gradient
1.	1.8000	–0.2000	11.5258
2.	1.9529	0.6489	3.9571
3.	2.2613	0.4625	0.5322
4.	2.2408	0.4415	0.4146E-02
5.	2.2410	0.4411	0.2236E-04
6.	2.2410	0.4411	0.4909E-14

CNDO/2 calculations. For the sake of comparison, the starting geometrical parameters were chosen to the same relative value with respect to the optimized parameters, as in the reference examples. The accuracy of the computations was also identical (RMS gradient 0.0003). The direction of negative curvature (z_1) was estimated for the vector pointing from the one minimum to the other.

It has to be mentioned, that SIMON's algorithm requires an analytically evaluated starting Hessian, while the present method requires only the direction/(and value) of the negative curvature.

B. The HCN ⟶ CNH reaction[8]

PM	G82	POP	SIM
7(12)	10(?)	9(?)	8(?)

(Final geometry: r(CN) = 1.221 Å, r(CH) = 1.121 Å, φ(HCN) = 87.14°)

C. The FCN ⟶ CNF reaction[9]

In BAKER's example [27] the start position was chosen very near to the minimum, and the Hessian has here only positive eigenvalues. This position is outside the region where the conditions of the present algorithm are fulfilled. In this case the midpoint of the line segment connecting the minima was used as a starting configuration

[8]The abbreviations used have the following meaning:
PM = present method
G82 = method of the standard GAUSSIAN 82 program package
POP = POPPINGER's method [3]
SIM = SIMON's method [12]
y(x) = y steps and x gradient evaluations

[9]see footnote 8

PM	G82	POP	SIM
8(13)	failed	15(?)	13(?)

(Final geometry: r(CN) = 1.263 Å, r(CF) = 1.333 Å, φ(FCN) = 93.30°)

The program system realizing the above ideas is able to locate also minima and points of (so called) gradient extremal curves [20,28]. Along a curve of this type, it is always possible to reach that region where the Hessian already has the required one negative eigenvalue.

D. The optimization of CH_3F[10]

The optimization of the structure of methyl fluoride is presented to show the working of the algorithm in minimizations. The efficiency of the program system is due to some particular modifications of the linear searching and updating steps respectively.

PM	G82	SIM
8(18)	11(?)	11(?)

(Final geometry: r(CF) = 1.344 Å, r(CH) = 1.118 Å, φ(FCH) = 109.30°)

Appendix

Under certain conditions the BELL–CHRIGHTON–FLETCHER (BCF) algorithm [17] and the present one generate an identical succession of points.

The procedure [17] is based on a separation of the n–dimensional space into a one–dimensional and (conjugated) (n–1)–dimensional subspaces. The functions will be

[10]see footnote 8

maximized in the one–dimensional subspace, while it will be minimized in the conjugated subspace. For general functions these steps will be repeated cyclically.

It will be shown that for a quadratic function (see (1.1)) identical steps will be produced by both algorithms, if the first step of the present procedure is a pure maximization. To illustrate the reason for this, those steps will be examined which are generated by the algorithms considered.

From the start point x, along the search direction z_i (see relations (2.2)–(2.6)) the BCF algorithm yields a step of length α_i:

$$0 = z_i^t g(x + \alpha_i z_i) = z_i^t g(x) + \alpha_i z_i^t G z_i, \tag{A.1}$$

$$\alpha_i = -\frac{z_i^t g(x)}{z_i^t G z_i}. \tag{A.2}$$

The first step is taken uphill in the BCF algorithm (*i.e.* $z_i \equiv z_1$), therefore

$$z_1^t g(x) > 0. \tag{A.3}$$

The vector z_1 satisfies condition (2.3) implying the relation:

$$\alpha_1 > 0. \tag{A.4}$$

The present algorithm determines a step of length from the same start point x, along the search direction c_i:

$$0 = c_i^t B^{(z)} g(x + \beta_i c_i) = c_i^t B^{(z)} g(x) + \beta_i c_i^t B^{(z)} G c_i, \tag{A.5}$$

$$\beta_i = - \frac{c_i^t B^{(z)} g(x)}{c_i^t B^{(z)} G c_i} \tag{A.6}$$

($B^{(z)}$ has been defined by (2.17).)

If the first step of the present procedure fulfills the identity

$$c_1 \equiv z_1 \tag{A.7}$$

then, because of the equality

$$B^{(z)} w_1 = - w_1, \tag{A.8}$$

the following relations are valid simultaneously:

$$c_1^t B^{(z)} g(x) < 0, \tag{A.9}$$

$$| c_1^t B^{(z)} g(x) | = | z_1^t g(x) | \tag{A.10}$$

and

$$c_1^t B^{(z)} G c_1 > 0, \tag{A.11}$$

$$| c_1^t B^{(z)} G c_1 | = | z_1^t G z_1 | \tag{A.12}$$

implying the identity

$$\beta_1 \equiv \alpha_1. \tag{A.13}$$

For those directions of search which are in the subspace conjugated to z_1, the matrix $B^{(z)}$ has no effect at all. The steps in the "positive subspace" are therefore identical.

While the above separation of the optimization problem (into pure maximization and pure minimizations) is an inherent basic assumption in the BCF algorithm, it is a special possible case in the present procedure.

Acknowledgement

In writing up this paper thanks are due to Dr. Imre Bálint for the consent of using many results of his work, consultations and advice during the period working in my group between January 1985 and July 1987. The support of this work is acknowledged to the Hungarian Ministry of Higher Education (grant Nos. P–437/84. and 746/86).

References

[1] *McIver,J.W., Komornicki,A:* J.Am.Chem.Soc.84,2625 (1972).

[2] *Komornicki,A., K.Morokuma, K.Ishida, R.Ditchfield, M.Conrad:* Chem.Phys.Lett.45,595 (1977).

[3] *Poppinger,D.:* Chem.Phys.Lett., 35, 550 (1975).

[4] *Halgren,T.A., W.N.Lipscomb:*Chem.Phys.Lett.43, 225 (1977).

[5] *Müller,K., L.D.Brown:* Theor.Chim.Acta 53,75 (1978).

[6] *Schlegel,H.B.:* J.Comp.Chem. 3,214 (1982).

[7] *Rothman,M.J., L.L.Lohr:* Chem.Phys.Lett. 70, 405 (1980).

[8] *Kato,S., K.Morokuma:* J.Chem.Phys. 73, 3800 (1980).

[9] *Crippen,G.M., H.A.Scheraga:* Arch.Biochem.Biophys. 144, 462 (1971).

[10] *Cerjan,C.J., W.H.Miller:* J.Chem.Phys. 75, 2800 (1981).

[11] *Simons,J., P.Jorgensen, H.Taylor, J.Ozment:* J.Phys.Chem. 87, 2745 (1983).

[12] *Banarjee,A., N.Adams, J.Simons, R.Shepard:* J.Phys.Chem. 89, 52 (1985)

[13] *Taylor,H., J.Simons:* J.Phys.Chem. 89, 684 (1985).

[14] *Pulay,P., G.Fogarasi, F.Pang, J.E.Boggs:* J.Am.Chem.Soc. 101, 2550 (1979).

[15] *Sinclair,J.E., R.Fletcher:* J.Phys. C7, 864 (1974).

[16] *Fletcher,R.:* Conj.Grad.Meth.for Ind.Syst.;Proc.of the 1975 Dundee Num.Anal.Conf.; Springer–Verlag, Berlin, p73–89 (1975).

[17] *Bell,S., S.Crighton, R.Fletcher:* Chem.Phys.Lett. 82, 122 (1981).

[18] *Oren,S.S.:* J.Opt.Theor.Appl. 43, 167 (1984).

[19] *Bálint,I., M.Bán:* Theor.Chim.Acta 63, 255 (1983).

[20] *Bálint,I., M.Bán:* Int.J.Quant.Chem. 25, 667 (1984).

[21] *Fletcher,R.:* Practical Methods of Optimization;Vol.1, Wiley, New York, 1980.

[22] *Murrell,J.N., K.J.Laidler:* Trans.Far.Soc. 64, 371 (1978).

[23] *Parlett,B.N.:* The Symmetric Eigenvalue Problem, Prentice–Hall Ser.in Comp.Math., Englewood Cliffs, 1980.

[24] *Gill,P.E., W.Murray, M.H.Wright:* Practical Optimization, Academic Press, New York, 1981.

[25] *Powell,M.J.D. (ed):* Non–linear Optimization, Academic Press, New York, 1982.

[26] *Scales,L.E.:* Introduction to Non–linear Optimization, Macmillan, Basingstoke, 1985.

[27] *Baker,J.:* J.Comp.Chem. 7, 385 (1986).

[28] *Hoffmann,D.K.,* R.S.*Nord, K.Ruedenberg:* Theoret. Chim. Acta 69, 265 (1986).

РАСПОЛОЖЕНИЕ СТАЦИОНАРНЫХ ТОЧЕК ПОВЕРХНОСТЕЙ ПОТЕНЦИАЛЬНОЙ ЭНЕРГИИ II. НОВЫЙ МЕТОД ДЛЯ НАХОЖДЕНИЯ СЕДЛОВЫХ ТОЧЕК

М.И. БАН

Разработан новый квази–ньютоновский метод для нахождения седловых точек. При преобразовании проблемы неопределенной оптимизации в положительно определенную, сохранена высокая нумерическая эффективность (в минимализации) характерная для этого класса алгоритмов. В то же время органические проблемы, возникающие в неопределенных оптимизациях, могут быть избежены.

LIST OF PAPERS, PUBLISHED BY THE AUTHORS OF THE DEPARTMENT OF PHYSICS AND THE DEPARTMENT OF CHEMISTRY, IN SCIENTIFIC JOURNALS, DURING 1989.

DEPARTMENT of PHYSICS

Institute of Experimental Physics

1. *Ambrózy A., E. Hähn, L.B. Kiss Gy., Trefán:* Study of the carrier transport in thick film resistors by 1/f noise measurements. Active and Passive Electronic Components 13, 191 (1989).
2. *Burista F., L. Nánai R., Vajtai I., Hevesi:* Physical fundamentals of laser–heat treatment (in Hungarian), Gépgyártástechnológia 29, 181 (1989).
3. *Galeczki G., J. Hajdu, L.B. Kiss:* Note on the interrelation between low–frequency dielectric response and 1/f noise in condensed matter systems. Sol. State Comm. 72 1131 (1989).
4. *Gingl Z., L.B. Kiss, R.Vajtai:* $1/f^k$ noise generated by scaled Brownian motion. Sol. State Comm. 71, 765 (1989).
5. *Kirichenko N.A., E.A. Morozova, A.V. Simakhin, L. Nánai:* Peculiarities of CW–CO_2 and YAG laser ignition of metals in air. Infrared Physics 29, 427 (1989).
6. *Kiss L.B., Gy. Trefán, K. Tompa, I. Hevesi, G. Gévay, A. Lovas:* 1/f noise in glassy metal ribbons. Physica Scripta 39, 771 (1989).
7. *Kiss L.B.:* A (high T_c) superconductor sample arragement of bistable nature. Sol. State Comm. 69, No. 3. 259 (1989).
8. *Kiss, L.B., J. Hajdu:* Transient diffusion 1/f noise model. Sol. State Comm. 72, 799 (1989).
9. *Mogyorósi, P. K. Bali Zs. Tóth I. Hevesi:* Pulsed laser ablative deposition of thin matal films. Applied Surface Science 36, 157 (1989).

10. *Holnár M.*: The application of Light Emitter Diodes in a simple physical. experiments (in Hungarian). Fizikai szemle 7, 264 (1989).

11. *Nánai L. V. Volken*: Sound speed anisotropy of V_2O_5 single crystals determined by laser generated acustic waves. Sol. State Comm. 70, 223 (1989).

12. *Nánai L., F. Vajtai, I. Kovács, I. Hevesi*: On the kinetics of laser–light–induced oxidation constans of vanadium. J. of Less–Common–Metals 152, L23 (1989).

13. *Nánai L., I. Hevesi, B.S. Luk'yanchuk, A.S. Rogachev, A.V. Simakhin, N.M. Sukhonkina, G.A. Shafeev:* Characteristic of laser–heated Titanium in a Nitrogen atmosphere. Acta Physica Hungarica 65, 405 (1989).

14. *Nánai L., I. Hevesi, V.A. Bobyrev, F.V. Bumkin, B.S. Luk'yanchuk, D.T. Alimov, S.A. Ubaydullaev, P.H. Habibullaev:* Dissipative structures and spiral waves at laser light induced oxidation of metals. Infrared Physics 29, 423 (1989).

15. *Nánai L., I. Hevesi, F.V. Bumkin, B.S. Luk'yanchuk, M.R.Brook, G.A. Shafeev, D.A. Jelski, Z.C. Wu, T.F. George:* Laser–induced metal deposition on semiconductors from liquid electrolytes. Appl. Phys. Lett., 54, 736 (1989).

16. *Simon P.:* Time–resolved ablation–site photography of XeCl–laser irradiated polyimid. Appl. Phys., B48, 253 (1989).

17. *Szatmáry, K., G.Dömény:* RS Cygni 1980–1987 (in Hungarian), Meteor, 1, 45 (1989).

18. *Szatmáry, K.*: Stellar Wind (in Hungarian). Föld és ég, 24, 265 (1989).

19. *Szatmári, S., G. Kühnle, J.Jasny, F.P. Schäfer:* KrF laser system with corrected pulse front and compressed pulse duration. Appl. Phys., B49, 239 (1989).

20. *Szatmári, S.:* Pulse shortening of $5x10^3$ by the combined pulse forming of dye oscillators, saturated amplifiers and gated saturable absorbers. Opticand Quantum Electronics, 21, 55 (1989).

21. *Szörényi, T., F. Piglmayer, D. Bäuerle:* Pyrolitic laser–induced chemical vapor depositon (LCVD) of microstructures. Proc., SPIE 1033, 319 (1989).

22. *Szörényi, T., Zs. Tóth:* Pulsed laser synthesis and printing of compound semiconductors. Proc., SPIE 1022, 93 (1989).

23. *Ursu, I., M.I. Birjega, I.N. Mihailescu, N. Popescu-Pogrion, L. Ribco, I. Ketskeméty, L. Nánai, E. Szil:* Crystallization of unsupported amorphous chromium films by 60 ns (0.694 m) single laser pulse. Rev. Roum. Phys., 34, 195 (1989).

24. *Wu, Z.C., D.A. Jelski, T.F. George, L. Nánai, I. Hevesi, F.V. Bunkin, B.S. Luk'yanchuk, M.R.Brook, G.A. Shafeev:* Model of laser–induced deposition on semiconductors from liquid electrolytes. Chemistry of Materials, 1, 353 (1989).

Institute of Optics and Quantum Electronics

1. *Bor, Zs.:* Distortion of femtosecond laser pulses in lenses. Optics Letter, 14, 119 (1989).

2. *Bor, Zs., Z. Gogolák, G. Szabó:* Femtosecond–resolution pulse–front distortion measurement by time–of–flight interferometry. Optics Letters, 14, 862 (1989).

3. *Feldman, J., R. Sattman, E.O. Göbel, J. Kuhl, J. Hebling, K. Ploog, R. Muralidharan, P. Dawson, C.T. Foxon:* Subpicosecond real–space charge transfer in type–II GaAs/AlAs superlattices. Physical Review Letters, 62, 1892 (1989).

4. *Hebling, J.:* Q–switched picosecond dye laser pumped by an excimer laser. Applied Optics, 28, 417 (1989).

5. *Hebling, J., J. Klebniczki, P. Heszler, Zs. Bor, B. Rácz:* Travelling have amplified spontaneous emission excited in a prismatic geometry. Applies Physics, B48, 401, (1989).
6. *Hebling, J., J. Kuhl:* Generation of tunable femtosecond pulses by travelling wave amplification. Optics Comm., 73, 375 (1989).
7. *Hebling, J., J. Kuhl:* Generation of femtosecond pulses by travelling wave amplified spontaneous emission. Optics Letters , 14, 278 (1989).
8. *Heszler, P., Zs. Bor, G. Kovács, G. Szabó:* Cu–vapor laser–excited short pulse dye laser. Applied Spectroscopy, 43, 728 (1989).
9. *Heszler, P., Zs. Bor, G. Hajos:* Incubation process in polyimid upon UV photoablation. Appl. Phys., A49, 739 (1989).
10. *Kovács, G., P. Heszler, Zs. Bor, J. Hebling, J. Klebniczki:* Improved jitter and long–term stability of N_2 lasers. J. Phys. E: Sci. Instrum., 22, 940 (1989).

Institute of Theoretical Physics

1. *Kapuy, E., C. Kozmutza, Zs. Ozoróczy:* Ab initio method for treatment of spatially extended systems I., II. and III. Acta Phys. Hung., 65, 85 (1989).
2. *Benedict, M.G., A.I. Zajcev, V.A. Malysev, E.D. Trifonov:* Резонанцное взанмодействне ультракороткого импулса света с тонкой пленкой (in Russian). Оптика и шпектроскопия, 66, 4, 726 (1989).
3. *Benedict, M.G., L.Gy. Fehér:* Quantum jumps, geodesics and topological phase. Physical Review D, 39, 10, 3194 (1989).
4. *Benedict, M.G., L.Gy. Fehér, Z. Horváth:* Monopols and instantons from Berry's phase. J. Math. Phys., 30, 8, 1727 (1989).

DEPARTMENT of CHEMISTRY

Institute of Applied Chemistry

1. *Fejes, P., I. Kiricsi, Gy. Tasi, I. Hannus, I. Bertóti, T. Székely:* Thermogravimetric and infrared spectroscopic investigations on the interactions between mordenites and phosgene. Zeolites, 9, 392 (1989).

2. *Fejes, P. H. Förster, I. Kiricsi, Gy. Tasi:* Transformation of allene over acidic and nonacidic zeolites, Poster at 8th Int. Zeol. Conf., Recent Research Rep., p.465 Amsterdam, 1989.

3. *Halász, J., K. Varga, P. Fejes:* Selective ammoxidation of propene over promoted tin–antimony mixed oxide catalysts. J. Mol. Catal., 51, 303 (1989).

4. *Kiricsi, I., H. Förster, Gy. Tasi:* Formation of carbocations from C_6 compound in zeolites. Stud. Surf. Sci. Catal., 46, 355 (1989).

5. *Kiricsi, I., Gy. Tasi, P. Fejes, F. Berger:* Adsorption of propene in zeolites possessing different adsorption energies. J. Mol. Catal., 51, 341 (1989).

6. *Kiricsi, I., H. Förster, Gy. Tasi, P. Fejes:* Chemisorption of neopentane in zeolites studied by UV–VIS spectroscopy. J. Catal., 115, 597 (1989).

7. *Kiricsi, I., H. Förster, Gy. Tasi, P. Fejes:* Formation of carbenium ions in zeolites II., Application of UV–VIS spectroscopy for monitoring surface species, formed from hydrocarbons in zeolites (in Hungarian). Magy. Kém. Folyóirat, 95, 193 (1989).

8. *Kiricsi, I., H. Förster, P. Fejes, Gy. Tasi*: Formation of carbenium ions in zeolites III., Formation of alkyl and alkenyl carbenium ions from propylene in NaHY zeolite (in Hungarian). Kém. Folyóirat, 95, 199 (1989).

9. *Kiricsi, I., H. Förster, P. Fejes, Gy. Tasi*: Formation of carbenium ions

in zeolites IV., Chemisorption of propene over HZSM–5 zeolites (in Hungarian). Kém. Folyóirat, 95, 207 (1989).

10. *Kiricsi, I., Gy. Tasi, P. Fejes, H. Förster:* Formation of carbenium ions in zeolites V.,Chemisorption of cyclopropane (in Hungarian). Kém. Folyóirat, 95, 434 (1989).

11. *Kiricsi, I., P. Fejes, Gy. Tasi, H. Förster*: Formation of carbenium ions in zeolites IV.,Formation of alkenyl–type carbenium ions from 1–butene (in Hungarian). Kém. Folyóirat, 95, 488 (1989).

12. *Harsi, I., P. Fejes, K. Varga:* Simulation of an adiabatic contact catalitic reactor. Comp. Chem., Engng., 13, 725 (1989).

13. *Tasi, Gy., I.Kiricsi, P. Fejes, H. Förster, S. Lovas:* Semiempirical quantum chemical calculations with microcomputers (in Hungarian). Kém. Folyóirat, 95, 520 (1989).

14. *Tlomak, P., I. Hannus, W.E. Brower, Jr.:* RHEED detection of near crystalline phases on a $Pd_{80}Si_{20}$ metallic glass surface with adsorbates present. Ultramicroscopy, 29, 192 (1989).

15. *Hannus, I., J. Halász, I. Kiricsi, Gy. Schöbel, Gy. Tasi, P. Fejes:* Adsorption of nitrogen oxides in zeolites. Acta Phys. et Chem. Szeged, 35, 3 (1989)

16. *Hannus, I., A. Ádász-Szücs, I. Kiricsi, Gy. Tasi, F. Berger, J. Halász, P. Fejes:* Treatment of natural gas with zeolites. Acta Phys. et Chem. Szeged, 35, 19 (1989)

Institute of Colloid Chemistry

1. *Dékány, I., F. Szántó, A. Weiss:* The liquid–crystal structure of adsorbed layers and the stability of dispersed systems in organic liquids. Colloids and Surfaces, 41, 107 (1989).

2. *Dékány, I., L.G. Nagy, G. Lagaly:* The structure of the surface layer on hydrophillic/hydrophobic solids in binary liquid mixtures, 34. Hauptversammlung der Kolloid–Gesellschaft in Bochum Kolloid–Tagung 1–4. Oktober, 1989. p.33.

3. *Dékány, I., T. Marosi, A. Weiss:* Model investigation of hydrocarbon replacement on expanded layer silicates: Adsorption, microcalorimetric and X–ray diffraction measurements, 3rd Int. Conf. Fundamentals of Adsorption, Sonthofenn May 7–12, 1989. p.136.

4. *Dékány, I., T. Marosi, Z. Király, L.G.Nagy:* The effect of surface modification on thermodynamical properties of the adsorption layer at S/L interfaces, 3rd Int. Conf. Fundamentals of Adsorption, Sonthofenn May 7–12, 1989. p.229.

5. *Király, Z., I. Dékány:* Thermodynamics of multilayer adsorption of aqueous butanol solution onto printex and graphitised printex carbon blacks. J. Chem. Soc. Faraday Trans. 1, 85(10), 3373 (1989).

6. *Király, Z., I. Dékány:* One–step and step–by–step methods in S/L chromatography and flow sorption microcalorimetry, 34. Hauptversammlung der Kolloid–Gesellschaft in Bochum Kolloid–Tagung 1–4. Oktober, 1989. p.91.

7. *Király, Z., I. Dékány:* Thermodynamics of the multilayer adsorption of aqueous alcohol solutions onto non–porous carbon surfaces, 3rd Int. Conf. Fundamentals of Adsorption, Sonthofenn May 7–12, 1989. p.170.

8. *Patzkó, Á., F. Szántó:* Adhesion of quartz particles in liquid mixtures, PORANAL '89, Szeged, Hungary, 13–15. September 1989, Proceedings of the 4th Symposium on Particle Size Analysis and Powder Technology, p.327 and

9. *Tombácz, E., J. Balázs, J. Lakatos, F. Szántó:* Influence of the exchangeable cations on stability and rheological properties of montmorillonite

suspensions. Colloid and Polymer Science, 267, 1016 (1989).

10. *Zimehl, E., I. Dékány, G. Lagaly:* Adsorption on gel networks and concentrated latex dispersions. 34. Hauptversammlung der Kolloid–Gesellschaft in Bochum Kolloid–Tagung 1–4. Oktober, 1989. p.153.

11. *Kóczó, F.,* Á. *Patzkó, M. Borbély:* The dielectric behaviour of monocationic montmorillonites. Acta Phys. et Chem. Szeged, 35, 65 (1989).

Institute of Inorganic and Analytical Chemistry

1. *Burger, K., P. Sipos, M. Véber, I. Horváth, B. Noszál, M. Löw:* Formation of microequilibria of the proton, calcium and magnesium complexes of γ–carboxyglutamic acid and related compounds (in Hungarian). Magy. Kém. Folyóirat, 95, 165 (1989).

2. *Csányi, L.J.:* Peroxide derivatives of molybdenum(VI) in acidic solution. Transition Met. Chem., 14, 298 (1989).

3. *Csányi, L.J., I. Horváth, Z.M. Galbács:* Peroxide derivatives of molybdenum(VI) in neutral and alkaline media. Transition Met. Chem., 14, 90 (1989).

4. *Gaizer, F.:* Protonation and zinc complex formation of insulin. Polyhedron 8, 2065 (1989).

5. *Gaizer, F.:* Protonation and zinc complex formation of insulin (in Hungarian). Magy. Kém. Folyóirat, 95, 327 (1989).

6. *Horváth, I., R. Rajkó, P. Huhn:* Application of robust regression methods to the linear calibration model, I. (in Hungarian). Magy. Kém. Folyóirat, 95, 327 (1989).

7. *Labádi, I., K. Burger, Gy. Liptay, A Horváth, S. Papp, L. Korecz:* Preparation and investigation of iron(II)–ethyleneglycol complexes (in Hungarian). Magy. Kém. Folyóirat, 95, 178 (1989).

8. *Lukács, F., A. Péter, G. Sipos-Nagy, K. Burger, M. Löw, I. Schön, L. Kisfaludy:* A novel approach for the quantitative study of reductions by metallic sodium in liquid ammonia. Cleavage of protecting groups from protected oxytocein. Inorg. Chim. Acta 157, 121 (1989).
9. *Nagy, L., H. Ohtaki, T. Yamaguchi, M. Nomura:* EXAFS study of iron(III) complexes of sugar–type ligands. Inorg. Chim. Acta, 159, 201 (1989).
10. *Nagy, L., H. Ohtaki, T. Yamaguchi, M. Nomura:* EXAFS study of iron(III) complexes of sugar–type ligands (in Hungarian). Magy. Kém. Folyóirat, 95, 8 (1989).
11. *Nagy, L., L. Zsikla, K. Burger:* Preparation and ESR study of copper(II) complexes with sugar type ligands. J. Crist. Spectr. Res., 19, 911 (1989).
12. *Rajkó, R., I. Horváth, P. Huhn:* Parameter estimation based on the fuzzy theory (in Hungarian). Magy. Kém. Folyóirat, 95, 323 (1989).
13. *Ishiguro, S., K. Ozutsumi, L. Nagy, H. Ohtaki:* Spectrophotometric and calorimetric studies on the formation of binary (2,2'–bipyridine)nickel(II) and ternary (2,2'–bipyridine)chloronickel(II) complexes in N,N–dimethylformamide. J. Chem. Soc. Dalton Trans., 655 (1989).
14. *Véber, M., P. Sipos, K. Burger:* Zinc, calcium and magnesium ion coordination of vinblastine and vindoline. Inorg. Chim. Acta, 156, 145 (1989).
15. *Veres, S., A. Csikkel–Szolnoki:* Spectrophotometric detrmination of arsenic using carrier gas prepared in the hydride generation chamber (in Hungarian). Magy. Kém. Folyóirat, 95, 87 (1989).

Institute of Organic Chemistry

1. *Bakos, T., I. Vincze:* Direct, high–yield transformation of tetrahydropyranyl ethers to acetates. Synth. Comm., 19, 523 (1989).

2. *Bartók, M., L. Cera, Gy. Göndös, Á. Molnár:* Hydrogenolysis of β–lactams on nickel: a new method for the preparation of 1,3–aminoalcohols. Transformation of compounds containing C–N bonds on heterogenous catalysts, 4. (in Hungarian). Magy. Kém. Folyóirat, 95, 173 (1989).
3. *Felföldi, F., M.S. Klyavlin, M. Bartók:* Transformation of organic compounds in the presence of metal complexes V. Cyclization of aminoalcohols on a ruthenium complex. J.Organom.Chem., 362, 193 (1989).
4. *Felföldi, F., I. Kapocsi, M. Bartók:* Transformation of organic compounds in the presence of metal complexes IV. Hydrosilylation of 2– and 4–alkylcyclohexanones on rhodium(I) complexes. J. Organomet. Chem., 362, 411 (1989).
5. *Göndös, Gy., I. Szécsényi, L. Cera:* Silica gel–assisted reversible ring–opening and ring–closure reactions on a thin layer silica gel chromatographic plate. J. Planar Chrom., 2, 163 (1989).
6. *Göndös, Gy., L. Cera, M. Bartók:* Transformation of compounds containing C–N bonds on heterogenous catalysts, Part V. Hydrogenolysis of C–N bonds in substituted azacycloalkanones: preparation of sterically hindered amines and amino derivatives. J. Mol. Catal, 57, 81 (1989).
7. *Göndös, Gy., L. Cera, M. Bartók, J.C. Orr:* Homogenous and heterogenous catalytic asymmetric reactions II. Asymmetric hydrogenation of steroid ketones. J. Organomet. Chem. 373, 365 (1989).
8. *Göndös, Gy., L.C. McGirr, C.R. Jablonski, V.Snedden, J.C. Orr:* The reduction of steroid 2α–fluoro–4–en–3–ones (in Hungarian). Magy. Kém. Folyóirat, 95, 33 (1989).
9. *Molnár, Á., M. Bartók, G. Czira, J. Tamás:* Transformation of compounds containing C–N bonds on heterogenous catalysts, Part IV. A new metal–catalysed reaction: isomeration of 1,3–oxazacycloalkanes to

carboxamides on palladium. J. Mol. Catal. 57, 1 (1989).

10. *Molnár, Á., Á. Mastalir, M Bartók:* 1,2–Bond shift isomerization of oxiranes on copper–graphimet, J.C.S., Chem. Comm., 1989, 124.

11. *Molnár, Á., J.T. Kiss, M. Bartók:* Isomerization of 2–methyl–1–butene on copper–on–silica catalysts prepared by ion–exchange. J. Mol. Catal., 51, 361 (1989).

12. *Molnár, Á., G.V. Schmidt, M. Bartók:* New catalytic materials from amorphus metal alloys. (In: Advances in Catalysis, Vol. 36. Ed. by D.D. Eley, H. Pines, P.B. Weisz. San Diego, CA, 1989. Academic Press, Inc. p.329.

13. *Molnár, Á., J.T. Kiss, M. Bartók:* Surface characterization of Cu/SiO_2 catalysts prepared by ion–exchange. (In: Structure and Reactivity of Surfaces. Proc. Eur. Conference, Trieste, Italy, Sept. 13–16, 1988. Eds.: C. Morterra, A. Zecchina, G. Costa. Amsterdam, 1989. Elsevier. p.685)(Studies in Surface Science and Catalysis, Vol. 48.)

14. *Nagy., L., L. Zsikla, K. Burger, A. Rockenbauer, J.F. Kiss:* Preparation and electron spin resonance study of copper(II) complexes with sugar type ligands. J. Crystallogr. Spectr. Res. 19, 911 (1989).

15. *Pálinkó, I., F. Notheisz, M. Bartók:* A competitive reaction which is able to make fine distinctions between reacting surfaces. (In: Structure and Reactivity of Surfaces. Proc. Eur. Conference, Trieste, Italy, Sept. 13–16, 1988. Eds.: C. Morterra, A. Zecchina, G. Costa. Amsterdam, 1989. Elsevier. p.729)(Studies in Surface Science and Catalysis, Vol. 48.)

16. *Sárkány, I., M. Bartók:* Infrared study of the effects of O–containing compounds on CO preadsorbed on PT/Cab–O–Sil. (In: Structure and Reactivity of Surfaces. Proc. Eur. Conference, Trieste, Italy, Sept. 13–16, 1988. Eds.: C. Morterra, A. Zecchina, G. Costa. Amsterdam, 1989. Elsevier.

p.845)(Studies in Surface Science and Catalysis, Vol. 48.)

17. *Schneider, Gy., S. Bottka, L. Hackler, J. Wölfling, P. Sohár:* Steroids, XLI. Neighbouring group participation, X. Neighbouring group participation and fragmentation during the solvolysis of the epimers on 3–methoxy–16(tolylsulfonyloxymethyl)–estra–1,3,5(10)–trien–17–ol. Liebigs Ann. Chem. 1989, 263.

18. *Sirokmán, G., Á. Molnár, M. Bartók:* Synthesis of deuterium–labelled alkanes. J. Label. Comp. Radiopharm., 27, 439 (1989).

19. *Sirokmán, G., Á. Mastalir, Á. Molnár, M. Bartók, Z. Schay, L. Guczi:* On the nature of catalytic activity of nickel and platinum graphimets. J. Catal. 117, 558 (1989).

Institute of Physical Chemistry

1. *Bán, M.I.:* Location of stationary points of potential energy surfaces I. Guide to a new program system developed for the determination of gradient extremal curves. Acta Phys. et Chem. Szeged, 35, 73 (1989).

2. *Bán, M.I.:* Location of stationary points of potential energy surfaces II., A new procedure for finding saddle points. Acta Phys. et Chem., Szeged, 35, 000 (1989).

3. *Bán, M.I.:* An acceleration method for iterative quantum chemical procedures. Acta Phys. et Chem., Szeged, 35, 99 (1989).

4. *Bán, M.I.:* A rapid iterative diagonalization method for large matrices. Acta Phys et Chem., Szeged, 35, 87 (1989).

5. *Berkesi, O., I. Dreveny, J. Andor:* in "Surfactants in solution" Plenum Press, 9, 63 (1989).

6. *Dömötör, Gy., M.I. Bán:* Dynamic level–shifting. Computers and Chemistry, 13, 53 (1989).

7. *Görgényi, M., Z. Fekete, L. Seres:* Estimation and prediction of the retention indices of selected trans-diazenes. Chromatographia, 27, 581 (1989).

8. *Kankare, J., T. Pajunen, J. Lukkari, Cs. Visy:* Spectroscopic studies of the oxidation–reduction mechanism of conducting polymers. J. Chem. Soc., Faraday Discussions 88, 296 (1989).

9. *Körtvélyesi, T., L. Seres:* Theoretical studies of the N–containing radicals formed in thermal decomposition of dimethyl– and diethyldiazenes. React. Kinet. Catal. Letters 40, 65 (1989).

10. *Kutsán, Gy.,* Á. *Rauscher:* Computer aided scanning electrode technique for investigation of corrosion failures in organic coated tinned plates. Acta Phys. Chem. Szeged, 35, 43 (1989).

11. *Novák, M.,* Á. *Szücs:* Study of electropolishing of a Zn anode in acidic medium. J. Electroanal. Chem., 266, 157 (1989).

12. *Szabó-Plánka, T., G. Peintler, A. Rockenbauer, M. Győr, M. Varga-Fábián, L. Institórisz, L. Balázspiri:* Electron spin resonance study of copper(II) complexes of X–glycine and glycil–X type dipeptides and related tripeptides. Variation of coordination modes with ligand excess and pH in fluid and frozen aqueous solutions. J. Chem. Soc., Dalton Trans., 1925 (1989).

13. *Szirovicza, L., I. Nagypál, E. Boga:* An algorithm for the design of propagating acidity fronts. J. Am. Chem. Soc., 111, 2842 (1989).

14. *Szirovicza, L., J. Woog, I. Bárdi:* Pyrolysis of pentanes in the presence of CCl_4 II. Kinetics of the reaction $C_2H_5+CCl_4$, $C_2H_5Cl+CCl_4$. Acta Chim. Hung., 126, 117 (1989).

15. *Szücs, Á., C.D. Hitchens, J.O'M. Bockris:* Electrochemical reaction of glucose oxidase at graphite electrodes. Bioeletrochem. Bioenerg., 21, 133

(1989).

16. *Szücs, Á., C.D. Hitchens, J.O'M. Bockris:* On the adsorption of glucose oxidase at a gold electrode. J. Electrochem., 136, 3748 (1989).

17. *Visy, Cs., J. Lukkari, T. Pajunen, J. Kosonen, J. Kankare:* Spectroscopic evidence fort the existence of long lived intermediates during the electrochemical transformation of poly–3–methylthiophene. J. Electroanal. Chem. 262, 297 (1989).

18. *Visy, Cs., J. Lukkari, T. Pajunen, J. Kankare:* Effect of Anions on the transient redox behaviour of polypyrrole in anhydrous acetonitrile. Synthetic Metals, 33, 289 (1989).

Institute of Solid State and Radiochemistry

1. *Berkó, A., F. Solymosi:* Adsorption and dissociation of CH_3Cl on clean and potassium–promoted Pd(100) surfaces. J. Phys. Chem., 93, 12 (1989).

2. *Bugyi, L., F. Solymosi:* On the negligible interaction between K and CO on the CaF_2 surface. Surface Science, 210, L 193 (1989).

3. *Kiss, J., K. Révész, F. Solymosi:* Segregation of boron and its reaction with oxygen on Rh. Applied Surface Science, 37, 95 (1989).

4. *Kiss, J., G. Klivényi, K. Révész, F. Solymosi:* Photoelectron spectroscopic studies on the dissociation of CO on potassium–dosed Rh(111) surface. Surface Science, 223, 551 (1989).

5. *Liu, Z.M., Y. Zhou, F. Solymosi, J.M. White*: Vibrational study of CO_2 on K–promoted Pt(111). J. Phys.Chem., 93, 4383 (1989).

6. *Solymosi, F.:* An infrared study of the influence of CO adsorption on the topology of by supported Ru. J. Catalysis, 115, 107 (1989).

7. *Solymosi, F., A. Berkó:* The properties of CO and K coadsorbed on Pd(100): LEED, EELS, TDS and work function studies. J. Chem. Phys. 90,

2492 (1989).

8. *Solymosi, F., I. Kovécs:* Effects of potassium adlayer on the adsorption and desorption of hydrogen on Pd(100) surface. J. Phys. Chem., 93, 7537 (1989).

9. *Zhou, X.L., F. Solymosi, P.M. Blass, K.C. Cannon, J.M. White:* Interactions of methyl halides (Cl, Br, I) with Ag(111). Surface Science, 219, 294 (1989).

INDEX

Adsorption of nitrogen oxides in zeolites
I. HANNUS, J. HALASZ, I. KIRICSI, GY. SCHUBEL, GY. TASI, P. FEJES 3
Treatment of natural gas with zeolites
I.HANNUS, A.ADASZ–SZUCS, I.KIRICSI, GY.TASI, F.BERGER, J.HALASZ, P.FEJES 19
Computeraided scanning electrode technique for the investigation of corrosion failures in organic–coated tinned plates
GY. KUTSAN, A. RAUSCHER 43
Absorption spectra of nitrones of N–(2–hydroxybenzylidene)aniline and N–(4–hydroxybenzylidene)aniline in various solvent mixtures
P. NAGY, R. HERZFELD 55
The dielectric behaviour of monocationic montmorrilonites
F. KOCZO, A. PATZKO, M. BORBELY 65
Location of stationary points of potential energy surfaces I. The determination of gradient extremal curves
M.I. BAN 73
A rapid iterative diagonalization method for large matrices
M.I. BAN 87
An acceleration method for iterative quantum chemical procedures
M.I. BAN 99
Location of stationary points of potential energy surfaces II. A new procedure for finding saddle points
M.I. BAN 107
List of papers published by the authors of the Department of Physics and the Department of Chemistry, in scientific journals, during 1989. 129

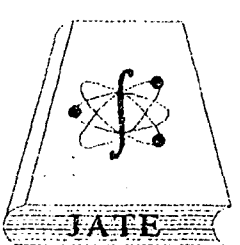

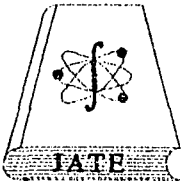

Publisher: The Dean Dr. L. Hatvani
(JATE TTK Dean's Office)
Published by the Editorial Office of Acta Phys. et Chem.
at JATE Institute of Physical Chemistry, Szeged
Wordprocessing and copying by *S. Kádár*
Size: B/5
No. of copies: 400

Fk.: Dr. Hatvani László
Készült az Acta Phys. et Chem. szerkesztőségében
(JATE, Fizikai Kémiai Tanszék, Szeged)
Szövegszerkesztési és sokszorosítási munka: *Kádár Sándor*
Engedélyszám: 16–3124/54–5/1990 Méret: B/5
Példányszám: 400